arXiv:cond-mat/0402203v2 [cond-mat.dis-nn] 6 Mar 2006

Disordered Electron Systems

Carlo Di Castro

Dipartimento di Fisica, Università di Roma "La Sapienza", and INFM Center for Statistical Mechanics and Complexity, Piazzale Aldo Moro 2, 00185 Roma, Italy

Roberto Raimondi

NEST-INFM and Dipartimento di Fisica, Università di Roma Tre, Via della Vasca Navale 84, 00146 Roma, Italy

1. – Introduction

These lectures provide an introduction to the theory of disordered interacting electron systems. As for the case of superconductivity, the understanding of the behavior of transport and thermodynamical properties of metals and semiconductors has required the invention of new and fascinating concepts.

In these lectures our focus is mainly on the effects of disorder, and its interplay with electron-electron interaction. The resulting theory, although still cannot answer some important questions, is simple and elegant. It describes the combined effects of interaction and disorder in terms of a renormalized Fermi liquid, whose Landau parameters become scale dependent and provide, together with the conductance, the couplings flowing under the action of the renormalization group. However, this final simple description, which has required several decades of intensive work from many people, is built on several conceptual steps. It is our aim to lead the reader through the development of these various steps. Our hope is that the reading of these lectures should allow people not expert in the field to access the original literature.

There are already several review articles which give an account of the problem from different view points and at different stages of the historical development [1, 2, 3, 4, 5, 6, 7, 8]. However, the most recent and complete are still quite hard to read for unprepared

© Società Italiana di Fisica

readers. For unprepared readers we mean those people that are not familiar with the complex technical jargon that the field experts have developed over the years.

We will concentrate on those aspects that we believe are fundamental for the problem of the metal-insulator transition due to disorder and interaction. This will force us to ignore a number of extensions and developments of the theory. These latter, however, may be found in the existing reviews.

We have also chosen to present the theory in the simple language of standard many-body perturbation theory. The field-theoretic approach based on the derivation of an effective non-linear σ-model[6] is certainly more elegant and powerful, but requires quite some effort to appreciate the beauty of it. We invite the reader to approach it after reading these lectures. These lecture notes are self-contained. A basic knowledge of many-body theory and diagrammatic technique is the only prerequisite.

After these warnings, we outline the contents of these lectures. In the next section we set the stage for the microscopic theory by introducing the reader to the metal-insulator transition in disordered systems and to phenomenological scaling. The necessary background for the microscopic theory is given in the following section. The fourth section deals with the non-interacting problem. A number of key physical and technical ingredients are introduced in a pedagogical way. Also, the experimental urgency to take into account interaction effects is presented. The fifth section goes to the heart of the problem by building the renormalized disordered Fermi liquid. Gauge invariance and Ward identities are the shining lighthouses which help us to navigate through the messy waves of the perturbation theory. Land is finally reached in the sixth section, where we discuss the renormalization group equations and look back to our journey and compare the theoretical understanding with the available experiments.

2. – Setting the stage for the metal-insulator transition

In this section, we begin by recalling the textbook theory of electrical transport in metals. Then we move to a description of the actual physical systems where the phenomena, which we describe theoretically, are observed. We conclude the section with the scaling theory of the metal-insulator transition due to disorder.

2˙1. *The semiclassical approach of Drude-Boltzmann.* – The conventional theory of electrical transport is due to Drude. In its original formulation, Drude suggested that electrons, under the action of an externally applied electric field, are accelerated according to Newton's equation of motion until they collide with the ions after a time τ. The distance between successive collisions determines the mean free path l. Due to this sequence of independent scattering events the electrical conductivity is given by

$$\sigma_0 = \frac{e^2 n_0 \tau}{m} \tag{2.1}$$

where n_0 is the density of electrons and e, m are the charge and electron mass.

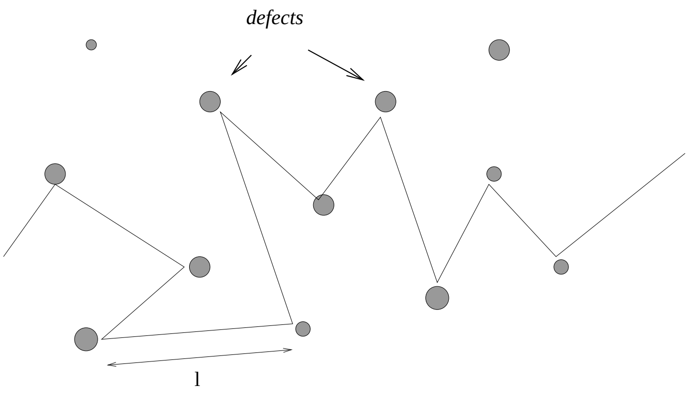

Fig. 1. – A pictorial representation of the semi-classical theory of transport.

After the birth of quantum mechanics, Sommerfeld reformulated Drude's theory to accomodate the Fermi statistics of electrons, providing the correct relation between τ and l via the Fermi velocity v_F. More importantly, with the work of Bloch, it was realized that the relaxation of electron momentum and the finite value of the conductivity is due to imperfections of the ion lattice, *i.e.* to *disorder*. Drude's law (2.1) may be obtained by a *semi-classical* approach based on the Boltzmann equation for the evolution of the electron distribution function in the presence of external fields. A pictorial description of Drude's model of electrical conduction is shown in fig.1.

As a consequence of the collisions, the electrons undergo a classical random walk of step l and a *diffusive* motion, with the diffusion coefficient D related to the conductivity by Einstein's relation

$$\sigma_0 = e^2 \frac{\partial n_0}{\partial \mu} D \tag{2.2}$$

where $\partial n_0/\partial\mu$ is the *compressibility*. In the case of the Fermi gas, $\partial n_0/\partial\mu = 2N_0$ is simply related to the density of states per unit volume per spin

$$N_0 = \frac{\Omega_d}{(2\pi\hbar)^d} 2^{\frac{d-2}{2}} m^{d/2} E_F^{\frac{d-2}{2}} \tag{2.3}$$

where Ω_d is the solid angle in d dimensions and E_F the Fermi energy. From the Drude formula (2.1) and Einstein's relation (2.2), with $n_0 = 2N_0 2E_F/d$, one gets the diffusion coefficient $D = (2E_F\tau)/(d\,m) = v_F^2\tau/d$. Within the independent electron approximation, only one diffusion constant D controls the charge, spin and heat transport, leading to relations similar to eq.(2.2) for the charge. In particular, the thermal conductivity, κ_E,

$$\kappa_E = C_{V,0} D \tag{2.4}$$

where $C_{V,0} = (2\pi^2/3)k_B^2 N_0 T$ is the specific heat for the electron gas.

In concluding this subsection, we introduce the conductance related to the conductivity by geometrical factors

$$G = \frac{\sigma_0 \mathcal{S}}{\mathcal{L}} = \sigma_0 L^{d-2} \tag{2.5}$$

where $\mathcal{S}$ and $\mathcal{L}$ are the cross section and length of the conductor to which we assign the typical size L. By using the explicit expression of the density of states, one may rewrite G as

$$G = \frac{2e^2}{h}\frac{\Omega_d}{(2\pi)^{d-1}\, d}\frac{2E_F\tau}{\hbar}\left(\frac{p_F L}{\hbar}\right)^{d-2} = \frac{2e^2}{h}\frac{\Omega_d}{(2\pi)^{d-1}\, d}\frac{p_F\; l}{\hbar}\left(\frac{p_F L}{\hbar}\right)^{d-2}, \tag{2.6}$$

which shows that, in the natural conductance units ($G_0 = 2e^2/h = 12.9\mathrm{k}\Omega^{-1}$), the value of G is controlled by the dimensionless parameters $p_F l/\hbar = 2\pi l/\lambda_F$ and L/λ_F. In two dimensions, in particular, conductivity and conductance have the same physical dimensions and the ratio between the Fermi wavelength and the mean free path is the only parameter that controls the value of the conductivity. In the semi-classical limit, $\lambda_F \ll l$, the Drude formula predicts a high conductivity. The rate of collisions τ^{-1} is proportional to the impurity concentration. By increasing the disorder in the semiclassical approach, one has that σ_0 diminishes, but remains finite. Ioffe and Regel[9] stated the criterion that in the metallic phase the mean free path l cannot be smaller than the average interelectron distance proportional to $\hbar/p_F$, i.e., $p_F l/\hbar \geq 1$. Mott[10] applied this criterion to the Drude conductivity arguing that for $d \geq 2$ there is a minimum metallic conductivity, $\sigma_{0\min}$ when $l \approx \hbar/p_F$,

$$\sigma_{0\min} = \frac{2e^2}{h}\frac{\Omega_d}{(2\pi)^{d-1}\, d}\left(\frac{p_F L}{\hbar}\right)^{d-2}. \tag{2.7}$$

As a result, there should be a discontinuity of the conductivity (which is universal in $d = 2$) at the transition from the metal to the insulator. However, when $l \approx \hbar/p_F$ we are deeply in the quantum limit and the Ioffe-Regel criterion cannot be naively applied to the semiclassical Drude formula. Indeed one expects that corrections beyond the semi-classical approximations will strongly modify eq.(2.1) opening the way to a new perspective in the metal-insulator transition. Most of these lectures concern precisely this type of corrections.

2˙2. *The metal-insulator transition.* – There are, of course, finite-temperature corrections to Drude's formula. In general, temperature-dependent corrections arise from inelastic scattering of electrons beween them and with the phonons, resulting in the characteristic $\approx T^2$ and $\approx T^3$ behavior of the conductivity. However, typical disordered systems show, at low temperature, strong anomalies. In metallic films, for instance, there are temperature dependent logarithmic corrections[11]

$$\sigma(T) = \sigma_0 + m \ln T, \tag{2.8}$$

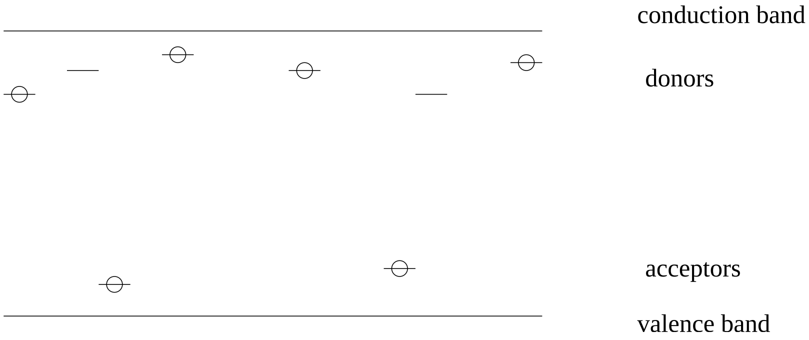

Fig. 2. – Energy diagram of an n-type semiconductor containing donors and acceptors. The horizontal lines represent centres, the circles electrons in them.

where m is positive. Besides metals, experimental realizations of disordered systems are obtained in doped semiconductors like $Si : P$, $Ge : Sb$ and amorphous alloys as $Nb : Si$, $Al : Ge$, $Au : Ge$. In a doped semiconductor, there are two types of conduction mechanisms. The first is due to the thermal activated carriers and dominates at high temperature. To understand the second mechanism, let us consider, for instance, an n-type semicondutor, as shown in fig.2. An electron sitting at its donor atom location, has a wave function exponentially localized around the impurity (the energy of such an electron is indicated by a short horizontal line in the figure). Due to the small, but finite overlap of wave functions centered at different impurity locations, the donor electrons can move around by tunneling from one impurity to another. This gives rise to what is called impurity conduction. A doped semiconductor is compensated when, besides the majority donor atoms, it contains also some minority acceptor atoms. In this way, some of the donor electrons are captured by the acceptor levels, by allowing the tunneling of a donor electron from an occupied level to an unoccupied one. By increasing the impurity concentration, the overlap of the wave functions sitting at different impurity sites becomes larger. One point to notice is that by increasing the impurity concentration, there are two competing effects. On the one hand, disorder increases due to the larger number of scattering centers. On the other, at a high enough concentration of impurities, the overlap is such that the impurity levels form a band, which behaves as an intrinsically disordered degenerate electron gas and yields a metallic conductivity. Hence disorder effects are stronger at lower concentration. The transition to metallic behavior of the impurity conduction occurs at a critical impurity concentration, n_c. $Si : P$, where P donors sit substitutionally and randomly in a dislocation-free Si lattice, is an ideal system to study the effect of disorder on transport properties. For instance, at enough impurity concentration to be in the metallic state, one measures

$$\sigma(T) = \sigma_0 + mT^n, \tag{2.9}$$

where the coefficient m can be both positive and negative and $n = 1/2$ [12]. By decreasing the P concentration below a critical value, the system undergoes a metal-insulator transition at $T = 0$ in the sense that

$$\sigma_0 \approx (n - n_c)^\mu, \tag{2.10}$$

with the critical exponent $\mu = 1/2$[13, 12] The value of μ for uncompensated $Si : P$ is still under debate and depends strongly on the identification of the critical region in the experimental data[14, 15, 16, 17, 18]. Compensated samples[19] and the alloys [20, 21, 22] have $\mu = 1$.

Besides the transport properties, anomalies are also seen in the tunneling density of states for $Au : Ge$[23], $NbSi$[20], in specific heat[24, 25, 26, 27], and in spin susceptibility [28, 29, 30, 31, 32] in SiP. As we will discuss in a more detailed way in the next sections, taking into account corrections both in transport and thermodynamic properties will be crucial in developing an effective Fermi-liquid theory for these systems.

In more recent years, the discovery of a metal-insulator transition in the two-dimensional electron gas[33] has stimulated a renovated effort to understand the interplay of disorder and interaction effects ([1]). This phenomenon has been first observed in Si-MOSFET devices and later also in other two-dimensional electron gas realizations as in semiconductor hetero-structures. In Si-MOSFETs devices, the two-dimensional electron gas is formed at the interface between the bulk silicon and an insulating layer of silicon oxide, as shown in fig.3. By applying a positive bias on the metallic gate deposited on the insulating silicon oxide layer one forces the electrons to move in the SiO_2-Si interface, in an almost two-dimensional environment. As compared with the doped semiconductor systems, these systems have the advantage that the density of the electron gas is almost continuously controlled by the degree of the band bending at the interface, i.e., by the applied bias. This allows a very fine scanning of the properties of the sample as function of density. Furthermore, the disorder is mainly due to scattering centers in the insulating layer, so that in principle one varies the density at fixed amount of disorder. By varying the electron density, n, one can change the effect of the interaction since $E_F \propto n$, and in 2D the Coulomb electron-electron interaction $E_C \propto n^{1/2}$. The ratio r_s between the Coulomb interaction evaluated at the average interparticle distance and the Fermi energy is given by

$$r_s = \frac{E_C}{E_{kin}} = \frac{e^2/(\varepsilon r_{av})}{E_F}, \tag{2.11}$$

where ε is the dielectric constant. By using $E_F = n/(2N_0)$ and $r_{av} = 1/\sqrt{n}$ and recalling

---

([1]) At present there is not yet a general consensus on whether we have a real zero-temperature transition or rather a crossover effect.

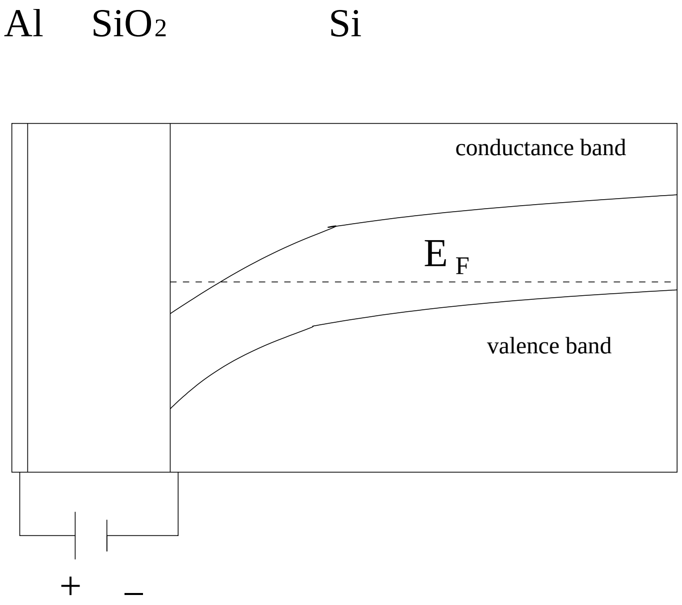

Fig. 3. – Scheme of a SiMOSFET device. The metallic gate (Al) is positevely biased so that it attracts the electrons, which on the other hand cannot enter the insulating layer of SiO_2. The electrons are then confined at the interface $Si - SiO_2$ and form a two-dimensional electron gas. In the proximity of the interface the slope of the energy bands determines the effective tickness of the two-dimensional electron gas.

the expression of the Bohr radius $a_B = \varepsilon\hbar^2/(me^2)$, one obtains

$$r_s = \frac{1}{\pi\varepsilon a_B\sqrt{n}}. \tag{2.12}$$

At the present, the origin of the metal-insulator transition in two-dimensional systems is still unclear and represents a very hot issue of debate in the literature. (A recent review may be found in refs.[34, 35]). For this reason, we prefer not to enter now in a detailed discussion of the experimental features of this phenomenon, which we will point out later on when relevant results of the theory will require it.

2·3. *The Anderson transition and quantum interference.* – All of this suggests that disorder cannot be treated only within a semi-classical approach. In 1958, Anderson invented the field of *localization*, proposing that under certain circumstances diffusion may be completely suppressed[36]. He proposed a lattice model where the site energies are randomly distributed. When disorder is absent, a small hopping amplitude is enough to delocalize the electron states and form Bloch waves. However, by increasing the disorder, the hopping processes may only spread an initially localized state over a finite distance, which defines the localization length ξ_0. Since in the process of the impurity band formation, localized states are more likely to form in the band tails, Mott argued[37] that there must exist a critical energy E_c, called the *mobility edge*, which separates localized from extendend states. When the Fermi energy E_F is below the mobility edge, the system is an insulator. When E_F passes through E_c, the system becomes metallic. From this point of view, for a given model and given amount of disorder, the problem is to compute E_c. For non-interacting systems, this can be tackled numerically, by exactly solving the Schrödinger equation in a disordered lattice. A review of the status of the numerical simulations may be found in ref.[7].

Even though these concepts played an important role in shaping our modern view of the metal-insulator transition, a great impulse to the development of the field came, however, by the discovery of the phenomenon of *weak localization*.

As remarked at the end of the previous subsection, the standard theory of transport is based on a semi-classical approach, where in evaluating the probability for electron diffusion one neglects the interference between the amplitudes corresponding to different trajectories and essentially treats a classical random walk with step l and diffusion constant D. This is indeed justified in many cases, where the semi-classical theory works. In fact, in a disorderd system the phase difference for any two different trajectories will vary randomly. The situation changes, however, for *self-intersecting* trajectories, which come from closed loops. In this case, trajectories naturally come in pairs, depending on whether one goes around the loop clockwise or counter-clockwise. One expects that interference between these pairs of trajectories modifies the semi-classical result. There is a simple argument to estimate the probability of having a self-intersecting trajectory. On the one hand, one has that the electron motion is described by a classical diffusion process such that the average distance after a time t is

$$\overline{\mathbf{r}^2} = Dt. \tag{2.13}$$

On the other hand, the quantum nature of the electron may be thought of in terms of a *tube* of size λ_F generated by the electron motion. In a time dt, the volume spanned by the tube increases by

$$\mathrm{d}V_{tube} = \lambda_F^{d-1}\ v_F \mathrm{d}t. \tag{2.14}$$

Let us consider the ratio between the increase of the tube volume in time dt and the total volume generated by the diffusion process. The total probability for self-intersection may be estimated by integrating this ratio over time

$$P \sim \int_{\tau}^{\tau_\phi} \frac{\lambda_F^{d-1} v_F \mathrm{d}t}{(Dt)^{d/2}}, \tag{2.15}$$

where the lower limit τ is the time above which the diffusive regime, after a few collisions, starts to set in. The upper limit, τ_ϕ, is the time until which phase coherence of the wave function persists. In general, *inelastic* processes at finite temperature make τ_ϕ a decreasing function of temperature. In two dimensions the probability grows logarithmically as temperature decreases. At zero temperature, when $\tau_\phi \to \infty$, the upper limit is provided by the system size via the diffusion relation $L^2/D \equiv \tau_L$. In this way, the probability of self-intersection acquires a scale dependence

$$P \sim \frac{v_F \lambda_F^{d-1}}{D^{d/2}\tau^{(d-2)/2}} \frac{2}{d-2}\left[\left(\frac{\tau}{\tau_L}\right)^{\frac{d-2}{2}} - 1\right] \propto \frac{G_0}{\sigma_0 l^{d-2}} \frac{2}{d-2}\left[\left(\frac{\tau}{\tau_L}\right)^{\frac{d-2}{2}} - 1\right]. \tag{2.16}$$

By assuming that the conductivity corrections are proportional to this probability, one obtains

$$\frac{\delta\sigma}{\sigma_0} \propto \frac{1}{g_0 \epsilon}\left[\left(\frac{l}{L}\right)^{\epsilon} - 1\right] \tag{2.17}$$

where $\epsilon = d-2$ and $g_0 \equiv G(l)/G_0$ is the conductance at the scale l in units of G_0. Equation (2.17) is valid at $T=0$ and the inverse scattering time or the inverse mean free path play the role of the ultraviolet cutoff, whereas τ_L^{-1} is the infrared cutoff. At $d=2$, the conductivity correction is log-singular.

At finite temperature, when $\tau_\phi < \tau_L$, the infrared cutoff becomes temperature dependent and in 2D the correction becomes logarithmic in temperature. This opens the way to the scaling theory discussed in the next subsection.

As a final remark to this subsection, we point out that the weak-localization phenomenon is sensitive to any perturbation that breaks the time reversal invariance. This is clear from the above argument of the interference between time reversed trajectories. For instance, in the presence of a magnetic field, the two trajectories acquire a phase difference $\phi_1 - \phi_2 = (2e/\hbar c)\Phi_B$, proportional to the magnetic flux Φ_B threading the surface delimited by the closed loop. Since at finite temperature the logarithmic singularity is cut off at time τ_ϕ, in order to cut off the singularity typical magnetic fields must be of the order of a flux quantum over a region whose size is of the order of the dephasing length $L_\phi = \sqrt{D\tau_\phi}$. This gives the condition $B \geq (h/ec)/L_\phi^2$. It is also clear that further dephasing mechanisms, as for instance, spin-flip scattering with typical time τ_s become important when $\tau_s < \tau_\phi$.

2·4. *The scaling theory of the metal-insulator transition.* – The starting point is the argument of Thouless concerning the evolution of the wave function as the system size is increased[38, 39]. To fix the ideas, let us imagine that the system of system size $2L$ is made up by combining blocks of size L, as shown in fig.4. Suppose we know the eigenstates for a block of size L. The level spacing for these is ΔE. We ask how are the states when we combine blocks together. Let δE be the energy brought about by the perturbation of joining the blocks together. Clearly, we expect that for $\delta E \ll \Delta E$ the new eigenstates for a system of size $2L$ will differ very little from those at scale L. The energy δE measures the sensitivity to a change in the boundary conditions. In a diffusive sytem this may be related to the time necessary to reach the boundary, $\delta E = \hbar D/L^2$. The level spacing, on the other hand, is related to the inverse density of

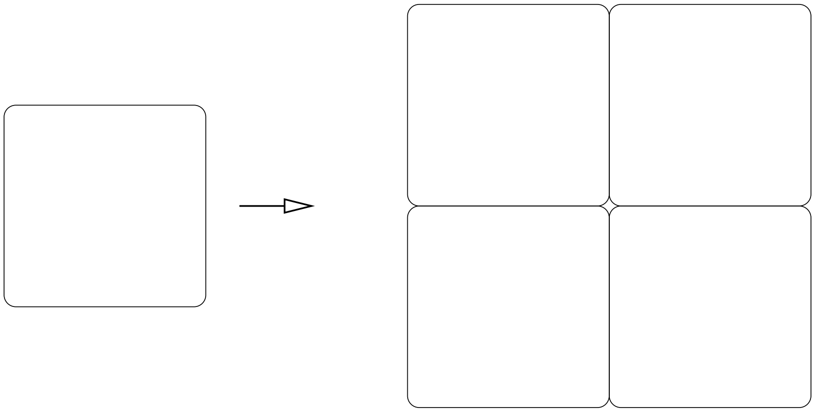

Fig. 4. – Block of size $2L$ obtained by blocks of size L.

states, $\Delta E = 1/(N_0 L^d)$. By using Einstein's relation, the ratio of the two energies gives

$$\frac{\delta E}{\Delta E} = N_0 L^d \frac{\hbar D}{L^2} = \frac{1}{2\pi}\frac{\sigma_0 L^{d-2}}{2e^2/h} = \frac{g(L)}{2\pi} \tag{2.18}$$

where $g(L)$ is the conductance at the scale L in units of $2e^2/h$. If $g \ll 1$, the new eigenstates are not modified much by the assembling of the blocks. On the other hand, when $g \gg 1$, the new states are delocalized on all the blocks. The scaling theory[40] assumes the $g(L)$ is the only parameter that controls the evolution of the eigenstates when we rescale the system size. Mathematically this is expressed by requiring that the conductance of a block of size $L' = bL$ is expressed in terms of the conductance of a block of size L by a function of L'/L and $g(L)$ only, i.e., $g(L') = f(L'/L, g(L))$. Its logarithmic derivative for $L' = L$, which defines the β-function of the corresponding renormalization group equations, depends on the scale L only through $g(L)$ itself

$$\frac{\mathrm{d}\ln g(L)}{\mathrm{d}\ln L} = \beta(g(L)). \tag{2.19}$$

The vanishing of the β-function controls the scale-invariant limit, i.e., provides the fixed point of the trasformation g^*. In the case of one-parameter equation the fixed g^* point coincides with the critical value g_c. Linearization of the transformation, starting from the fixed point, provides the scaling behavior of the physical quantities. The β-function is relatively well known in the two limits of a good metal, where Ohm's law is valid and σ is a constant, and in the strongly localized insulating regime, where the scale-dependent conductance falls off exponentially over a localization length ξ_0 as

$$g(L) = g_0 e^{-L/\xi_0}. \tag{2.20}$$

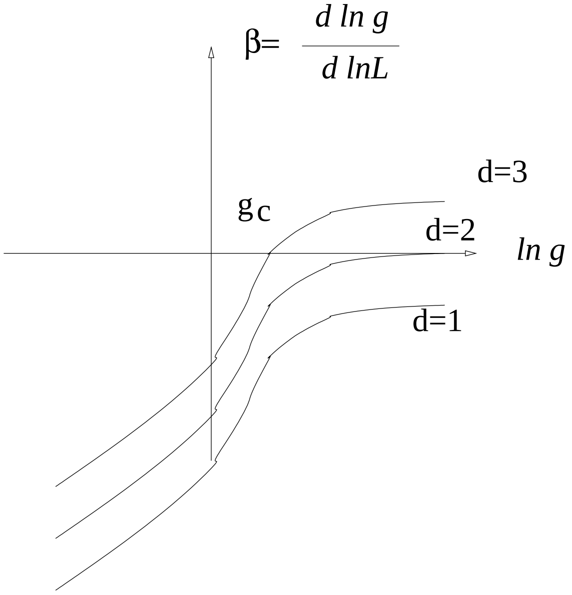

Fig. 5. – Schematic β-function.

One then immediately gets

$$\beta(g) = d - 2, \quad g \gg 1 \tag{2.21}$$

$$\beta(g) = \ln \frac{g}{g_0}, \quad g \ll 1 \tag{2.22}$$

where g_0 is the conductance at some initial microscopic scale l. Under reasonable assumptions, the β-function has the qualitative behavior shown in fig.5. A positive (negative) value for β means that upon increasing the system size, g increases (decreases) corresponding to a metallic (insulating) behavior.

A zero g_c such that $\beta(g_c) = 0$, signals an unstable fixed point for the flow of g. This represents a metal-insulator transition. One consequence of eqs.(2.21),(2.22) is that, for $d \leq 2$, the system is always an insulator at zero temperature and all states are localized. Close to a critical point at $d > 2$ we may linearize the β-function to get

$$\frac{\mathrm{d}(g - g_c)}{\mathrm{d}\ln L} = g_c \beta'(g_c)(g - g_c), \quad \beta'(g_c) = \left(\frac{\mathrm{d}\beta(g)}{\mathrm{d}g}\right)_{g=g_c} \tag{2.23}$$

from which

$$g(L) - g_c = (g_0 - g_c)\left(\frac{L}{l}\right)^{x_g} \tag{2.24}$$

where g_0 is the conductance at scale l and

$$x_g = g_c \beta'(g_c). \tag{2.25}$$

By defining a correlation length, which coincides with the localization length in the insulating side, it diverges at criticality as

$$\xi \sim (g_0 - g_c)^{-\nu}. \tag{2.26}$$

By assuming that ξ is the only relevant length, it scales as $\xi' = \xi/(L/l)$ and one deduces $\nu = 1/x_g$. Furthermore, from the critical behavior of the conductivity

$$\sigma \sim (g_0 - g_c)^{\mu} \sim \frac{g(\xi)}{\xi^{d-2}} \rightarrow \frac{g_c}{\xi^{d-2}} \tag{2.27}$$

one derives the scaling law[41]

$$\mu = (d-2)\nu \equiv \epsilon\nu. \tag{2.28}$$

In the metallic regime, where g is large, we can assume that the β-function can be expandend in a power series in $1/g$[42, 40]

$$\beta(g) = d - 2 - \frac{a}{g} - \frac{b}{g^2} + \dots\ . \tag{2.29}$$

Above two dimensions, if $a > 0$, one has a fixed point $g_c = a/\epsilon$ and $\nu = 1/\epsilon$ leading to $\mu = 1$. On the other hand, if $a = 0$, the fixed point is determined by the second order term, $g_c^2 = b/\epsilon$, which implies $\nu = 1/(2\epsilon)$ and $\mu = 1/2$. Finally, when $a < 0$, there is no fixed point at this order.

At $d = 2$ the scaling equation reduces to

$$\frac{\mathrm{d}g}{\mathrm{d}\ln L} = -\frac{a}{g}. \tag{2.30}$$

For $a > 0$ the system scales to an insulator, whereas for $a < 0$ it scales to a perfect conductor. This phenomenological theory does not allow for a metallic phase in $d = 2$.

3. – The microscopic approach

In this section we introduce a few general tools that will be used in building a microscopic theory. First we discuss how physical observables may be evaluated in terms of response functions. Secondly, we show how conservation laws impose constraints, *e.g.* Ward Identities, on these correlation functions, which are useful when performing perturbative expansions. We mainly follow ref.[43].

3˙1. *Linear response theory, Kubo formula and all that.* – The coupling with an external electromagnetic field is given by the Hamiltonian(2)

$$H_{emi} = \frac{1}{c} \int \mathrm{d}\mathbf{r} A^{\mu}(\mathbf{r}) J_{\mu}(\mathbf{r}) \tag{3.1}$$

where the Greek index runs over time ($\mu = 0$) and space indices ($\mu = 1, ..., d$). The latter will be later on indicated by Latin letters . As it is standard, lower indices have space components with a minus sign, *e.g.*, $J_{\mu} = (c\rho, -\mathbf{J})$. With $\mathbf{r}$ we indicate the position vector in any dimension d. The external scalar, $\phi(\mathbf{r})$, and vector potential, $\mathbf{A}(\mathbf{r})$, are coupled with the charge and current density, defined by

$$\rho(\mathbf{r}) = e\psi^{\dagger}_{\sigma}(\mathbf{r})\psi_{\sigma}(\mathbf{r}) \tag{3.2a}$$

$$\mathbf{J}(\mathbf{r}) = -\mathrm{i}\frac{e\hbar}{2m}\left[\psi^{\dagger}_{\sigma}(\mathbf{r})\nabla\psi_{\sigma}(\mathbf{r}) - (\nabla\psi^{\dagger}_{\sigma}(\mathbf{r}))\psi_{\sigma}(\mathbf{r})\right] - \frac{e^2}{mc}\mathbf{A}(\mathbf{r})\psi^{\dagger}_{\sigma}(\mathbf{r})\psi_{\sigma}(\mathbf{r}) \tag{3.2b}$$

$$\equiv \mathbf{j}(\mathbf{r}) - \frac{e^2}{mc}\mathbf{A}(\mathbf{r})\psi^{\dagger}_{\sigma}(\mathbf{r})\psi_{\sigma}(\mathbf{r}). \tag{3.2c}$$

In the following, for the sake of simplicity we shall set $\hbar$, c, and k_B equal to one. In eqs.(3.2), $\psi_{\sigma}(\mathbf{r})$ ($\psi^{\dagger}_{\sigma}(\mathbf{r})$) is the annihilation (creation) Fermion field operator. Our goal is to study the system response to an external electromagnetic field within linear response. The second term in eq.(3.2c), the diamagnetic contribution, being already linear in the field, may be evaluated as

$$\mathbf{j}^{dia} = -\frac{e^2}{m} n_0 \mathbf{A} \tag{3.3}$$

where n_0 is the equilibrium (number) density. By the compact notation $x = (t, \mathbf{r})$, the linear response is given by

$$J^{\mu}(x) = \int \mathrm{d}x' \; K^{\mu\nu}(x, x') A_{\nu}(x') \tag{3.4}$$

where the response kernel $K^{\mu\nu}(x, x')$ is the four-current correlation function, which includes both the density-density and current-current correlation functions,

$$K^{\mu\nu}(x, x') = R^{\mu\nu}(x, x') + \frac{e^2}{m} n_0 \delta^{(4)}(x - x')\delta_{\mu\nu}(1 - \delta_{\nu 0}) \tag{3.5}$$

and

$$R^{\mu\nu}(x, x') = -\mathrm{i}\theta(t - t') < [j^{\mu}(x), j^{\nu}(x')] >, \tag{3.6}$$

---

(2) We adopt the relativistic notation: upper and lower indices indicate contravariant and covariant vectors, respectively, *i.e.* $A^{\mu} = (\phi, \mathbf{A})$ and $A_{\mu} = (\phi, -\mathbf{A})$.

with the average taken over the appropriate statistical ensemble(3) . If the unperturbed system is traslationally invariant and has a time-independent Hamiltonian, we can use Fourier transforms with respect to both $\mathbf{r} - \mathbf{r}'$ and $t - t'$,

$$K^{\mu\nu}(\mathbf{r} - \mathbf{r}', t - t') = \int_{-\infty}^{\infty} \frac{\mathrm{d}\omega}{2\pi} \sum_{\mathbf{q}} e^{\mathrm{i}\mathbf{q}\cdot(\mathbf{r}-\mathbf{r}')-\mathrm{i}\omega(t-t')} K^{\mu\nu}(\mathbf{q}, \omega). \tag{3.7}$$

The sum over the momenta is left unspecified for the time being. It depends on the choice of boundary conditions. In the limit of an infinite system, the sum gets replaced by an integral over all space in the standard way. In Fourier space, eq.(3.4) becomes local

$$J^{\mu}(q) = K^{\mu\nu}(q) A_{\nu}(q), \tag{3.8}$$

where $q = (\omega, \mathbf{q})$. Physical observables are now readily obtained. For instance, the DC electrical conductivity, by making the choice of a time-dependent vector gauge, $\mathbf{E} = -\partial_t \mathbf{A}(t)$, reads

$$\sigma_{ij} = -\lim_{\omega \to 0} \frac{K^{ij}(\mathbf{0}, \omega)}{\mathrm{i}\omega}. \tag{3.9}$$

3˙2. *Conservation laws and gauge invariance.* – Charge conservation is expressed by the continuity equation

$$\partial_t \rho + \nabla \cdot \mathbf{J} = 0, \tag{3.10}$$

while gauge invariance requires that the physics is unchanged by the replacement

$$A^{\mu}(x) \to A^{\mu}(x) - \partial^{\mu} f(x), \tag{3.11}$$

with f an arbitrary function and $\partial^{\mu} = (\partial_t, -\nabla)$. Equations (3.10,3.11) imply

$$q_{\mu} K^{\mu\nu} = 0, \tag{3.12a}$$

$$K^{\mu\nu} q_{\nu} = 0. \tag{3.12b}$$

More explicitly, one has the following relations connecting the various correlation functions:

$$\omega K^{00} = q^j K^{j0}, \tag{3.13a}$$

$$\omega K^{0i} = q^j K^{ji}, \tag{3.13b}$$

$$\omega K^{00} = q^j K^{0j}, \tag{3.13c}$$

$$\omega K^{i0} = q^j K^{ij}, \tag{3.13d}$$

---

(3) The plus sign in front of the diamagnetic term is due to the fact that by using a lower index for A_{μ} the space part has a minus sign.

from which $K^{0i} = K^{i0}$, $K^{ij} = K^{ji}$, and

$$\omega^2 K^{00} = q^i K^{ij} q^j. \tag{3.14}$$

The conductivity tensor may be decomposed into *longitudinal* and *transverse* components as

$$\sigma_{ij} = \frac{q^i q^j}{\mathbf{q}^2}\sigma_L + \left(\delta_{ij} - \frac{q^i q^j}{\mathbf{q}^2}\right)\sigma_T \tag{3.15}$$

so that eq.(3.9) reads

$$\sigma_L = \mathrm{i} \lim_{\omega\to 0} \lim_{|\mathbf{q}|\to 0} \frac{\omega}{\mathbf{q}^2} K^{00}(\mathbf{q},\omega). \tag{3.16}$$

The charge response to a static and homogeneous external potential, *e.g.* the compressibility, is given as

$$\frac{\partial n}{\partial \mu} = -\frac{1}{e^2} \lim_{|\mathbf{q}|\to 0} K^{00}(\mathbf{q}, 0). \tag{3.17}$$

To appreciate the physical meaning of eqs.(3.16,3.17), let us consider the *phenomenological* expression of the current for a good metal

$$\mathbf{J} = \sigma_L \mathbf{E} - D\nabla\rho \tag{3.18}$$

where D is the diffusion coefficient, which, under general statistical considerations, is related to σ_L by Einstein's relation

$$\sigma_L = e^2 \frac{\partial n}{\partial \mu} D. \tag{3.19}$$

Equation (3.18) may be used together with the continuity equation (3.10) to find an expression for the *density-density*, K^{00}, response function. By taking the divergence of eq.(3.18) and replacing it into eq.(3.10), one gets

$$(\partial_t - D\nabla^2)\rho = \sigma_L \nabla^2 \phi, \tag{3.20}$$

from which, after Fourier transforming, the density-density response function reads

$$K^{00} = -\sigma_L \frac{\mathbf{q}^2}{-\mathrm{i}\omega + D\mathbf{q}^2} = -e^2 \frac{\partial n}{\partial \mu} \frac{D\mathbf{q}^2}{-\mathrm{i}\omega + D\mathbf{q}^2}. \tag{3.21}$$

The above equation, of course, agrees with eq.(3.16) and gives the compressibility (3.17) as required by Einstein's relation. Notice that the latter, within the linear response, is derived from the eq.(3.14), connecting the density-density and current-current response functions. The task of a *microscopic* theory, as it will be shown in the following sections, is to derive the expression for the current instead of *phenomenologically* assuming eq.(3.18).

3˙3. *Response functions and Ward identities.* – We begin by introducing a vertex function

$$\Lambda^\mu(x,x',x'') =< T_t J^\mu(x)\psi(x')\psi^\dagger(x'') >, \tag{3.22}$$

where T_t is the time-ordering operator and the average is over a statistical ensemble. In this subsection, for the sake of simplicity, we confine ourselves to the zero-temperature limit with the average taken over the ground state. We also neglect spin indices for a little while to keep the notation as simple as possible. When the derivative $\partial/\partial_{x_\mu}$ acts on the right-hand side of eq.(3.22), one obtains two contributions. One is due to the derivative acting on J^μ and gives zero due to the continuity equation (3.10). A second contribution comes from the time-derivative of the T_t-product. As a result one gets the following Ward Identity:

$$\frac{\partial}{\partial x_\mu}\Lambda^\mu(x,x',x'') = \mathrm{i}e\ \delta(x-x'')G(x',x) - \mathrm{i}e\ \delta(x-x')G(x,x''), \tag{3.23}$$

where we have introduced the single-particle Green function

$$G(x,x') = -\mathrm{i} < T_t\psi(x)\psi^\dagger(x') > . \tag{3.24}$$

One may also consider Fourier transforms with respect to the relative coordinates $x-x''$ and $x'-x$ (The arguments of the two Green's functions in the right-hand side of eq.(3.23)). We define the Fourier transform of eq.(3.22) as

$$\Lambda^\mu(x,x',x'') = \int \mathrm{d}q\ \mathrm{d}p\ e^{\mathrm{i}(p-q/2)(x'-x)}\ e^{\mathrm{i}(p+q/2)(x-x'')}\ \Lambda^\mu(p,q) \tag{3.25}$$

in terms of which the Ward Identity becomes

$$q_\mu \Lambda^\mu(p,q) = e\ G(p-q/2) - e\ G(p+q/2). \tag{3.26}$$

In the above $p=(\epsilon,\mathbf{p})$ and in eq.(3.25)

$$\mathrm{d}p\ = \frac{\mathrm{d}\epsilon}{2\pi}\sum_{\mathbf{p}},$$

and similarly for q. The connection between the vertex function and response functions is obtained by introducing the truncated vertex Γ^μ defined as

$$\Lambda^\mu(p,q) = G(p+q/2)\Gamma^\mu(p,q)G(p-q/2). \tag{3.27}$$

In terms of Γ^μ the response functions read

$$K^{\mu\nu}(q) = -\mathrm{i}\int \mathrm{d}p\ \gamma^\mu(p,q)G(p+q/2)\Gamma^\nu(p,q)G(p-q/2), \tag{3.28}$$

where $\gamma^\mu = (e, e\,\mathbf{p}/m) \equiv (e, \gamma^i_{\mathbf{p}})$ is the *bare* vertex. As a check, the bare vertex is found by writing the Ward Identity in terms of Γ^μ

$$q_\mu \Gamma^\mu(p,q) = e\, G^{-1}(p+q/2) - e\, G^{-1}(p-q/2), \tag{3.29}$$

and using the *bare* Green's function expression

$$G(p) = \frac{1}{\epsilon - \xi_{\mathbf{p}} + \mathrm{i}\ sign\ (|\mathbf{p}| - p_F)}, \tag{3.30}$$

p_F being the Fermi momentum and $\xi_{\mathbf{p}} = \mathbf{p}^2/2m - \mu$.

We conclude this section by giving a few more consequences of the Ward identity (3.26). First, we notice that, while in the *static* limit, the density-density response function gives the compressibility (compare eq.(3.17)), in the *dynamic* limit we have

$$\lim_{\omega \to 0} K^{00}(\mathbf{0}, \omega) = 0. \tag{3.31}$$

The above result, which is a mathematical formulation of the particle number conservation, follows from eq.(3.26) after taking the $\mathbf{q}$-zero limit and upon integration over momentum $\mathbf{p}$ and the entire energy ϵ range.

Finally, by restricting the frequencies to the region $(\epsilon+\omega/2)(\epsilon-\omega/2) < 0$, and taking advantage of the Ward Identity in the zero-momentum limit, one gets for the density response function

$$\begin{aligned} K^{00}_{+-}(\mathbf{0},\omega) &= -\mathrm{i}e \int_{-\omega/2}^{\omega/2} \frac{\mathrm{d}\epsilon}{2\pi} \sum_{\mathbf{p}} \Lambda^0(\epsilon, \mathbf{p}; \omega, \mathbf{0}) \\ &= -\mathrm{i}e^2 \int_{-\omega/2}^{\omega/2} \frac{\mathrm{d}\epsilon}{2\pi} \sum_{\mathbf{p}} \frac{1}{\omega} \left(G^R(\mathbf{p}, \epsilon - \omega/2) - G^A(\mathbf{p}, \epsilon + \omega/2) \right) \\ &\approx_{\omega \to 0} \mathrm{i}e^2 \frac{1}{2\pi} \sum_{\mathbf{p}} \left(G^R(\mathbf{p}, 0) - G^A(\mathbf{p}, 0) \right), \end{aligned} \tag{3.32}$$

where we made use of the fact that the sign of the frequency determines whether the Green's function is analytical in the upper (retarded R) or in the lower (advanced A) half of the complex plane as a function of frequency. By recalling the expression for the single-particle density of states

$$N(\epsilon) = -\frac{1}{\pi} \sum_{\mathbf{p}} \mathcal{I}m\ G^R(\mathbf{p}, \epsilon),$$

one obtains an expression for the single-particle density of states at the Fermi energy

$$N(0) \equiv N = \lim_{\omega \to 0} \frac{1}{2e^2} K^{00}_{+-}(\mathbf{0}, \omega), \tag{3.33}$$

where the factor of 2 in the denominator is due to the spin degeneracy.

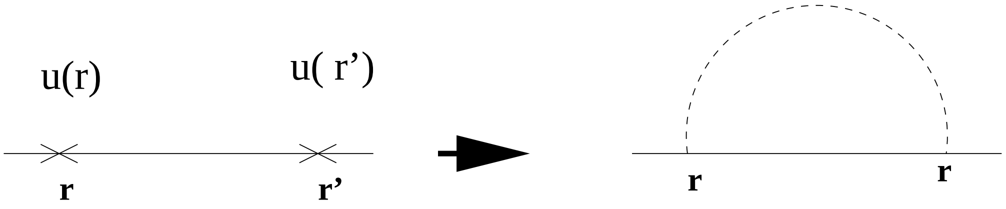

Fig. 6. – Self-energy in the Born approximation before and after averaging over the impurity distribution. The dashed line represents the average of two impurity insertions. When the internal Green's function line (solid line) is replaced with the dressed Green's function one obtains the self-consistent Born approximation.

4. – Non-interacting Disordered Electrons

4·1. *Self-consistent Born approximation.* – Quite generally, non-interacting electrons in the presence of disorder are described by the following Hamiltonian:

$$H = \int \mathrm{d}\mathbf{r}\ \psi^{\dagger}_{\sigma}(\mathbf{r}) \left[-\frac{\nabla^2}{2m} + u(\mathbf{r}) \right] \psi_{\sigma}(\mathbf{r}) \tag{4.1}$$

where $u(\mathbf{r})$ is taken as a *Gaussian* random variable defined by

$$\overline{u(\mathbf{r})} = 0, \quad \overline{u(\mathbf{r})u(\mathbf{r}')} = \overline{u^2}\delta(\mathbf{r}-\mathbf{r}') \equiv \frac{1}{2\pi N_0 \tau}\delta(\mathbf{r}-\mathbf{r}'). \tag{4.2}$$

In the above, N_0 is the *free* single-particle density of states per spin and τ is a parameter inversely proportional to the impurity concentration and whose physical meaning will be evident in a few moments. In the Born approximation[44] one has for the self-energy the expression (see fig.6)

$$\Sigma^1(\mathbf{r},t;\mathbf{r}',t') = \frac{\delta(\mathbf{r}-\mathbf{r}')}{2\pi N_0 \tau} G^0(\mathbf{r},t;\mathbf{r},t'). \tag{4.3}$$

The superscript 0 for G indicates that we are considering the unperturbed expression (3.30). In Fourier space, eq.(4.3) reads

$$\Sigma^1(\mathbf{p},\epsilon) = \frac{1}{2\pi N_0 \tau} \sum_{\mathbf{p}'} \frac{1}{\epsilon - \xi_{\mathbf{p}'} + \mathrm{i}\ sign\ (|\mathbf{p}'| - p_F)}. \tag{4.4}$$

For large values of $\mathbf{p}'$, the real part of the sum over $\mathbf{p}'$ diverges, but its value *does* not depend on the energy ϵ. This divergency is a consequence of the simple model taken for the scattering potential. A more realistic momentum-dependent scattering potential will generally cure the divergence and give rise to a finite contribution that may be absorbed into a redefinition of the chemical potential. The main contribution to the energy dependence of the sum comes from the values of $\mathbf{p}'$ close to the Fermi surface. By following the standard procedure we pass from momentum to energy integration

$$\sum_{\mathbf{p}} ... = N_0 \int_{-\mu}^{\infty} \mathrm{d}\xi_{\mathbf{p}} ... \approx N_0 \int_{-\infty}^{\infty} \mathrm{d}\xi_{\mathbf{p}} ... \tag{4.5}$$

where we have sent to minus infinity the lower limit of integration, since $\mu \approx E_F$ is the biggest energy scale in the problem. Then, by residue integration, we obtain

$$\Sigma^1(\mathbf{p}, \epsilon) = -\frac{\mathrm{i}}{2\tau} sign(\epsilon). \tag{4.6}$$

To proceed in the perturbative expansion one replaces the above result into the Green's function and computes Σ^2. At second order one has exactly the same expression as before except that the pole of the Green's function is now moved away from the real axis by the quantity $1/2\tau$. However, the residue integration does not depend on the distance of the pole from the real axis and one realizes that the right-hand side of eq.(4.6) is indeed a self-consistent solution which yields

$$G(\mathbf{p}, \epsilon) = \frac{1}{\epsilon - \xi_{\mathbf{p}} + \frac{\mathrm{i}}{2\tau}\ sign\ (\epsilon)}, \tag{4.7}$$

from which emerges the meaning of τ as the *elastic* quasiparticle relaxation time. We stress that the consistency of the above approximation for evaluating integrals over momentum is based on the fact that the distance from the real axis of the pole in the Green's function remains small compared to the Fermi energy, which corresponds to the condition

$$E_F \tau \gg 1 \tag{4.8}$$

and one finds the *effective* expansion parameter discussed previously. The *self-consistent* Born approximation effectively selects a subset of diagrams characterized by the absence of *crossing* of impurity average lines. This sequence of independent scattering events leads to a ladder resummation of diagrams for the vertex part, as it will be shown in the next subsection.

4$\dot{}$2. *Vertex part and diffuson ladder*. – This subsection has a twofold aim. On the one hand we show that the microscopic approach, at leading order in the parameter $1/E_F\tau$, reproduces the semiclassical theory of Drude-Boltzmann. On the other hand, we introduce a number of technical ingredients that will be used extensively in these lectures. In particular, we will perform the evaluation of both the density-density and current-current correlation function. We begin with the density-density response function. The expression to evaluate reads

$$K^{00}(\mathbf{q}, \omega) = -2\mathrm{i}e^2 \int_{-\infty}^{\infty} \frac{\mathrm{d}\epsilon}{2\pi} \sum_{\mathbf{p}} G\left(\mathbf{p}_+, \epsilon_+\right) \Gamma^0(\mathbf{p}, \epsilon; \mathbf{q}, \omega) G\left(\mathbf{p}_-, \epsilon_-\right) \tag{4.9}$$

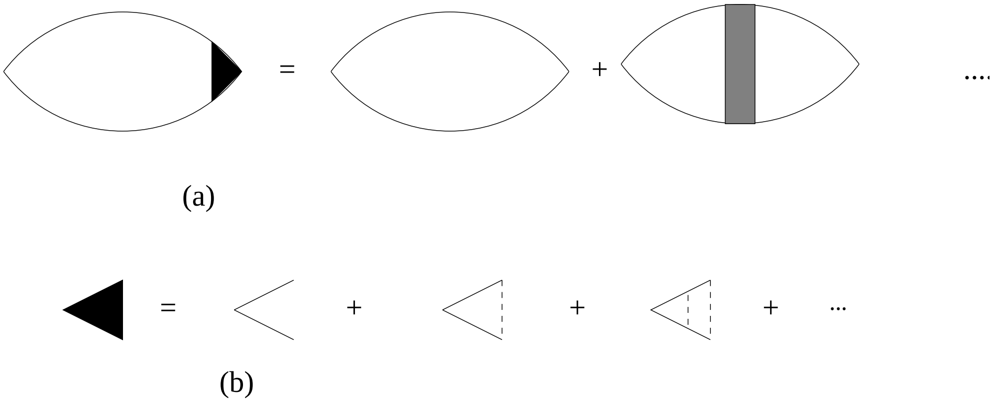

Fig. 7. – (a) Diagram for the correlation function. The black triangle indicates the vertex part. (b) The vertex part is obtained as an infinite resummation of non crossing impurity lines.

where $\mathbf{p}_{\pm} \equiv \mathbf{p} \pm \mathbf{q}/2$ and $\epsilon_{\pm} \equiv \epsilon \pm \omega/2$ and we have introduced a factor of two due to the spin. The truncated vertex Γ^0 is indicated by a black triangle in fig.7. The Green's functions appearing in the diagrams are those evaluated within the self-consistent Born approximation, as explained in the previous subsection. The evaluation of the vertex requires the evaluation of the series of ladder diagrams shown in fig.8. The series of ladder diagrams, to be called ladder from now on, may be evaluated by solving the integral equation

$$L_{\mathbf{p},\mathbf{p}',\epsilon}(\mathbf{q},\omega) = L^{(0)} + L^{(0)} \sum_{\mathbf{p}''} G\left(\mathbf{p}''_{+}, \epsilon_{+}\right) G\left(\mathbf{p}''_{-}, \epsilon_{-}\right) L_{\mathbf{p}'',\mathbf{p}',\epsilon}(\mathbf{q},\omega), \tag{4.10}$$

where $L^{(0)} = \frac{1}{2\pi N_0 \tau}$. The ladder generally depends on three momenta and two energies. However, as it will be shown in a few moments, the actual dependence is only on $\mathbf{q}$ and ω. This is the reason of the notation adopted. Later on we will drop the subscripts $\mathbf{p}$,$\mathbf{p}'$

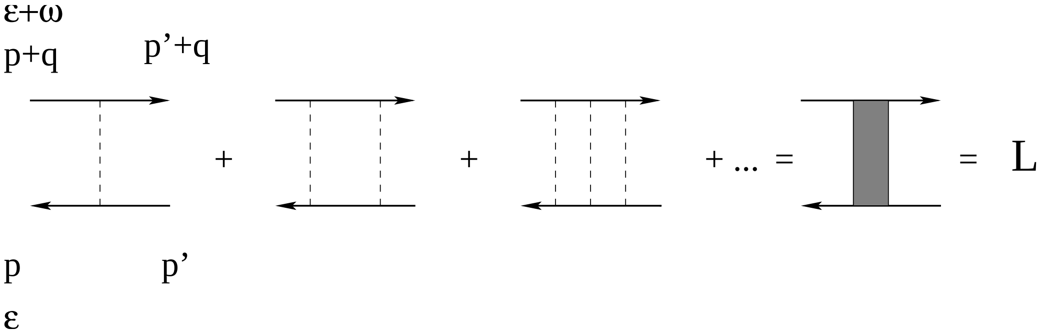

Fig. 8. – Ladder resummation.

and ϵ. The kernel of the integral equation (4.10) gives a non-vanishing contribution when the poles of the two Green's functions lie on opposite sides of the real axis. To see this, let us consider the term with two impurity lines in the ladder series. It reads

$$\Pi = \sum_{\mathbf{p}} G\left(\mathbf{p}_+, \epsilon_+\right) G\left(\mathbf{p}_-, \epsilon_-\right). \tag{4.11}$$

To evaluate the integral we go to the energy variable introduced in eq.(4.5). We have $\xi_{\mathbf{p}\pm\mathbf{q}/2} = \xi_{\mathbf{p}} \pm \mathbf{p}\cdot\mathbf{q}/2m + q^2/8m$. Since the integral is dominated by the contribution coming from the poles we set to p_F the absolute value of $\mathbf{p}$ in the scalar product with $\mathbf{q}$. The integral over the energy $\xi_{\mathbf{p}}$ may then be carried out by residue method as explained in the previous subsection. Also we notice that the condition of having poles on opposite sides of the real axis implies a restriction on the frequencies, i.e., $\epsilon + \omega/2 > 0$ and $\epsilon - \omega/2 < 0$. As a result we get

$$\Pi = \theta(\omega^2/4 - \epsilon^2) 2\pi N_0 \tau \int \frac{\mathrm{d}\Omega_{\hat{\mathbf{p}}}}{\Omega_{\hat{\mathbf{p}}}} \frac{1}{1 - \mathrm{i}\omega\tau + \mathrm{i}lq\cos(\theta)}, \tag{4.12}$$

where $\Omega_{\hat{\mathbf{p}}}$ is the solid angle and θ is the angle between $\mathbf{p}$ and $\mathbf{q}$. $l = v_F\tau$ represents the mean free path due to *elastic* scattering. Although the angular integral may be evaluated exactly, in the following we will be interested in the limits $\omega\tau \ll 1$ and $lq \ll 1$, which define the *diffusive* (4) transport regime. It is then convenient to expand for small frequency and momentum the right-hand side of eq.(4.12) and perform the angular integral. We get finally

$$\Pi = \theta(\omega^2/4 - \epsilon^2) 2\pi N_0 \tau \left(1 + \mathrm{i}\omega\tau - Dq^2\tau\right), \tag{4.13}$$

where the diffusion coefficient is given by $D = v_F l/d$, d being the dimensionality. As anticipated, the ladder does not depend on the momenta $\mathbf{p}$ and $\mathbf{p}'$. It depends on the difference of the incoming and outgoing momenta only and the integral equation becomes an algebraic one. The final solution reads

$$\begin{aligned} L(q,\omega) &= \frac{L^{(0)}}{1 - L^{(0)}\Pi} \\ &= \frac{1}{2\pi N_0 \tau^2} \frac{\theta(\omega^2/4 - \epsilon^2)}{-\mathrm{i}\omega + Dq^2}. \end{aligned} \tag{4.14}$$

This is the most important equation of this subsection. It shows how the diffusive pole one expects emerges from the repeated elastic scattering. In terms of the ladder the vertex reads

---

(4) This expansion is sufficient in the low temperature regime when $T\tau \ll 1$. At higher temperature with $T\tau \geq 1$ one must retain the full frequency and momentum dependence of Π. This defines the quasi-ballistic regime. A detailed discussion can be found in ref.[45].

$$\begin{aligned}\Gamma^0(\mathbf{p},\epsilon,\mathbf{q},\omega) &\equiv \gamma_0+\delta\Gamma^0\\ &= e\left(1+\sum_{\mathbf{p}'}G\left(\mathbf{p}'_+,\epsilon_+\right)G\left(\mathbf{p}'_-,\epsilon_-\right)L_{\mathbf{p}',\mathbf{p},\epsilon}(\mathbf{q},\omega)\right)\\ &= e(1+2\pi N_0\tau L(q,\omega)) = e\left(1+\frac{\theta(\omega^2/4-\epsilon^2)}{-\mathrm{i}\omega\tau+D\tau q^2}\right).\end{aligned}\tag{4.15}$$

One notices that in the zero-momentum limit the expression for Γ^0 may be obtained directly from the Ward Identity (3.29) and agrees with the above equation. With the vertex we may now complete the evaluation of the density-density response function. It is natural to split it in two parts corresponding to the two contributions in the vertex. The contribution, which does not contain the diffusive pole and does not have restrictions on the frequency range, reads

$$\begin{aligned}K^{00}_{++}+K^{00}_{--} &= -2\mathrm{i}e^2\int_{-\infty}^{\infty}\frac{\mathrm{d}\epsilon}{2\pi}\sum_{\mathbf{p}}G\left(\mathbf{p}_+,\epsilon_+\right)\ G\left(\mathbf{p}_-,\epsilon_-\right)\\ &\approx -2\mathrm{i}e^2\int_{-\infty}^{\infty}\frac{\mathrm{d}\epsilon}{2\pi}\sum_{\mathbf{p}}G\left(\mathbf{p},\epsilon\right)^2\\ &= -2\mathrm{i}e^2\frac{1}{2\pi}\sum_{\mathbf{p}}\left[G^R\left(\mathbf{p},0\right)-G^A\left(\mathbf{p},0\right)\right]\\ &= -2e^2N_0,\end{aligned}\tag{4.16}$$

where the superscripts $R(A)$ indicate the retarded and advanced Green's functions

$$G^{R(A)}(\mathbf{p},\epsilon)=\frac{1}{\epsilon-\xi_{\mathbf{p}}\pm\frac{\mathrm{i}}{2\tau}}.\tag{4.17}$$

In obtaining the above result, we have taken the *static* limit (frequency goes to zero first, and then momentum). Given the restriction in the frequencies for the second part in the vertex, one could naively think that in the small frequency and momentum limit, this contribution would be vanishingly small. This however depends on the order the two limits are performed. Due to the presence of the diffusive pole in the ladder, one obtains for the second *dynamic* contribution

$$\begin{aligned}K^{00}_{+-} &= -2\mathrm{i}e^2\int_{-\omega/2}^{\omega/2}\frac{\mathrm{d}\epsilon}{2\pi}\sum_{\mathbf{p}}G\left(\mathbf{p}_+,\epsilon_+\right)\ G\left(\mathbf{p}_-,\epsilon_-\right)\frac{1}{-\mathrm{i}\omega\tau+D\tau q^2}\\ &\approx -2e^2N_0\frac{\mathrm{i}\omega}{-\mathrm{i}\omega+Dq^2},\end{aligned}\tag{4.18}$$

where due to the diffusive pole one may set $\mathbf{q}=\mathbf{0}$ and $\omega=0$ in the Green's functions and perform the integral with residue methods. By combining together eqs.(4.16),(4.18) one

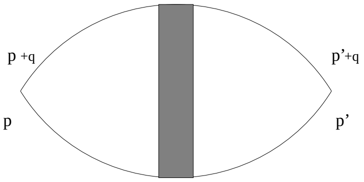

Fig. 9. – Diagram contributing to the leading correction to the current-current response function in the dynamical region. In the ladder flows the momentum $\mathbf{q}$.

obtains the total density-density response function at leading order in $E_F\tau$, in complete agreement with the result of eq.(3.21) based on the phenomenological expression of the current. We also note that, as expected, both the compressibility and the single-particle density of states are given by the Fermi gas expression N_0.

We now turn to the evaluation of the current-current response function. For the purpose of computing the electrical conductivity, this is not strictly necessary since the Ward identity (3.16) allows us to get σ from the density-density correlation function(3.21). We believe however that it is instructive to show how the calculation goes. The expression reads

$$R^{ij}(\mathbf{q},\omega) = -2\mathrm{i}\int_{-\infty}^{\infty}\frac{\mathrm{d}\epsilon}{2\pi}\sum_{\mathbf{p}}\gamma^i_{\mathbf{p}}\, G\left(\mathbf{p}_+,\epsilon_+\right)\ \Gamma^j(\mathbf{p},\epsilon;\mathbf{q},\omega)G\left(\mathbf{p}_-,\epsilon_-\right). \tag{4.19}$$

The first observation concerns the vectorial nature of the vertex. By going through the same steps as for the density-density response function, the integral contains a vertex γ^i which makes the integral vanish upon angular integration. As a result the current vertex Γ^i remains unrenormalized. This can be illustrated with the help of fig.9. Since the region of small $\mathbf{q}$ gives the dominant contribution to the integral, one can set $\mathbf{q}=0$ in the Green's functions. As a consequence the two $\mathbf{p}$ and $\mathbf{p'}$ integrations in fig.9 decouple from one another and vanish for the presence of the vectorial vertex. The diagram of fig.9, which is the diffusive polar contribution to the density-density response function, does not contribute to the current-current response functions. However, the evaluation of the remaining part of the response function is more delicate as compared to the case of the density-density response. The reason is due to the fact that in performing the small-frequency limit we need to divide by ω according to eq.(3.9). One then cannot simply take the zero-frequency limit by setting $\omega=0$ before performing the integral, but it is necessary to make an expansion in powers of ω. After a few manipulations we get

$$\begin{aligned} R^{ij}(\mathbf{0},\omega) &= -2\mathrm{i}\sum_{\mathbf{p}}\gamma^i_{\mathbf{p}}\gamma^j_{\mathbf{p}}\left[\int_{-\infty}^{\infty}\frac{\mathrm{d}\epsilon}{2\pi}\,G^2\left(\mathbf{p},\epsilon\right)\right.\\ &\quad\left.-\,\frac{\omega}{2}\frac{1}{2\pi}\left(G^R\left(\mathbf{p},0\right)-G^A\left(\mathbf{p},0\right)\right)^2\right]\\ &= -\frac{e^2n_0}{m}-\mathrm{i}\omega\frac{e^2n_0\tau}{m}. \end{aligned} \tag{4.20}$$

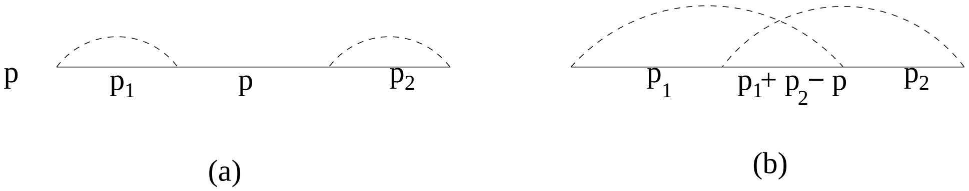

Fig. 10. – (a) A diagram without crossing. (b) A diagram with crossing.

The first term, by recalling eq.(3.5), cancels exactly with the diamagnetic contribution. The remaining term, by using eq.(3.9), gives the Drude formula for the electrical conductivity.

To summarize, in this subsection we have evaluated the linear response of a disordered Fermi gas to an electromagnetic external field to the leading order in the parameter $1/(E_F\tau)$. This parameter is also the natural dimensionless coupling of the present microscopic problem which deals with the Fermi gas (characterized by the unique energy scale E_F) in the presence of disorder which introduces the (other) energy scale $N_0\overline{u^2} \sim \tau^{-1}$. At this order, one recovers the results of the semiclassical approach of Drude-Boltzmann. However, we have developed a formalism within which next-to-leading corrections may be investigated systematically. This will be the subject of the next subsections as far as non-interacting electrons are concerned. Interaction effects will be considered in the next section.

4·3. *Weak localization.* – We have stated that the leading approximation in an expansion in the parameter $1/(E_F\tau)$ is obtained by considering diagrams without crossing. We begin our discussion of the next-to-leading corrections, by showing how crossing of impurity lines increases the order of a diagram. A simple example is shown in fig.(10), where both diagrams are of the same order in the impurity lines. Let us estimate these diagrams. By recalling the self-energy expression (4.6) and the Green's function (4.7), the diagram (a) reads

$$\begin{aligned}(a) \quad &= \quad \left(\frac{\mathrm{i}\,sign\epsilon}{2\tau}\right)^2 G(\mathbf{p},\epsilon)\\ &\approx_{\epsilon,\xi_{\mathbf{p}}\to 0} \frac{1}{\tau^2}\tau = \frac{1}{\tau}\end{aligned}$$

while the diagram (b) yields

$$\begin{aligned}(b) &= \left(\frac{1}{2\pi N_0\tau}\right)^2 \sum_{\mathbf{p}_1,\mathbf{p}_2} G(\mathbf{p}_1,\epsilon)G(\mathbf{p}_2,\epsilon)G(\mathbf{p}_1+\mathbf{p}_2-\mathbf{p},\epsilon)\\ &= \frac{1}{(2\pi N_0\tau)^2}\sum_{\mathbf{p}_1,\mathbf{p}_2}\frac{1}{(\epsilon-\xi_1+\mathrm{i}\delta_\epsilon)(\epsilon-\xi_2+\mathrm{i}\delta_\epsilon)(\epsilon-\xi_1-\xi_2-\xi+2\mu-\frac{\mathbf{p}_1\cdot\mathbf{p}_2}{m}+\frac{\mathbf{p}\cdot(\mathbf{p}_1+\mathbf{p}_2)}{m}+\mathrm{i}\delta_\epsilon)}\end{aligned}$$

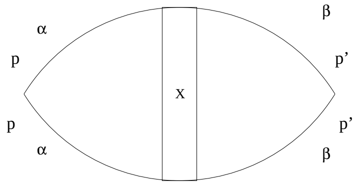

Fig. 11. – Diagram contributing to the next-to-leading correction to the current-current response function. The Greek indices label the spin of the Green's function line. Notice that at the density vertex the spin is conserved.

$$\approx \frac{1}{\tau^2\mu},$$

where for brevity $\delta_\epsilon = sign(\epsilon)/2\tau$ and $\xi_1 \equiv \xi_{\mathbf{p}_1}$ and similarly for $\mathbf{p}_2$ and $\mathbf{p}$. The above result is obtained by noting that, due to the poles of the first two Green functions, we can set $\xi_1 = \xi_2 = 0$ in the third one. Clearly (b) is smaller of (a) by a factor $1/\mu\tau$. In general to take diagrams with crossing of impurity lines becomes a very complicated problem. There is, however, a subset of diagrams, the so-called maximally crossed diagrams, which can be evaluated. The contribution of the series of these diagrams to the current-current response function is shown in fig.11. The corresponding expression reads

$$\delta K^{ij}(\mathbf{0},\omega) = -2\mathrm{i}\sum_{\mathbf{p},\mathbf{p}'}\gamma^i_{\mathbf{p}}\gamma^j_{\mathbf{p}'}\int_{-\infty}^{\infty}\frac{\mathrm{d}\epsilon}{2\pi}\,G\left(\mathbf{p},\epsilon_+\right)\,G\left(\mathbf{p},\epsilon_-\right)\,L_c(\mathbf{p},\mathbf{p}',\omega)G\left(\mathbf{p}',\epsilon_+\right)\,G\left(\mathbf{p}',\epsilon_-\right), \tag{4.21}$$

where with $L_c(\mathbf{p},\mathbf{p}',\omega)$ we have indicated the series of the maximally crossed diagrams. As for the leading order calculation, the first step requires the evaluation of the series giving $L_c(\mathbf{p},\mathbf{p}',\omega)$. This can be done by observing that the series of the maximally crossed diagrams, from now on called crossed ladder, L_c, may be expressed in terms of the direct ladder by reversing one of the electron Green's function lines, as shown in fig.12. This corresponds to

$$L_c(\mathbf{p},\mathbf{p}',\omega) = L(\mathbf{p}+\mathbf{p}',\omega) - \frac{1}{2\pi N_0\tau}. \tag{4.22}$$

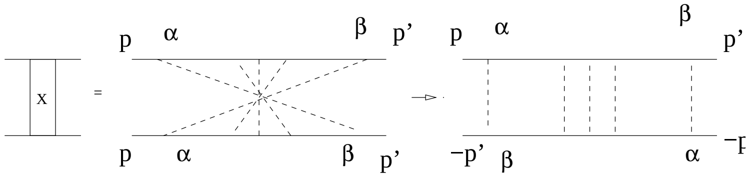

Fig. 12. – Crossed ladder expressed in term of the direct ladder. Notice that, upon the reversal of the bottom Green's function line, the in and out combination of spin indices are $\alpha\beta$ and $\beta\alpha$, respectively.

Hence, the crossed ladder has a diffusive form with respect to the combination $\mathbf{p}+\mathbf{p}'$ since one of the two Green's function lines has been reversed. This means that the dominant contribution comes from the region $\mathbf{p}\sim-\mathbf{p}'$ and the integration over the two vector vertices is no longer decoupled as in the leading order case with the direct ladder. The direct ladder studied in the previous subsection describes the propagation of a particle-hole pair. The crossed ladder, when one of the lines is reversed, describes the propagation of a particle-particle pair and the diffusive pole is with respect to the total incoming momentum of the pair. This is reminiscent of the interaction scattering channel relevant for superconductivity and for this reason the crossed ladder is called the cooperon ladder. The direct ladder, on the other hand, is, in the technical jargon, called the diffuson. A key point to keep in mind about the difference between the diffuson and the cooperon is the total electric charge of the pair. While for the diffuson this is zero, it is twice the electron charge for the cooperon. As a consequence, in the diffusive regime, the cooperon is affected by the presence of a magnetic field, while the diffuson is not touched. We will see how a magnetic field affects the cooperon in the next subsection. We are now ready to complete our derivation of the correction to the current response. By performing the integrals (see Appendix A) in the standard way, eq.(4.21) becomes

$$\begin{aligned}\delta K^{ij} &= -2\mathrm{i}\int_{-\omega/2}^{\omega/2}\frac{\mathrm{d}\epsilon}{2\pi}\sum_{\mathbf{p},\mathbf{p}'}\gamma^i_{\mathbf{p}}\gamma^j_{\mathbf{p}'}G^R(\mathbf{p},\epsilon)\;G^A(\mathbf{p},\epsilon)\,G^R(\mathbf{p}',\epsilon)\,G^A(\mathbf{p}',\epsilon)\\ &\quad\frac{1}{2\pi N_0\tau^2}\frac{1}{-\mathrm{i}\omega+D(\mathbf{p}+\mathbf{p}')^2}\\ &= -2\mathrm{i}\int_{-\omega/2}^{\omega/2}\frac{\mathrm{d}\epsilon}{2\pi}\sum_{\mathbf{p}}\sum_{\mathbf{Q}}\gamma^i_{\mathbf{p}}\gamma^j_{\mathbf{Q}-\mathbf{p}}G^R(\mathbf{p},\epsilon)\;G^A(\mathbf{p},\epsilon)\,G^R(\mathbf{Q}-\mathbf{p},\epsilon)\,G^A(\mathbf{Q}-\mathbf{p},\epsilon)\\ &\quad\frac{1}{2\pi N_0\tau^2}\frac{1}{-\mathrm{i}\omega+D\mathbf{Q}^2}\\ &= d\mathrm{i}\;\omega\;\frac{e^2}{\pi}\sum_{\mathbf{Q}}\frac{1}{-\mathrm{i}\omega/D+\mathbf{Q}^2}\end{aligned}$$

from which and from eq.(3.9), at $d=2$, we get the correction to the conductivity

$$\delta\sigma=-\frac{e^2}{\pi^2\hbar}\ln\left(\frac{L}{l}\right)=-\sigma_0 2t\ln\left(\frac{L}{l}\right),\tag{4.23}$$

where we have resumed the physical units. The above equation represents the *weak-localization* correction[46] and $t=(4\pi^2N_0D\hbar)^{-1}=(2\pi E_F\tau/\hbar)^{-1}$ is the effective small expansion parameter in the metallic regime. To make connection with the phenomenological scaling theory, we note that the parameter t coincides with the inverse conductance in units of G_0 divided by 2π, $t=1/(2\pi g)$. The logarithmic divergence has been cutoff at large $\mathbf{Q}$ by the inverse mean free path, *i.e.* the distance beyond which diffusive motion starts to set in. The small $\mathbf{Q}$ cutoff is instead provided by the inverse of some length scale, L. In the zero frequency and zero temperature limit, this scale is given by the system size. At finite temperature, inelastic processes provide a so called dephasing length L_ϕ.

As discussed in the first section, the physical origin of the weak-localization correction is due to quantum interference. We are now in a position to appreciate the exact meaning of this statement. In a Feynman diagram a Green's function line describes the amplitude for going from one point to another. In the response functions, the two Green's function lines represent the operation of taking the product of one amplitude with its complex conjugate. Each amplitude is a sum over all possible paths so that in the product there will appear interference terms. The leading approximation, by restricting to ladder diagrams, makes an *effective* selection of paths. When we average over the impurity configurations, by connecting two impurity insertions by a dashed line, this corresponds to the fact that both the upper and lower Green's function lines are going through the same scattering center, *i.e.*, one is considering the product of the amplitude of a given path with its complex conjugate. Hence, in the leading approximation there is no interference. When considering, on the other hand, the maximally crossed diagrams, one observes that the upper Green's function line goes through a sequence of scattering events which is exactly the opposite of the one followed by the lower line. This represents the interference between trajectories that are one the time reversed of the other. One also notices that these trajectories are made by closed loops and always come in pairs, due to the fact the loop may be gone around clock- or anticlockwise.

So far we have established that the electrical conductivity acquires a logarithmic correction at order $1/E_F\tau$. The correction has a negative sign and signals a slowing-down of the electron diffusion. It is then legitimate to ask what this implies for the full momentum and frequency dependence of the density response function. To this end, we now consider the corresponding corrections with the bare density vertex $\gamma_0 = e$. In the presence of the scalar vertex, as we have seen in subsec. 4.2 already for the Drude approximation, the direct ladder contributes to the density response function to obtain the diffusive form (3.21). At the order t we are now considering, many more diagrams have to be taken into account. Most of them cancel each other [43] and we are left with those shown in fig.13. The expression for the first diagram reads

$$\delta K^{00}_{+-} = -\frac{2\mathrm{i}\;\omega}{2\pi}\sum_{\mathbf{p},\mathbf{p}'}\delta\Gamma^0(\mathbf{q},\omega)G^R\left(\mathbf{p}_+\right)\;G^A\left(\mathbf{p}_-\right)\;L_c(\mathbf{p},\mathbf{p}',\omega)G^R\left(\mathbf{p}'_+\right)G^A\left(\mathbf{p}'_-\right)\delta\Gamma^0(\mathbf{q},\omega). \tag{4.24}$$

In eq.(4.24) we have already performed the sum over the frequency ϵ, which gives rise to the factor ω in front. In the Green's functions, consistently with the approximations used up to now, we have set the frequency to zero and only the momentum argument is explicitly shown. The two vertex corrections $\delta\Gamma^0$ at the extreme left and extreme right describes the direct ladders appearing in the diagram and are given by eq.(4.15). To evaluate the integrals over the momenta $\mathbf{p}$ and $\mathbf{p}'$, we note that the cooperon ladder gives a big contribution to the integral when $\mathbf{p}+\mathbf{p}'$ is small. It is then convenient to introduce the variable $\mathbf{Q} = \mathbf{p}+\mathbf{p}'$ and set $\mathbf{Q} = 0$ everywhere except that in the cooperon

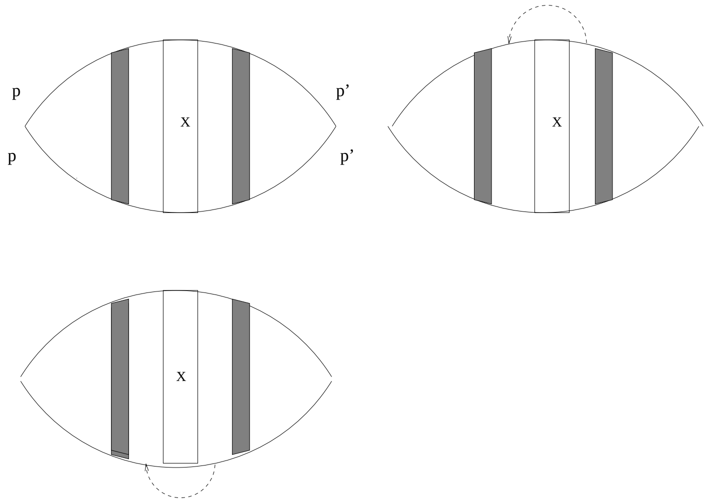

Fig. 13. – Diagram contributing to the next-to-leading correction to the density-density response function.

ladder. We are then left with an integral over the cooperon ladder and a second over a product of four Green's functions. However, this is not yet the full story. It turns out that there exist further diagrams (the second and the third) that may be obtained by simply *decorating* the first diagram of fig.13 with an extra impurity line. Such a decoration only adds two Green's functions and an extra summation over a fast momentum. To proceed we have then to integrate the Green's functions in the diagrams of fig.13 according to the expression

$$
\begin{aligned}
I_H = & \sum_{\mathbf{p}} G^R(\mathbf{p}_+)G^A(-\mathbf{p}_+)G^R(-\mathbf{p}_-)G^A(\mathbf{p}_-) \\
& + \frac{1}{2\pi N_0 \tau} \sum_{\mathbf{p}} G^R(\mathbf{p}_+)G^R(-\mathbf{p}_-)G^A(\mathbf{p}_-) \sum_{\mathbf{p}'} G^R(\mathbf{p'}_+)G^A(-\mathbf{p'}_+)G^R(-\mathbf{p'}_-) \\
& + \frac{1}{2\pi N_0 \tau} \sum_{\mathbf{p}} G^R(\mathbf{p}_+)G^A(-\mathbf{p}_+)G^A(\mathbf{p}_-) \sum_{\mathbf{p}'} G^A(-\mathbf{p'}_+)G^A(\mathbf{p'}_-)G^R(-\mathbf{p'}_-).
\end{aligned}
\tag{4.25}
$$

Notice the factor $\frac{1}{2\pi N_0 \tau}$ for the extra impurity line. Since we are interested in the small-momentum limit, we make an expansion in powers of $\mathbf{q}$. After a straightforward, but lengthy calculation, one gets

$$
I_H = 4\pi\tau^4 N_0 D\mathbf{q}^2. \tag{4.26}
$$

Finally, from eq.(4.15) and the expression (4.22) for the crossed ladder, we get as a correction to first order in t to eq.(4.18) for K^{00}_{+-}

$$\delta K^{00}_{+-} = -\frac{2\mathrm{i}\,\omega D\mathbf{q}^2}{(D\mathbf{q}^2-\mathrm{i}\omega)^2}\frac{e^2}{\pi}\sum_{\mathbf{Q}}\frac{1}{D\mathbf{Q}^2-\mathrm{i}\omega} \equiv +\frac{2e^2\mathrm{i}\,\omega N_0\mathbf{q}^2}{(D\mathbf{q}^2-\mathrm{i}\omega)^2}\delta D, \tag{4.27}$$

where

$$\delta D = \frac{\delta\sigma}{2e^2N_0} = -\frac{D}{\pi N_0}\sum_{\mathbf{Q}}\frac{1}{D\mathbf{Q}^2-\mathrm{i}\omega}$$

agrees with the expression for $\delta\sigma$ found in eq.(4.23) derived from the current-current response function. The above equation shows that the correction to K^{00}, made of many different contributions, can at the end be absorbed into a renormalization of the diffusion coefficient $D_R = D + \delta D$. Hence we conclude that at this order eq.(4.18) changes into

$$K^{00}_{+-} = -2e^2N_0\frac{\mathrm{i}\omega}{-\mathrm{i}\omega + D_R\mathbf{q}^2} \tag{4.28}$$

and by virtue of eq.(3.17) and eq.(3.33) the compressibility and the density of states are not renormalized. Only one renormalization ($D \rightarrow D_R$) is required in this case. The one-parameter scaling theory follows. Given the expression (4.23) for $\delta\sigma$, the group equation for the conductance g has an expansion in t of its β-function (eq.(2.29)) with the coefficient $a = 1/\pi$. The critical index for the conductivity, at order ϵ in $d = 3$, is $\mu = 1$. The frequency cuts off the singularity in the diffusion ladder and acts in this transition as an external field in ordinary transitions. Its scaling index x_ω has the same value as the dimension of the D_Rq^2, i.e., $x_\omega = \epsilon + 2 = d$.

4·4. *Effect of a magnetic field.* – As we have pointed out in sec.2.3, the magnetic field will cut off the weak-localization corrections. To see this explictly, it is useful to switch to a space and time representation of the cooperon ladder, as shown in fig.14. The cooperon describes the propagation of a pair of electrons that have coiciding space coordinates (within the spatial resolution given by the mean free path l). t, t' and η, η' are center-of-mass and relative times of the electron pair. For instance, an incoming pair has a temporal evolution factor

$$e^{-\mathrm{i}(\epsilon+\omega/2)(t'+\eta'/2)}e^{-\mathrm{i}(\epsilon-\omega/2)(t'-\eta'/2)} = e^{-2\mathrm{i}\epsilon t'}e^{-\mathrm{i}\omega\eta'/2}. \tag{4.29}$$

In this representation the cooperon reads

$$L_c^{\eta,\eta'}(\mathbf{r},\mathbf{r}') = \frac{\theta(\eta-\eta')}{2\pi N_0\tau^2}\frac{e^{-|\mathbf{r}-\mathbf{r}'|^2/D(\eta-\eta')}}{(2\pi D(\eta-\eta'))^{d/2}}, \tag{4.30}$$

and obeys the diffusion equation

$$\left(2\frac{\partial}{\partial\eta} - D\nabla^2_{\mathbf{r}}\right)L_c^{\eta,\eta'}(\mathbf{r},\mathbf{r}') = \frac{1}{2\pi N_0\tau^2}\delta(\eta-\eta')\delta(\mathbf{r}-\mathbf{r}'). \tag{4.31}$$

We note that the formula for the weak-localization correction of eq.(4.23) involves the Fourier transform with respect to time of the cooperon at coinciding space points. In terms of $L_c^{\eta,\eta'}(\mathbf{r},\mathbf{r}')$, the weak-localization correction eq.(4.23), in $d=2$, is recovered as

$$\delta\sigma = -e^2 4N_0 D\tau^2 \int_\tau^{\tau_\phi} \mathrm{d}\eta L_c^{\eta,-\eta}(\mathbf{r},\mathbf{r}) = -\frac{e^2}{\pi^2\hbar}\ln\frac{L_\phi}{l}. \tag{4.32}$$

The space and time representation makes more transparent the physical origin of the weak localization correction. The cooperon propagator $L_c^{\eta,-\eta}(\mathbf{r},\mathbf{r})$ represents the propagation of a pair of electrons going around the same closed trajectory in opposite directions, or one electron going through the time reversed trajectory of the other electron. The time nedeed to go around the loop is 2η and one has to integrate over all possible values of η between τ and τ_ϕ. The lower limit, τ, sets the time over which diffusive behavior develops. The upper limit, τ_ϕ, sets the time over which phase coherence between the two electrons going around the loop is maintained. For both times, we switch to the corresponding lengths via the diffusion constant.

We are now ready to consider the effect of an external magnetic field. It enters the diffusion equation via the minimal substitution as

$$\nabla \to \nabla - 2ie\mathbf{A}(\mathbf{r}), \tag{4.33}$$

which is to be expected for the minimal substitution of the two electrons described by the cooperon. In fact, as the established name cooperon may suggest, this is completely analogous to the minimal substitution that it is usually made when considering the Landau-Ginzburg equations for superconductivity. In the absence of the external magnetic field, the diffusion equation is solved via the knowledge of the eigenvalues of the laplacian operator exactly as for the Schrodinger equation at imaginary time. The analogy is made precise by saying that one may define particle-like parameters as a mass $m^* = 1/(2D)$ and a charge $e^* = 2e$. A magnetic field will modify this mass and act as a cutoff for the singularity in σ. In the presence of a uniform external magnetic field, the diffusion equation may be solved in terms of Landau levels. More precisely, in two dimensions for a magnetic field perpendicular to the plane, the cooperon at coinciding space points reads

$$L_c^{\eta,\eta'}(\mathbf{r},\mathbf{r}) = \frac{\theta(\eta-\eta')}{2\pi N_0\tau^2} g_s \sum_{n=0}^{\infty} e^{-E_n(\eta-\eta')/2} = \frac{\theta(\eta-\eta')}{2\pi N_0\tau^2} g_s \frac{e^{-\omega_c(\eta-\eta')/4}}{1-e^{-\omega_c(\eta-\eta')/2}}, \tag{4.34}$$

where $g_s = e^* B/(2\pi)$, $E_n = \omega_c(n+1/2)$, and $\omega_c = 2e^* DB$ are the degeneracy and energy of the effective Landau level, and the ciclotron frequency, respectively. By inserting the eq.(4.34) into the expression for the weak-localization correction of eq.(4.32) one gets

$$\delta\sigma(B) = -e^2 D\frac{g_s}{\pi}\int_\tau^{\tau_\phi} \mathrm{d}\eta\, \frac{1}{\sinh(\omega_c\eta/2)} = -\frac{e^2}{2\pi^2\hbar}\ln\left[\frac{\tanh(\omega_c\tau_\phi/4)}{\tanh(\omega_c\tau/4)}\right]. \tag{4.35}$$

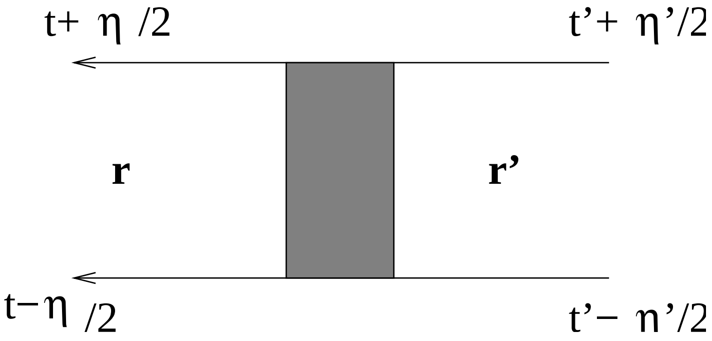

Fig. 14. – The cooperon ladder in time and space representation. Notice that both particles in the incoming (outgoing) pair have the same (center-of-mass) coordinate $\mathbf{r}'$ ($\mathbf{r}$). The lack of explicit dependence on the relative coordinate corresponds to the fact the ladder resummation does not depend on the fast momentum.

In the metallic regime, where $\tau \ll \tau_\phi$, at low magnetic field ($\omega_c\tau_\phi \ll 1$), the above correction reads

$$\delta\sigma(B) = -\frac{e^2}{2\pi^2\hbar}\left[\ln\left(\frac{\tau_\phi}{\tau}\right) - \frac{4}{3}\left(\frac{\Phi(B)}{\Phi_0}\right)^2\right], \tag{4.36}$$

where $\Phi_0 = hc/2e$ and $\Phi(B) = \pi L_\phi^2 B$ is the magnetic flux through a circle with radius the dephasing length. The effect of the magnetic field is felt for fields such that $\Phi(B)$ is of the order of the flux quantum Φ_0. Then it suppresses the weak localization correction and gives rise to a negative magnetoresistance. Experimentally, by measuring the magnetoconductance one may obtain the value of the dephasing time at a given temperature, $\tau_\phi(T)$.

In the opposite limit, such that $\omega_c\tau_\phi \gg 1$ (but $\omega_c\tau \ll 1$), eq.(4.35) reads

$$\delta\sigma(B) = \frac{e^2}{2\pi^2\hbar}\ln(\omega_c\tau), \tag{4.37}$$

which is no longer singular. The crossover between the two regimes occurs when the infrared cut off τ_ϕ^{-1} is replaced by ω_c. This condition amounts to $\Phi(B) \sim \Phi_0$, as was already stressed in subsec.2.3.

As far as the metal-insulator transition is concerned, the suppression of the weak localization correction corresponds to the vanishing of the coefficient a of the perturbative expansion of the β-function (cf. eq.(2.29)). Then, corrections arise when a crossing of two direct ladders is considered in current-current response function and appear at the second order in the expansion in power of $t \sim 1/g$. This, as mentioned at the end of subsection **2**˙3, implies a change of the critical conductivity exponent from $\mu = 1$ to $\mu = 1/2$. This is contrast with several experiments, as discussed at the end of this section.

4˙5. *Spin effects.* – The weak-localization correction is also affected by the presence of magnetic impurities. These latter make the cooperon propagator massive. In the presence of spin-dependent scattering, it is useful to decompose the ladder into singlet and triplet components with respect to the total spin for the incoming pair. The latter is a particle-hole and particle-particle pair for the diffuson and cooperon, respectively. In Appendix B, we give the details on how to derive the expression for the ladder in the presence of spin-flip scattering by magnetic impurities. The final result, in the limit when the spin-flip scattering time is much larger than the elastic scattering time, $\tau_s \gg \tau$, reads

$$L^S = \frac{1}{2\pi N_0 \tau^2} \frac{1}{Dq^2 - \mathrm{i}\omega}, \tag{4.38}$$

$$L^T = \frac{1}{2\pi N_0 \tau^2} \frac{1}{Dq^2 - \mathrm{i}\omega + \frac{4}{3\tau_s}}, \tag{4.39}$$

$$L_c^S = \frac{1}{2\pi N_0 \tau^2} \frac{1}{Dq^2 - \mathrm{i}\omega + \frac{2}{\tau_s}}, \tag{4.40}$$

$$L_c^T = \frac{1}{2\pi N_0 \tau^2} \frac{1}{Dq^2 - \mathrm{i}\omega + \frac{2}{3\tau_s}}. \tag{4.41}$$

One sees that only the singlet channel of the diffuson remains massless. While it is obvious that both triplet channels become massive, magnetic impurities as well as magnetic field break the time reversal symmetry and introduce a mass in the cooperon singlet as well. The a-coefficient of the β-function expansion is again vanishing and the singlet channel diffuson gives rise to corrections to second order in $t \sim 1/g$, yielding the value $\mu = 1/2$. Comparison with available experiments is postponed at the end of the section.

Spin-orbit scattering has the global effect of reversing the sign of the quantum interference contribution to the conductivity. In Appendix C we derive for both the diffuson and cooperon ladders the expression

$$L^S = \frac{1}{2\pi N_0 \tau^2} \frac{1}{Dq^2 - \mathrm{i}\omega}, \tag{4.42}$$

$$L^T = \frac{1}{2\pi N_0 \tau^2} \frac{1}{Dq^2 - \mathrm{i}\omega + \frac{d+1}{d\tau_{so}}}, \tag{4.43}$$

$$L_c^S = \frac{1}{2\pi N_0 \tau^2} \frac{1}{Dq^2 - \mathrm{i}\omega}, \tag{4.44}$$

$$L_c^T = \frac{1}{2\pi N_0 \tau^2} \frac{1}{Dq^2 - \mathrm{i}\omega + \frac{d+1}{d\tau_{so}}}. \tag{4.45}$$

We see that in this case the cooperon singlet remains massless in contrast to the magnetic impurities case. In the non magnetic impurity case the weak localization correction to the conductivity comes from both the cooperon singlet and triplet channels. As is shown in Appendix C, the singlet contribution is antilocalizing and amounts to 1/3 of the localizing triplet contribution. The latter being now suppressed, we are left with the singlet antilocalizing interference contribution. In terms of the β-function expansion, this means that the coefficient a changes sign. Also in this case, the comparison with the experiments is postponed to the next subsection.

In all the cases discussed above, no corrections arise to the thermodynamic quantities like the single-particle density of states, the specific heat, and the spin susceptibility.

4˙6. *A review of the experimental situation.* – It is now time to compare the theoretical predictions obtained from the microscopic approach with the experiments. As we will see, there are a number of facts that suggest that a proper description of the metal-insulator transition cannot be obtained without taking into account the effects of the electron-electron interaction. 1) In semiconductor-metal alloys, as we have already pointed out, the metal-insulator transition is observed with a conductivity critical exponent $\mu = 1$. This is in agreement with the non-interacting scaling theory. On the other hand, tunneling measurements reveal that the density of states has strong anomalies. For instance, in [23], the single particle density of states of $Ge_{1-x}Au_x$ is measured for different values of the Au concentration above and below the critical concentration for the metal-insulator transition. On the metallic side, the density of states shows a dip at the Fermi energy, which in the insulating regime, at lower Au concentrations, develops in a gap. In the case of the Nb_xSi_{1-x} alloy, the value of the density of states, as obtained from tunneling measurements, is plotted as a function of the Nb concentration, and it is seen scaling to zero linearly by approaching the critical concentration for the metal-insulator transition[20]. 2) The presence of magnetic impurities, in the non-interacting theory, should lead to a value $\mu = 1/2$. However, in metal films of $Cu : Mn$, one finds experimentally $\mu = 1$[47]. 3) In the amorphous alloy $SiAu$, it has been observed[48] $\mu = 1$ both in the absence and presence of a magnetic field of 5 Tesla. This systems has a strong spin-orbit coupling which, within the single-particle scheme, should switch from an antilocalizing term in the absence of the magnetic field, to a transition with $\mu = 1/2$ in the presence of the field. 4) Similarly, a value $\mu = 1$, both with and without a magnetic field, has also been observed in $Al_{0.3}Ga_{0.7}As : Si$ with a fine tuning of the electron concentration close to the metal-insulator transition, by using the photoconductivity effect[49, 50]. Also in this system, it is estimated that spin-orbit scattering is relevant. 5) The experiments in uncompensated doped semiconductors are even more puzzling. First, as we mentioned in the introduction, there is the problem of the experimental determination of the value of the critical conductivity exponent in $Si : P$, whose value $\mu = 1/2$[13, 51, 12] has been questioned[14]. In another $n - type$ system, e.g., $Si : As$ [52], also a value $\mu = 1/2$ has been observed, whereas a close value of $\mu = 0.65$ has been reported for a p-type system as $Si : B$[53], where the spin-orbit scattering is expected to be strong. The situation is further complicated by the experimental observation that the introduction of a magnetic field changes the value of the conductivity exponent to $\mu = 1$[54] as for the alloys. Besides the interpretation of the issues raised by the transport measurements, the experiments also show that there is a strong enhancement at low temperature of the electronic specific heat[25] and the spin susceptibility[29]. 6) Finally, we want to comment on the problem of the metal-insulator transition in the two-dimensional electron gas. Although there is quite a rich experimental literature on this phenomenon, very little is really understood. First, the real occurrence of a zero-temperature metal-insulator transition has not gathered the general consensus. In any case, from the point of view of the present discussion about the relevance of the electron-electron interaction in disordered systems, Si-MOSFET devices and semiconducting heterostructures are even a stronger case. In fact, if there is a metal-insulator transition, this is clearly beyond the conventional non-interacting scaling theory for which all states are localized in two dimensions for any value of the disorder. Secondly, the Coulomb interaction in these systems is expected to be very strong.

By considering the effective mass of Si, $m = 0.19 m_0$ (m_0 being the bare electron mass), and taking a value for $\varepsilon \sim 11.9$, at typical electron densities $n \sim 10^{11} cm^{-2}$ from eq.(2.12) one gets $r_s \sim 2-3$, which has also led to suggest that Wigner cristallization may play a role [55]. A last point to make about two dimensional systems is their strong parallel magnetic field magnetoresistance. When the applied field gives a Zeeman energy $g\mu_B B \sim E_F$, the resistivity increases by more than an order of magnitude[56].

The interplay between disorder and electron-electron interaction will account for most of the questions arisen above.

5. – Interacting Disordered Electrons

In this section, we consider the interplay of disorder and interaction[57, 58, 59]. In addition to the Hamiltonian (4.1) we have now to consider the interaction term

$$
\begin{aligned}
H_I &= \frac{1}{2}\int \mathrm{d}\mathbf{r}\ \mathrm{d}\mathbf{r}' \psi^\dagger_\alpha(\mathbf{r})\psi^\dagger_\beta(\mathbf{r}')V(\mathbf{r}-\mathbf{r}')\psi_\beta(\mathbf{r}')\psi_\alpha(\mathbf{r}) \\
&= \sum_{\mathbf{p},\mathbf{p}',\mathbf{q}} V(\mathbf{q}) a^\dagger_{\alpha\mathbf{p}} a^\dagger_{\beta\mathbf{p}'+\mathbf{q}} a_{\beta\mathbf{p}'} a_{\alpha\mathbf{p}+\mathbf{q}}.
\end{aligned}
\tag{5.1}
$$

In the above summation over repeated spin indices is understood. We show that adding the interaction leads, in perturbation theory, to additional logarithmic corrections in two dimensions to both thermodynamic and transport quantities. We discuss how these corrections may be interpreted in terms of a disorder-renormalized Fermi liquid[60, 61, 62, 63, 64]. To achieve such a goal, a key step is the identification of which additional parameters besides t are required to take into account the interaction in the scaling description of disordered systems[65]. In the next subsection, we will see how the above mentioned logarithmic corrections arise in the single-particle density of states, the electrical conductivity (which was the only quantity affected by disorder in the non-interacting case), the specific heat, and the spin susceptibility. The last two will be evaluated via the correction to the thermodynamic potential. We will recognize how disorder selects particular regions of transferred momentum in electron-electron interaction giving rise to the effective couplings of the theory. In the following subsection, these will turn out to be related to the Landau scattering amplitudes. Once the skeleton structure of the theory is developed, via the Ward identities we will identify the singular scale-dependent terms

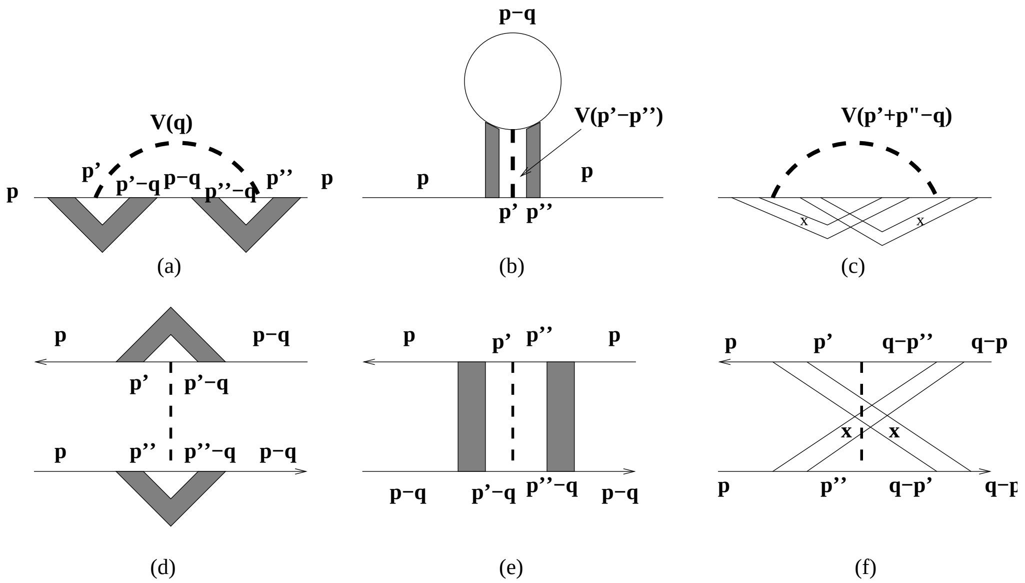

Fig. 15. – Diagrams for the correction to the Green's function to the lowest order in the interaction. (a) and (c) are exchange-type diagrams, while (b) is Hartree-type. Interaction is shown as a thick dashed line. The effective interaction diagrams ((d),(e),(f)) are obtained by cutting the internal Green's function with momentum $\mathbf{p}-\mathbf{q}$. The impurity "dressing" of the basic interaction diagrams selects three different regions of transferred momentum. In diagram (a), the momentum $q \sim 0$, that flows in the ladder, is also present in the interaction. (See (d)). In diagram (b), instead, the different position of the impurity ladder makes the momentum flowing in the interaction line, $p'-p''$, unrelated to q flowing in the ladder. (See (e)). Finally, the crossed ladders in diagram (c) select, in the small-q limit, the interaction in the Cooper channel. (See (f)).

with the Landau parameters themselves and derive the corresponding group equations in $d = 2 + \epsilon$.

5˙1. *Perturbation theory and the search for the effective couplings. –*

5˙1.1. Density of states. We begin by considering the diagrams for the Green's function to lowest order in the interaction. These are shown in fig.15. The basic diagrams are the usual exchange and Hartree contributions. Here, these two basic diagrams are "dressed" by the presence of disorder. As before, this is done by averaging over the impurity configurations. To illustrate how the mechanism now works, let us consider first the exchange diagram (a) in fig.15. Its expression, before the impurity averaging, reads

$$\begin{aligned}\delta\mathcal{G}(\mathbf{r},\mathbf{r}';\epsilon_n) = -T\sum_{\omega_m}\int \mathrm{d}\mathbf{r}_1\,\mathrm{d}\mathbf{r}_2\;\mathcal{G}(\mathbf{r},\mathbf{r}_1;\epsilon_n)\mathcal{G}(\mathbf{r}_1,\mathbf{r}_2;\epsilon_n-\omega_m)\\ \times\,\mathcal{G}(\mathbf{r}_2,\mathbf{r}';\epsilon_n)\mathcal{V}(\mathbf{r}_1,\mathbf{r}_2;\omega_m)\end{aligned} \tag{5.2}$$

where we use the Matsubara formalism. $\epsilon_n = (2n+1)\pi T$ and $\omega_m = 2m\pi T$ are fermionic and bosonic frequencies. The above expression is written in real space and is valid for a given impurity configuration. The electron-electron interaction is assumed to depend on frequency, since this will allow us to include retardation effects usually introduced by screening effects. As a matter of convention, we use calligraphic letters to indicate quantities depending on the Matsubara frequency. As a general strategy, we first perform the analytical continuation to real frequencies and then average over the impurity configurations by exploiting the technique developed in the previous section. Upon analytic continuation, $\mathrm{i}\epsilon_n \to \epsilon + \mathrm{i}0^+$[44], from eq.(5.2) the correction to the retarded Green's function becomes

$$\begin{aligned}\delta G^R(\mathbf{r},\mathbf{r}';\epsilon) = -\int \frac{\mathrm{d}\omega}{2\pi\mathrm{i}} \int \mathrm{d}\mathbf{r}_1 \int \mathrm{d}\mathbf{r}_2\, G^R(\mathbf{r},\mathbf{r}_1;\epsilon)\, \big[b(\omega) G^R(\mathbf{r}_1,\mathbf{r}_2;\epsilon-\omega) \\ (V^R(\mathbf{r}_1,\mathbf{r}_2;\omega) - V^A(\mathbf{r}_1,\mathbf{r}_2;\omega)) \\ + \; f(\omega-\epsilon) V^R(\mathbf{r}_1,\mathbf{r}_2;\omega)(G^R(\mathbf{r}_1,\mathbf{r}_2;\epsilon-\omega) - G^A(\mathbf{r}_1,\mathbf{r}_2;\epsilon-\omega))\big]\, G^R(\mathbf{r}_2,\mathbf{r}';\epsilon)\end{aligned} \tag{5.3}$$

where b and f are the Bose and Fermi function, respectively. $V^{R,A}$ are the analytical continuations of the dynamical interaction $\mathcal{V}$. The average over the impurity configurations has two effects. First, each Green's function is replaced by expression (4.7) obtained within the self-consistent Born approximation. Secondly, one has to insert direct and crossed ladders wherever possible. This gives the leading approximation. We have learned that the insertion of ladders is only possible when Green's functions have poles on opposite sides of the real axis, *i.e.*, when the ladder connects a retarded and an advanced Green's function. As a result we need to keep only the last term of eq.(5.3). The correction to the density of the states then reads

$$\begin{aligned}\delta N(\epsilon) = -\frac{1}{\pi}\mathcal{I}m \sum_{\mathbf{q},\mathbf{p}} \int_{-\infty}^{\infty} \frac{\mathrm{d}\omega}{2\pi\mathrm{i}}\; f(\omega-\epsilon) V^R(\mathbf{q},\omega) L^2(\mathbf{q},\omega) G^R(\mathbf{p},\epsilon) G^A(\mathbf{p}-\mathbf{q},\epsilon-\omega) G^R(\mathbf{p},\epsilon) \\ \times \sum_{\mathbf{p}'} G^R(\mathbf{p}',\epsilon) G^A(\mathbf{p}'-\mathbf{q},\epsilon-\omega) \sum_{\mathbf{p}''} G^R(\mathbf{p}'',\epsilon) G^A(\mathbf{p}''-\mathbf{q},\epsilon-\omega)\end{aligned} \tag{5.4}$$

where the average over the impurities has restored the translational invariance and we have gone to the momentum representation. The $\mathbf{q}$-integral is dominated by the diffusive pole of the impurity ladder. This implies that in the remaining momentum integrals one can perform, as usual, a small-$\mathbf{q}$ expansion. As it was also remarked in the non-interacting microscopic theory, we will perform the *fast* momenta (flowing in the Green's functions) integrals first, since they contribute only to the coefficient of the singular terms arising from the integration over the *slow* momenta flowing in the ladders. We then set $\mathbf{q} = 0$ in all the $\mathbf{p}$-, $\mathbf{p}'$-, and $\mathbf{p}''$-integrals, which can be carried out in the standard way with the residue method and, using the results of Appendix A, one gets

$$\delta N(\epsilon) = \frac{1}{\pi}\mathcal{I}m \sum_{\mathbf{q}} \int_{-\infty}^{\infty} \mathrm{d}\omega\; f(\omega-\epsilon) \frac{N_0 V^R(\mathbf{q},\omega)}{(D\mathbf{q}^2 - \mathrm{i}\omega)^2}. \tag{5.5}$$

At zero temperature, the Fermi function becomes a step function giving the condition $\omega < \epsilon$. In the case of short-range interaction V^R remains finite in the small frequency and momentum limit. Due to the presence of a double diffusive pole, the integration in the region $D\mathbf{q}^2\tau, |\omega|\tau < 1$ over frequency and momenta gives a logarithmic divergence

$$\frac{\delta N(\epsilon)}{N_0} = N_0 V^R(0,0) t \ln|\epsilon\tau| \equiv V_1 t \ln|\epsilon\tau|. \tag{5.6}$$

The Hartree diagram (b) may be evaluated in a similar way. Its expression, after impurity averaging, reads

$$\begin{aligned}\delta N(\epsilon) = \frac{1}{\pi}\mathcal{I}m \sum_{\mathbf{q},\mathbf{p}} 2V_2 \int_{-\infty}^{\infty} \frac{\mathrm{d}\omega}{2\pi \mathrm{i}}\, f(\omega-\epsilon) L^2(\mathbf{q},\omega)\\ \times G^R(\mathbf{p},\epsilon) G^A(\mathbf{p}-\mathbf{q},\epsilon-\omega) G^R(\mathbf{p},\epsilon)\end{aligned} \tag{5.7}$$

where the relative minus sign and the factor of 2 are due to the extra fermionic loop in the Hartree diagram. The interaction parameter V_2 takes into account the scattering at large angle across the Fermi surface, as shown in diagrams (b) and (e) of fig.15.

$$\begin{aligned}V_2 = \frac{1}{N_0} \sum_{\mathbf{p}',\mathbf{p}''} G^R(\mathbf{p}',\epsilon) G^A(\mathbf{p}'-\mathbf{q},\epsilon-\omega) V^R(\mathbf{p}'-\mathbf{p}'',0)\\ \times G^R(\mathbf{p}'',\epsilon) G^A(\mathbf{p}''-\mathbf{q},\epsilon-\omega).\end{aligned} \tag{5.8}$$

We then see that the presence of the diffusive pole of the ladder, by making the small q region more relevant, effectively selects the electron-electron scattering at small, V_1 (exchange contribution), and large momentum transfer, V_2 (Hartree contribution). A similar analysis can be carried out for the exchange contribution with crossed ladders (diagram (c)) and one has a third parameter V_3,

$$\begin{aligned}V_3 = \frac{1}{N_0} \sum_{\mathbf{p}',\mathbf{p}''} G^R(\mathbf{p}',\epsilon) G^A(\mathbf{q}-\mathbf{p}',\epsilon-\omega) V^R(\mathbf{p}'+\mathbf{p}'',0)\\ \times G^R(\mathbf{p}'',\epsilon) G^A(\mathbf{q}-\mathbf{p}'',\epsilon-\omega).\end{aligned} \tag{5.9}$$

Actually, there is also the Hartree contribution with crossed ladders, but it contributes with minus twice the same scattering amplitude. The total correction to the density of states reads then

$$\frac{\delta N(\epsilon)}{N_0} = (V_1 - 2V_2 - V_3) t \ln|\epsilon\tau|. \tag{5.10}$$

We notice that V_3 corresponds to the interaction in the Cooper scattering channel(see fig.(15)). Since its presence does not change the results qualitatively, to simplify the exposition, we let it drop from our subsequent discussion. On a formal level, one may assume the presence of a small magnetic field which, as we have seen, by introducing a mass, kills the singularity in the Cooper channel. The same selection of relevant momenta appear also in the perturbative calculation of the electrical conductivity and thermodyamic potential, as we are going to show. Before leaving the density of states, we notice that the above results are modified in the presence of long-range Coulomb interaction, which leads to log-square singularity in two dimensions. Details are provided in Appendix D.

5˙1.2. Electrical conductivity. The impurity-averaged diagrams responsible for the corrections to the conductivity are obtained in Appendix E. The procedure is similar to that followed in the case of the density of states, but there are many more diagrams. For this reason, the detailed derivation of how to perform the impurity average and the integration over the fast momenta is left to the Appendix E. Here we give directly the final result for the exchange diagram containing the interaction amplitude V_1 before the last integration over the slow momentum and frequency. We have

$$\delta\sigma = -\frac{2\sigma_0}{\pi\ d}\sum_{\mathbf{q}} D\mathbf{q}^2 \int_{-\infty}^{\infty} \mathrm{d}\omega \frac{\partial}{\partial\omega}\left(\omega \coth\left(\frac{\omega}{2T}\right)\right) \mathcal{I}m\ \left[\frac{V^R(\mathbf{q},\omega)}{(D\mathbf{q}^2 - \mathrm{i}\omega)^3}\right] \tag{5.11}$$

where the dimensionality factor d comes from the angular integration over $\mathbf{q}$. In two dimensions, in the case of short-range interaction, eq.(5.11) yields[58, 59]

$$\delta\sigma = -\frac{e^2}{\pi^2\hbar}(V_1 - 2V_2)\frac{1}{2}\ln\left(\frac{1}{T\tau}\right), \tag{5.12}$$

where, as for the density of states, the factor $-2V_2$ takes into account the contribution coming from the Hartree diagram. In the case of Coulomb long-range forces, , at small q, the screened interaction introduces an extra singularity (see Appendix D) $V^R(q,\omega) \approx -2\pi\mathrm{i}e^2\omega/(Dq^2)$. In contrast to the case of the single-particle density of states, the $1/q^2$ singularity arising from the interaction is compensated from the additional q^2 factor in the integrand. By using eq.(D.1) for $V^R(\mathbf{q},\omega)$ one obtains for the exchange contribution

$$\delta\sigma = -\frac{e^2}{2\pi^2\hbar}\ln\left(\frac{1}{T\tau}\right), \tag{5.13}$$

which has the same form as the weak localization correction. The same will hold for both short- and long-range case in the renormalized perturbation theory as we shall see in the next subsection.

5˙1.3. Thermodynamic potential. Contrary to the non-interacting case, the interplay between disorder and interaction introduces singular corrections to the specific heat and spin susceptibility. We present here the derivation of the correction to the thermodynamic potential. The effective diagrams are shown in fig. 16. We have to carry out the

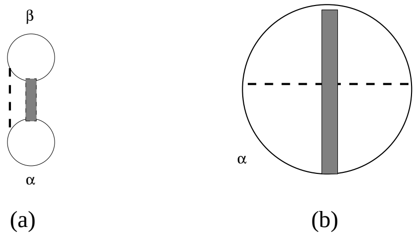

Fig. 16. – Diagrams for the thermodynamic potential. (a) Hartree. (b) Exchange. The ladder arising from the impurity average is already shown. Notice that in the Hartree diagram the spin on the two lines of the ladder may differ from zero, whereas it is always zero for the exchange one.

integration over the fast momenta flowing in the Green's functions. After doing that, we obtain

$$\Delta\Omega = -(V_1 - 2V_2)T\sum_{\omega_m}\sum_{\mathbf{q}} \frac{|\omega_m|}{D\mathbf{q}^2 + |\omega_m|}. \tag{5.14}$$

In Appendix F, we provide the details of the derivation. The Matsubara frequency sum is limited by $|\omega_m|\tau < 1$. To relax the constraint in the sum, we introduce a cutoff function

$$\left(\frac{\tau^{-1}}{|\omega_m| + \tau^{-1}}\right)^2$$

and the sum runs between minus and plus infinity. We may then perform analytical continuation to get

$$\Delta\Omega = -\frac{1}{2}(V_1 - 2V_2)\sum_{\mathbf{q}}\int_{-\infty}^{\infty}\frac{\mathrm{d}\omega}{\pi}b(\omega)\mathcal{I}m\left[\left(\frac{\tau^{-1}}{-\mathrm{i}\omega + \tau^{-1}}\right)^2 \frac{-2\mathrm{i}\omega}{D\mathbf{q}^2 - \mathrm{i}\omega}\right]. \tag{5.15}$$

In two dimensions, the sum over $\mathbf{q}$ may be done and eq.(5.15) becomes

$$\begin{aligned}\Delta\Omega &= -\frac{(V_1 - 2V_2)}{4\pi^2 D}\int_{-\tau^{-1}}^{\tau^{-1}} \mathrm{d}\omega\ \omega\ b(\omega)\ \ln(|\omega|\tau) \\ &= -t(V_1 - 2V_2)\frac{\pi^2 N_0 T^2}{3}\ln(T\tau),\end{aligned} \tag{5.16}$$

where we have dropped non singular terms in temperature. The thermodynamic potential then acquires a logarithmic correction that implies for the specific heat[66]

$$\delta C_V = C_{V,0}t(V_1 - 2V_2)\ln(T\tau), \tag{5.17}$$

where $C_{V,0} = (2\pi^2 N_0 T)/3$ is the non-interacting value.

In order to evaluate the spin susceptibility, we must include the Zeeman coupling. As shown in the eq.(G.2) of Appendix G, only the ladder corresponding to total spin ±1 of the incoming particle-hole pair are affected by the magnetic field via the Zeeman energy $\omega_s = g\mu_B B$. In this respect, we notice that only the Hartree diagram of fig.16 contributes, since in this case the total spin of the particle-hole pair is given by the combination $\alpha - \beta$, with both indices running over $\pm 1/2$. In the exchange diagram the total spin of the particle-hole pair entering the ladder is $\alpha - \alpha$ and is always zero. The combination of the two diagrams may be arranged as the sum of a singlet and triplet component with respect to the total spin of the particle-hole ladder. Hence, the magnetic field only affects the triplet component with value $M = \pm 1$. For the purpose of isolating the magnetic-field dependent contribution to the thermodynamic potential, it is convenient to write the difference, with and without the magnetic field, of the triplet as

$$\begin{aligned}
\Delta\Omega_B &= \frac{1}{2}T\sum_{\omega_m}\sum_{M\pm 1}\sum_{\mathbf{q}} V_2|\omega_m|\left[\frac{1}{D\mathbf{q}^2+|\omega_m|-\mathrm{i}M\omega_s sgn(\omega)}-\frac{1}{D\mathbf{q}^2+|\omega_m|}\right]\\
&= \frac{1}{2}T\sum_{\omega_m}\sum_{\mathbf{q}} V_2|\omega_m|\left[\frac{2(D\mathbf{q}^2+|\omega_m|)}{(D\mathbf{q}^2+|\omega_m|)^2+\omega_s^2}-\frac{2}{D\mathbf{q}^2+|\omega_m|}\right]\\
&= -\frac{1}{2}\pi t N_0 V_2 T\sum_{\omega_m}|\omega_m|\ln\left(\frac{\omega_m^2+\omega_s^2}{\omega_m^2}\right)\\
&\approx -\pi t N_0 V_2 \omega_s^2 T\sum_{\omega_m>0}\frac{1}{\omega_m}\\
&= \frac{tN_0V_2}{2}\omega_s^2\ln(T\tau). \qquad (5.18)
\end{aligned}$$

Now a few words concerning the steps leading to the final expression of eq.(5.18). Since the factor $|\omega_m|$ in the sum excludes the term with $\omega_m = 0$ and the expression in the sum is even in ω_m, we have rewritten the sum as twice the sum over the strictly positive frequencies. Then we observe that the smallest frequency is $2\pi T$, which allows us to make a small magnetic field expansion $\omega_s < T$. From eq.(5.18) one finally gets, by differentianting twice with respect to the magnetic field, the correction to the spin susceptibility

$$\chi = -\chi_0 2tV_2\ln(T\tau), \qquad (5.19)$$

where we have introduced the non-interacting value $\chi_0 = 2N_0(g\mu_B/2)^2$. No correction is instead found for the compressibility.

The two parameters V_1 and V_2 that appear in the perturbative expression of the density of states (5.10), conductivity (5.12), specific heat (5.17), and spin susceptibility (5.19) are the natural candidates for the additional running couplings to be used with the dimensionless resistance t to obtain the renormalized perturbation theory in $2+\epsilon$ dimensions.

5˙2. *The renormalized perturbation theory and effective Fermi-liquid description.* – In this subsection we show how the perturbative results derived in the previous one may be generalized to all orders in the interaction and how the effective scattering amplitudes are related to the Landau parameters. We then develop the renormalized perturbation theory for the various response functions by making use of the Ward identities that implement the conservation laws for charge, spin, and energy. Finally, we go back to the perturbative results which will be generalized to all orders in the interaction and derive the group equations.

5˙2.1. Effective scattering amplitudes and Landau parameters. According to the discussion of the previous section, the relevant interaction terms in the Hamiltonian are reduced to

$$H_I = \sum_{\mathbf{p},\mathbf{p}'} \sum_{\mathbf{q}}{}^{\prime} \left[V_1 a^\dagger_{\alpha\mathbf{p}} a^\dagger_{\beta\mathbf{p}'+\mathbf{q}} a_{\beta\mathbf{p}'} a_{\alpha\mathbf{p}+\mathbf{q}} + V_2 a^\dagger_{\alpha\mathbf{p}} a^\dagger_{\beta\mathbf{p}'+\mathbf{q}} a_{\beta\mathbf{p}+\mathbf{q}} a_{\alpha\mathbf{p}'} \right], \tag{5.20}$$

where the primed **q**-summation will be confined to small **q** values as implied when performing the disordere averaging.

Up to now our discussion has been limited to the first order in the interaction. However, we do not want to confine our theory to small interaction and the only true expansion parameter must be the dimensionless resistance $t = 1/(2\pi g)$. The good metal condition, $g \gg 1$ ($E_F\tau/\hbar \gg 1$), implies that the disorder only affects electron states within a small distance $\hbar/\tau$ away from the Fermi surface. Under these circumstances, one may go beyond the first-order interaction correction by replacing V_1 and V_2 with the Fermi-liquid scattering amplitudes Γ_1 and Γ_2, whose lowest order diagrams are depicted in fig.17.

We note that in the absence of spin-flip mechanisms, the total spin of two colliding particles is a conserved quantity. It is then convenient to introduce the *singlet* Γ_s and *triplet* Γ_t scattering amplitudes. After the selection of the relevant momentum transfer terms (cf. eqs.(5.6)-(5.8)) the corresponding spin structures can be decomposed as

$$\Gamma_1 \delta_{\alpha\delta}\delta_{\beta\gamma} - \Gamma_2 \delta_{\alpha\beta}\delta_{\gamma\delta} = (\Gamma_1 - \frac{1}{2}\Gamma_2)\delta_{\alpha\delta}\delta_{\beta\gamma} - \frac{1}{2}\Gamma_2 \sigma_{\alpha\delta}\cdot\sigma_{\beta\gamma} \tag{5.21}$$

where we have used the identity

$$\delta_{\alpha\beta}\delta_{\gamma\delta} = \frac{1}{2}\delta_{\alpha\delta}\delta_{\beta\gamma} + \frac{1}{2}\left[\sigma^x_{\alpha\delta}\sigma^x_{\beta\gamma} + \sigma^y_{\alpha\delta}\sigma^y_{\beta\gamma} + \sigma^z_{\alpha\delta}\sigma^z_{\beta\gamma}\right]. \tag{5.22}$$

We then define

$$\Gamma_s = \Gamma_1 - \frac{1}{2}\Gamma_2, \quad \Gamma_t = \frac{1}{2}\Gamma_2. \tag{5.23}$$

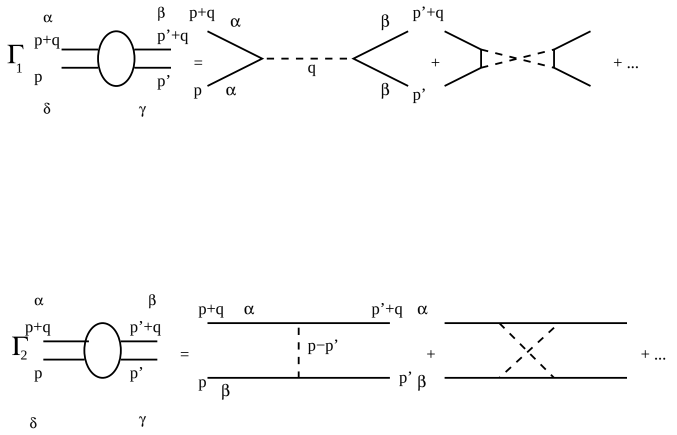

Fig. 17. – Lowest order diagrams for the small (Γ_1) and large (Γ_2) scattering angle. Notice the different momenta flowing through the interaction propagator. Also the two diagrams have a different spin structure.

The scattering amplitudes Γ_s and Γ_t are related to the Landau Fermi-liquid parameters F^0_s and $F^0_a$by[44]

$$\Gamma_s = \frac{1}{2N_0}\frac{F^0_s}{1+F^0_s}, \qquad \Gamma_t = -\frac{1}{2N_0}\frac{F^0_a}{1+F^0_a}. \tag{5.24}$$

From now on, when necessary, N_0 is assumed to include the Landau effective-mass correction. In terms of the Landau parameters, compressibility, spin susceptibility and specific heat are given by

$$\begin{aligned}
\frac{\partial n}{\partial \mu} &= \frac{2N_0}{1+F^0_s} = 2N_0(1-2N_0\Gamma_s) \equiv 2N_0 Z^0_s \\
\chi &= \frac{\chi_0}{1+F^0_a} = \chi_0(1+2N_0\Gamma_t) \equiv \chi_0 Z^0_t \\
C_V &= C_{V,0} \equiv C_{V,0} Z^0,
\end{aligned} \tag{5.25}$$

where Z^0 will be different from one in the presence of disorder and is here introduced for symmetry in the equations.

5˙2.2. Renormalized response functions. We begin our discussion of the interplay between interaction and disorder in the renormalization of the response functions, by considering the density-density response function. As in the case of the non-interacting theory of eqs.(4.16),(4.18), we split the response function in static and dynamic contributions. The effect of the interaction may be understood in terms of a skeleton perturbation

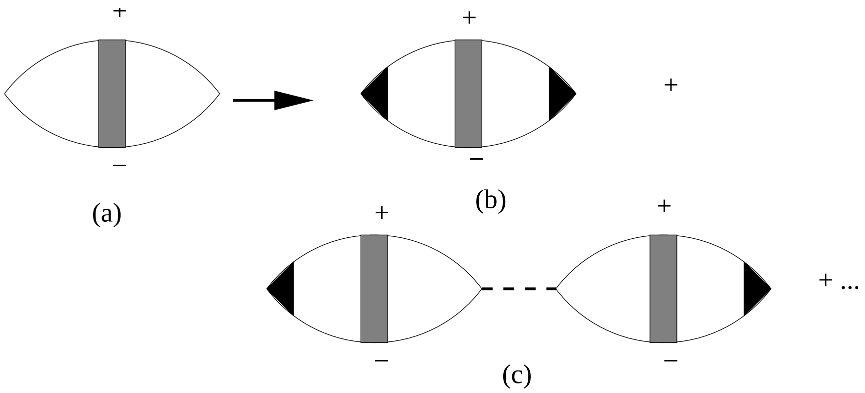

Fig. 18. – Skeleton structure of the perturbative evaluation of the response function in the presence of interaction. The plus and minus signs indicate the sign of the energy flowing in the line. We remind that the ladder insertion is only possible between a pair of retarded and advanced Green's functions. The first diagram (a) is the one used in the non-interacting theory. Diagram (b) represents how the interaction "dresses" (a). It leads to i) a "dressing" of the vertex, here indicated as a black triangle, ii) renormalization of the ladder. Interaction appears explicitly in diagram (c), which has to be considered together with all the other diagrams, indicated by the dots, obtained by the infinite resummation of the interaction. Depending on whether we consider the charge or spin response function one has the vertex $\Lambda_{s,t}$ and interaction $\Gamma_{s,t}$. For the energy response function, there is also a vertex Λ_E, but there is no infinite resummation of the interaction for the reasons explained in the text.

theory, as shown in fig.18. The first diagram (a), due to the ladder insertion, gives the dynamic contribution in the non-interacting case (cf. eq.(4.18)). Its "dressing" due to the interaction is represented by the diagram (b), whose contribution can be written in the form

$$K^{00}_{(b)} = -\frac{\mathrm{i}\omega 2e^2 N_0 \zeta^2 \Lambda_s^2}{Dq^2 - \mathrm{i}\omega Z} \equiv K^{00}_{+-}\Lambda_s, \tag{5.26}$$

which generalizes eq.(4.18). We now discuss it in detail. We begin with the ladder, which is the most important ingredient of the theory. The ladder in fact is the effective propagator of the diffusive mode, responsible for the singularities appearing in perturbation theory. It requires a wave function renormalization ζ, a frequency (effective external field) renormalization Z, and a renormalization of the diffusion constant(5)

$$L(q,\omega) = \frac{1}{2\pi N_0 \tau^2}\frac{1}{Dq^2 - \mathrm{i}\omega} \to \frac{1}{2\pi N_0 \tau^2}\frac{\zeta^2}{Dq^2 - \mathrm{i}Z\omega}. \tag{5.27}$$

---

(5) We leave the same symbol as before for the interaction-renormalized diffusion constant to keep the notation simple. Everywhere in this subsection this is understood whenever we are dealing with the renormalized ladder.

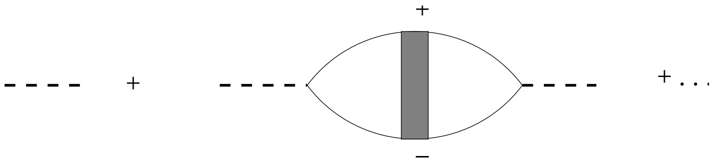

Fig. 19. – Dynamical resummation of the interaction.

In Appendix H we show that the interaction corrections to the ladder do not destroy its diffusive pole behavior and indeed lead to the renormalized form of eq.(5.27). Furthermore, the logarithmically singular corrections to the single-particle density of states, specific heat, and conductivity which appear in two dimensions can be absorbed in the above three renormalizations ζ, Z, and D, respectively. Here, by exploiting the constraints given by the general conservation laws embodied in the Ward identities, we will be able to directly express the ladder renormalization parameters in terms of physical quantities.

The vertex Λ_s is one in the non-interacting case. In the interacting case, it represents the vertex which, when multiplied by K^{00}_{+-}, gives the total dynamic part of K^{00}, which includes also terms ending with two advanced $(++)$ or two retarded $(--)$ Green's functions. The vertex Λ_s is irreducible for cutting a ladder propagator.

Besides "dressing" the non-interacting diagram, interaction leads to new diagrams as diagram (c) of fig.18, which gives

$$K^{00}_{(c)} = e^2 \frac{\omega 2 N_0 \zeta^2 \Lambda_s}{Dq^2 - \mathrm{i}\omega Z} \Gamma_s \frac{\omega 2 N_0 \zeta^2 \Lambda_s}{Dq^2 - \mathrm{i}\omega Z}. \tag{5.28}$$

By keeping in mind that the order in the expansion parameter t is determined by the number of integrations over the momenta flowing in the ladder propagator, we can replace, without changing the order in t, the scattering amplitude Γ_s by its screened form

$$\Gamma_s(q,\omega) = \Gamma_s - \Gamma_s \mathrm{i}\frac{2\omega}{2\pi}(2\pi N_0 \tau)^2 L(q,\omega)\Gamma_s(q,\omega) = \Gamma_s \frac{Dq^2 - \mathrm{i}Z\omega}{Dq^2 - \mathrm{i}Z_s\omega}, \tag{5.29}$$

obtained by an RPA-like infinite resummation (shown in fig.19) and using eq.(5.27). In eq.(5.29) $Z_s = Z - 2\zeta^2 N_0 \Gamma_s$ will turn to be the expression dressed by the disorder of Fermi-liquid renormalization of the compressibility Z^0_s. If we insert the dynamical amplitude (5.29) in the expression (5.28) for the first interaction correction and combine it with the contribution (5.26) of the first diagram, we arrive at the final form of the response function which resums all the infinite series of diagrams indicated by dots in fig. 18:

$$K^{00}_{+-} = -\frac{\mathrm{i}\omega 2 e^2 N_0 \zeta^2 \Lambda_s}{Dq^2 - \mathrm{i}\omega Z_s}, \qquad K^{00} = -e^2 \frac{\partial n}{\partial \mu} + K^{00}_{+-}\Lambda_s. \tag{5.30}$$

We are now ready to make use of the Ward identities (3.31),(3.33), where now K^{00}_{+-} is given by eq.(5.30), and we get

$$\frac{N}{N_0} = \frac{\zeta^2 \Lambda_s}{Z_s}, \tag{5.31}$$

$$\frac{\partial n}{\partial \mu} = 2N_0 \frac{\zeta^2 \Lambda_s^2}{Z_s}. \tag{5.32}$$

We can now follow two alternative routes leading to the same result. We can first remember from Appendix H that N/N_0 coincides with ζ. It then follows from eq.(5.31) that $\zeta\Lambda_s = Z_s$, which when used in eq.(5.32) gives

$$\frac{\partial n}{\partial \mu} = 2N_0 Z_s. \tag{5.33}$$

Alternatively, it can be shown that the compressibility has no logarithmic corrections, i.e., is given by the Fermi-liquid value in the absence of disorder with $Z_s = Z_s^0 = \zeta\Lambda_s$. This means that, although both Λ_s and ζ have logarithmic corrections, the combination $\zeta\Lambda_s$ does not. The final expression for the density response function has the conserving form

$$K^{00}(q,\omega) = -e^2 \frac{\partial n}{\partial \mu} \frac{D_c q^2}{D_c q^2 - \mathrm{i}\omega} \tag{5.34}$$

where the charge diffusion constant $D_c = D/Z_s$ has been introduced.

A similar analysis can be done for the spin susceptibility and the specific heat. First we note that the dynamical scattering amplitude in the triplet channel reads

$$\Gamma_t(q,\omega) = \Gamma_t + \Gamma_t \mathrm{i}\frac{2\omega}{2\pi}(2\pi N_0 \tau)^2 L(q,\omega)\Gamma_t(q,\omega) = \Gamma_t \frac{Dq^2 - \mathrm{i}Z\omega}{Dq^2 - \mathrm{i}Z_t\omega}, \tag{5.35}$$

where $Z_t = Z + 2N_0\zeta^2\Gamma_t$ is the expression dressed by the disorder of the Fermi-liquid renormalization of the spin susceptibility $Z_t^0 = 1 + 2N_0\Gamma_t$, which as for the compressibility is given by the static limit ($\omega = 0, q \to 0$) of the spin-spin response function $\chi(\mathbf{q},\omega)$. To analyze the spin-spin response function, one introduces, in analogy with the density-density response function, the i-th component of the spin density

$$S^i(x) = \frac{g\mu_B}{2} \psi^\dagger_\alpha(x) \sigma^i_{\alpha\beta} \psi_\beta(x), \tag{5.36}$$

and the associated spin-current density $\mathbf{S}^i$. By proceeding as in the charge density case of eq.(3.22), we introduce a vertex function

$$\Lambda^{i,\mu}_{\alpha\beta}(x,x',x'') =< T_t S^{i,\mu}(x)\psi_\alpha(x')\psi^\dagger_\beta(x'') >, \tag{5.37}$$

where the first upper index indicates which component of the spin density we are dealing with while the second one, μ, distinguishes between density and current component. In the presence of a magnetic field, one may derive for $\Lambda^{i,\mu}$ the following Ward identity

$$q_\mu \Lambda^{i,\mu}_{\alpha\beta}(p,q) = \frac{g\mu_B}{2}\left[\sigma^i_{\alpha\beta}\; G_\beta(p-q/2) - G_\alpha(p+q/2)\;\sigma^i_{\alpha\beta}\right] + \mathrm{i}\epsilon_{ij3}\omega_s\Lambda^{j,0}_{\alpha\beta}(p,q), \tag{5.38}$$

where ϵ_{ijk} is the full antisymmetric tensor and we have assumed the magnetic field in the z-direction. We now consider the consequences of eq.(5.38) in the vanishing momentum limit. Instead of working with the x and y components, it is convenient to switch to the circularly polarized ones defined as

$$\Lambda^{\uparrow\downarrow,0} = \frac{1}{2}\left(\Lambda^{1,0} + \Lambda^{2,0}\right), \tag{5.39}$$

$$\Lambda^{\downarrow\uparrow,0} = \frac{1}{2}\left(\Lambda^{1,0} - \Lambda^{2,0}\right), \tag{5.40}$$

corresponding to the spin-density in the $M = \mp 1$ triplet channels, respectively. By including the $M = 0$ channel of the triplet corresponding to $\Lambda^{3,0}$, one gets the Ward identity (5.38) in the form

$$(\omega + M\omega_s)\Lambda^{M,0}_{\alpha\beta}(\epsilon,\omega) = \frac{g\mu_B}{2}\left[\sigma^M_{\alpha\beta}\; G_\beta(\epsilon-\omega/2) - G_\alpha(\epsilon+\omega/2)\;\sigma^M_{\alpha\beta}\right], \tag{5.41}$$

where σ^M are defined as in eq.(5.39),(5.40) and we have dropped the explicit dependence on momentum $\mathbf{p}$ both in the vertex and in the Green's functions. (6) The dynamical resummation of the skeleton structure, analog to eq.(5.30) for K^{00}, with Γ_s replaced by Γ_t and $\partial n/\partial\mu$ or $2N_0$ by χ, gives

$$\chi^M_{+-}(q,\omega) = \frac{\mathrm{i}\omega\chi_0\zeta^2\Lambda_t}{Dq^2 - \mathrm{i}\omega Z_t - \mathrm{i}MZ_H\omega_s}, \qquad \chi^M(q,\omega) = \chi + \chi^M_{+-}(q,\omega)\Lambda_t, \tag{5.42}$$

where we have introduced a renormalization factor for the Zeeman energy, Z_H. Equation (5.41) together with the analog of eq.(3.31) for the spin-spin response function in the M-th channel leads to

$$\chi^M(0,\omega) = \chi\frac{M\omega_s}{\omega + M\omega_s}, \tag{5.43}$$

$$\chi^M_{+-}(0,\omega) = -\chi_0\frac{N}{N_0}\frac{\omega}{\omega + M\omega_s}. \tag{5.44}$$

Indeed, in the limit of zero magnetic field eq.(5.43) gives the total spin conservation by the vanishing of the response function at finite ω as q goes to zero, while eq.(5.44) reproduces the single-particle density of states in term of the dynamical part of the spin response function. Finally, by making use of the Ward identities (5.43),(5.44) in (5.42), one obtains

---

(6) Notice that the Green's function gets a spin label in the presence of Zeeman coupling.

$$(5.45)\chi^M(q,\omega) = \chi \frac{D_s q^2 - \mathrm{i} M\omega_s}{D_s q^2 - \mathrm{i}(M\omega_s + \omega)}, Z_t = \zeta\Lambda_t, \chi = \chi_0 Z_t, Z_H = Z_t, D_s = D/Z_t.$$

Notice that the result $Z_H = Z_t$[68] implements, to all orders in the expansion in the parameter t, the Fermi-liquid zero-order result.

The energy-energy response function χ_E can also be decomposed according to the eq.(5.42), where χ is replaced by χ_E and Z_t and $2N_0\Lambda_t^2$ by Z and $C_{V,0}T\Lambda_E^2$[69, 70]. (^{7}) The analogous Ward identity gives

$$Z = \zeta\Lambda_E, \; C_V = C_{V,0}Z, \quad D_E = D/Z \tag{5.46}$$

and the frequency renormalization Z of the ladder is identified with the specific-heat renormalization. In the presence of Coulomb long-range forces, to avoid double counting, one has to subtract the statically screened long-range Coulomb Γ_0 from the full singlet scattering amplitude entering the ladder resummation for the density-density response function. Hence, $\Gamma_s \to \Gamma_s - \Gamma_0$ in Z_s, where

$$\Gamma_0(q,\omega = 0) = \frac{V_C(q)\Lambda_s^2}{1 + V_C(q)\partial n/\partial\mu} \rightarrow_{q\to 0} \frac{\Lambda_s^2}{\partial n/\partial\mu}. \tag{5.47}$$

As a consequence of eq.(5.32), from $Z_s = Z - 2N_0\zeta^2(\Gamma_s - \Gamma_0)$ we derive the constraint

$$Z = 2N_0\zeta^2\Gamma_s. \tag{5.48}$$

In this way we have completed the general formulation of the effective renormalized Fermi-liquid theory.

5˙2.3. Derivation of the group equations. We now come back to the perturbative expressions of the electrical conductivity (5.12), specific heat (5.17) and spin susceptibility (5.19). These expressions were derived to first order in the interaction. However, we have seen that we may relax this condition in two ways. First, we may use the Fermi liquid scattering amplitudes. Second, we can make an infinite dynamical resummation

---

(^{7}) In contrast to the density and spin response functions, in the energy response function the renormalization parameter does not require additional terms due to the interaction besides Z, i.e., the Fermi-liquid renormalization, the analog of diagram (c) of fig. (18), is missing. This occurs since the interaction separates the integration at the two vertices in the response function diagrams. Due to the presence of the energy in the thermal vertex, each integration over the energy contributes at least a term with the second power of the frequency. Hence the terms due to the dynamical resummation of the interaction give rise to negligible contributions going with the fourth power in the frequency.

(eqs. (5.29),(5.35)). For the electrical conductivity, by inserting the dynamical scattering amplitudes in eq.(5.11) one has

$$\begin{aligned}\frac{\delta\sigma}{\sigma} &= -\frac{2}{2\pi \mathrm{i}}\int_{-\infty}^{\infty}\mathrm{d}\omega\frac{\partial}{\omega}\left(\omega\coth\left(\frac{\Omega}{2T}\right)\right)\sum_{\mathbf{q}}\frac{Dq^2(\Gamma_s(q,\omega)-3\Gamma_t(q,\omega))}{(Dq^2-\mathrm{i}Z\omega)^3}\\ &= t\left[1+\frac{Z_s}{2N_0\zeta^2\Gamma_s}\ln\frac{Z_s}{Z}\right.\\ &\quad\left. +\ 3\left(1-\frac{Z_t}{2N_0\zeta^2\Gamma_t}\ln\frac{Z_t}{Z}\right)\right]\ln\left(T\tau\right),\end{aligned} \tag{5.49}$$

which coincides with $\delta D/D$ found from the ladder renormalization in Appendix H. In the case of Coulomb interaction, when $2N_0\zeta^2\Gamma_s = Z$, the singlet part of eq.(5.49) reproduces eq.(5.13). Furthermore for small Γ_s and Γ_t ($Z = 1$) one recovers the first order short range interaction result of eq.(5.12). However, in the short-range case, by allowing the group equations to flow, $Z_s = Z_s^0$ is invariant, while, as we shall see, Z and $2N_0\zeta^2\Gamma_s$ diverge and the singlet strength becomes again universal in Eq(5.49) and equal to one.

The full expression for the correction to the thermodynamic potential is obtained by introducing in eqs.(5.14),(5.18) the singlet and triplet dynamical scattering amplitudes and the renormalized ladder, including the magnetic-field renormalization $Z_H = Z_t$. For the magnetic-field independent part one then gets

$$\begin{aligned}\Delta\Omega = &-T\sum_{q\omega_m}\int_0^1\mathrm{d}\lambda\left[\frac{N_0\zeta^2\Gamma_s|\omega_m|}{Dq^2+(Z-\lambda 2N_0\zeta^2\Gamma_s)|\omega_m|}\right.\\ &\left.-\ \frac{3N_0\zeta^2\Gamma_t|\omega_m|}{Dq^2+(Z+\lambda 2N_0\zeta^2\Gamma_t)|\omega_m|}\right],\end{aligned} \tag{5.50}$$

while the field-dependent contribution reads

$$\begin{aligned}\Delta\Omega_B = T\sum_{q\omega_m}\int_0^1\mathrm{d}\lambda\sum_{M\pm 1}&\left[\frac{N_0\zeta^2\Gamma_t|\omega|}{Dq^2+(Z+\lambda 2N_0\zeta^2\Gamma_t)|\omega_m|-\mathrm{i}M(Z+2N_0\zeta^2\Gamma_t)\omega_s\mathrm{sgn}(\omega)}\right.\\ &\left.-\ \frac{N_0\zeta^2\Gamma_t|\omega|}{Dq^2+(Z+\lambda 2N_0\zeta^2\Gamma_t)|\omega_m|}\right].\end{aligned} \tag{5.51}$$

In the above equations, due to the presence of the dynamical resummation of the interaction we used the standard trick[44] of multiplying the interaction by a parameter $0 < \lambda < 1$. However, this must not be introduced in the amplitude present in the magnetic field insertion since it will generate spurious diagrams. As a result, the corrections to the specific heat and to the spin susceptibility are

$$\delta C_V = C_{V,0}t(N_0\zeta^2\Gamma_s - 3N_0\zeta^2\Gamma_t)\ln(T\tau), \tag{5.52}$$

$$\delta\chi = -\chi_0 4tN_0\zeta^2\Gamma_t\frac{Z_t}{Z}\ln(T\tau). \tag{5.53}$$

The renormalization of the specific heat may be interpreted as the renormalization of the quasi-particle density of states $N_{QP} = ZN_0$. Accordingly, the renormalization of the spin susceptibility must contain both the renormalization of the quasi-particle mass and of the Landau parameter F_a^0. To show this we write

$$\chi = \chi_0 Z \frac{Z_t}{Z} = \chi_0 Z \left(1 + \frac{2N_0\zeta^2\Gamma_t}{Z}\right) \equiv \chi_0 Z \left(1 + \gamma_t\right) \tag{5.54}$$

with $\gamma_t = 2N_0\zeta^2\Gamma_t/Z$ being the renormalised Landau static amplitude. We note that ζ^2 is always associated either with Γ_s or Γ_t and drops out from the following group equations. It however renormalizes the single-particle density of states, which, in the interacting case, becomes scale dependent even though in a complicated way. Let us define the flow variable $s = -\ln T\tau$ so that $s \to \infty$ corresponds to the infrared limit. Then we have

$$\frac{\mathrm{d}Z}{\mathrm{d}s} = -\frac{t}{2} Z(1 - 3\gamma_t), \tag{5.55}$$

$$\frac{\mathrm{d}Z_t}{\mathrm{d}s} = 2tZ\gamma_t(1 + \gamma_t). \tag{5.56}$$

According to eq.(5.54) one has

$$\frac{\mathrm{d}Z_t}{\mathrm{d}s} = Z\frac{\mathrm{d}\gamma_t}{\mathrm{d}s} + (1 + \gamma_t)\frac{\mathrm{d}Z}{\mathrm{d}s}, \tag{5.57}$$

from which, by using eqs.(5.55),(5.56), one obtains

$$\frac{\mathrm{d}\gamma_t}{\mathrm{d}s} = \frac{t}{2}(1 + \gamma_t)^2, \tag{5.58}$$

in complete agreement with the explicit diagrammatic evaluation of the disorder induced corrections to the scattering amplitudes[61, 62]. By writing the correction to the conductivity in eq.(5.49) in terms of γ_t, the dependence on Z drops out. One gets

$$\frac{\mathrm{d}t}{\mathrm{d}s} = t^2 \left[1 + 3\left(1 - \frac{1 + \gamma_t}{\gamma_t} \ln(1 + \gamma_t)\right)\right]. \tag{5.59}$$

By resuming the weak-localization contribution, one obtains a term identical to the singlet contribution (the first one in the square brakets). The two terms although identical, have therefore a complete different origin and this shows up in the presence of a magnetic field which kills the weak-localization contribution and does not affect the singlet one. Equations (5.58),(5.59) together with eq.(5.55) are the renormalization group equations at one-loop order for the problem of interacting disordered systems at $d = 2$. Their analysis is the task for the next section.

6. – The Renormalization Group equations

By resuming our maritime metaphor, we finally have land in sight. In the present section, we approach the end of our trip by examining the consequences of the physical picture we have developed in the previous sections and briefly compare[71] the results with the experiments. To this end we discuss here in some detail the solution of the renormalization group (RG) equations for the inverse conductance t, triplet scattering amplitude γ_t and the parameter Z. We begin our discussion with the general case when there is no magnetic coupling in the system. In this case the RG equations read

$$\frac{\mathrm{d}t}{\mathrm{d}s} = -\epsilon\frac{t}{2} + t^2\left[1 + 3\left(1 - \frac{1+\gamma_t}{\gamma_t}\ln(1+\gamma_t)\right)\right], \tag{6.1}$$

$$\frac{\mathrm{d}\gamma_t}{\mathrm{d}s} = \frac{t}{2}(1+\gamma_t)^2, \tag{6.2}$$

$$\frac{\mathrm{d}Z}{\mathrm{d}s} = -\frac{t}{2}Z(1-3\gamma_t), \tag{6.3}$$

where in eq.(6.1) we have added the contribution due to the bare dimension due to Ohm's law, $\epsilon = d-2$. The first observation is that eqs.(6.1),(6.2) do not depend on Z. After solving for t and γ_t one may successively solve eq.(6.3) for Z.

Let us consider first the case $d = 2$, i.e., $\epsilon = 0$. Equation (6.2) for γ_t implies a continuous growth. By integrating it between s_0 and s, one has

$$\frac{1}{1+\gamma_t(s)} = \frac{1}{1+\gamma_t(s_0)} - \frac{1}{2}\int_{s_0}^{s}\mathrm{d}s' t(s'), \tag{6.4}$$

from which one sees that γ_t diverges at a finite value, s_c, of the flow parameter:

$$1 = \frac{1}{2}(1+\gamma_t(s_0))\int_{s_0}^{s_c}\mathrm{d}s' t(s'). \tag{6.5}$$

The eq.(6.1) for t says that after an initial increase for not too large $\gamma_t(s_0)$, the growth of γ_t makes the triplet contribution, which is antilocalizing, the dominating one. As a result, t goes through a maximum. In fig.20 we show the RG flow in terms of the variable $t/(1+t)$ and $\gamma_t/(1+\gamma_t)$. For all the RG trajectories $\gamma_t = \infty$ at some finite value s_c, which depends on the initial values. Due to this, one cannot seriously trust the above equations quantitatively. Nevertheless, the physical indication of some type of ferromagnetic instability is rather clear due to the diverging spin susceptibility associated with γ_t. The appearance of a finite length scale may indicate a formation of local magnetic moments on the same scale. Furthermore, the dominating antilocalizing effect of the triplet while t remains finite strongly supports the possibility of a metallic phase at low temperature[73, 72, 67, 74, 75], in contrast with the non-interacting theory based on WL only. Indeed, this metallic phase in $d = 2$ has recently been observed (see refs. in [34]). In any case, both experimentally and theoretically, it is not clear whether a possible ferromagnetic phase occurs before the transition to the insulating phase. Almost all the experimental information is based on transport measurements and the spin susceptibility is obtained indirectly. Very recently, a new method for measuring directly the spin susceptibility in a two dimensional electron gas has been invented and the first result suggests that, although there is a spin susceptibility enhancement, no ferromagnetic instability is observed[76].

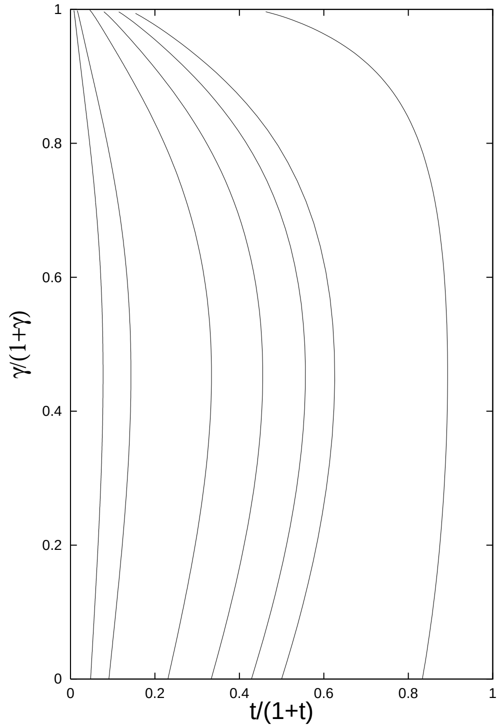

Fig. 20. – The RG flow, for $d = 2$, in terms of the variable $t/(1+t)$ (x-axis) and $\gamma_t/(1+\gamma_t)$ (y-axis). In the figure the flow lines start on the x-axis with $\gamma_t = 0$. For all of them $\gamma_t = \infty$ at some finite value s_c, which depends on the initial values.

In addition, due to the divergence of γ_t also Z goes to the strong coupling regime, leading to an enhancement of the specific heat, which is however hardly observable in two dimensions. Close to the value s_c, one has from eq.(6.4) that

$$\gamma_t \approx (s - s_c)^{-1}, \tag{6.6}$$

which together with the eq.(6.3) for Z gives

$$Z \approx (s - s_c)^{-3}, \ Z_t \approx (s - s_c)^{-4}. \tag{6.7}$$

To convert the above behavior as function of temperature, one may reason in the following way. In general, the divergence of the length scale corresponds to a vanishing temperature, as required by the diffusion law condition $L^2 = D/T$. In the present case, however, the parameter Z renormalizes the temperature so that one has the renormalized condition $L^2 = D/(ZT)$. At finite length scale, the vanishing of T is compensated by the divergence of Z in such a way that $T \approx (s - s_c)^3$. This implies for the specific heat and spin susceptibility

$$\frac{C}{T} \sim T^{-1}, \chi \sim T^{-4/3}. \tag{6.8}$$

We may finally notice that the inclusion of the cooperon contribution would modify the above group equations, without qualitative changes in the overall behavior (see ref.[74] for details).

In $d = 3$ one has a richer scenario depending on the initial value of the running variables. In the limit of large γ_t and small t the product $t\gamma_t$ obeys the equation

$$\frac{\mathrm{d}(t\gamma_t)}{\mathrm{d}s} = \gamma_t \frac{\mathrm{d}t}{\mathrm{d}s} + t\frac{\mathrm{d}\gamma_t}{\mathrm{d}s} = \frac{t\gamma_t}{2}\left(t\gamma_t - \epsilon\right), \tag{6.9}$$

which has a fixed point for $t_c\gamma_{t,c} = \epsilon$. This condition gives the asymptotic expression for a critical line in the $t - \gamma_t$ plane. Close to this critical line, for large values of γ_t, one has the approximate solution

$$t(s) = t(s_0)e^{-\epsilon(s-s_0)/2}, \tag{6.10}$$

$$\gamma_t^{-1}(s) = \gamma_t^{-1}(s_0) - \frac{t(s_0)}{\epsilon} + \frac{t(s_0)}{\epsilon}e^{-\epsilon(s-s_0)/2}. \tag{6.11}$$

One immediately sees from the above equations that for low disorder, $t(s_0) < \epsilon/\gamma_t(s_0)$, t scales to zero and γ_t scales to a finite value. In the high-disorder regime, $t(s_0) > \epsilon/\gamma_t(s_0)$, γ_t diverges at a finite value of s as in the two-dimensional case and t stays finite. In fig.21 we report the flow obtained by numerically integrating the RG equations. We note, however, that the strong-coupling runaway flow requires to go beyond the one-loop approximation we have presented here leaving open the issue whether this proposed scenario is realized or not. An approximate treatment of the two-loop correction is possible, but its discussion is well outside the scope of this paper. We refer the reader to ref. [8].

Along the critical line or nearby in the low-disorder regime, by converting to a length scale via $s = -\ln T\tau = -\ln(\tau D/L^2) \sim 2\ln(L/l)$, one has that, while t vanishes, the conductivity stays finite

$$\sigma(L) = t_c^{-1}(L)L^{-\epsilon}. \tag{6.12}$$

Equation (6.12) may be interpreted in terms of a modification of the scaling law (2.28)

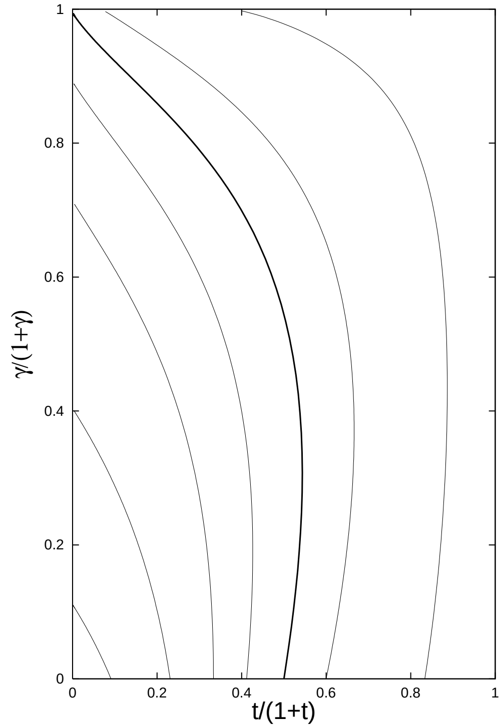

Fig. 21. – The RG flow, in $d = 3$, in terms of the variable $t/(1+t)$ and $\gamma_t/(1+\gamma_t)$. In the figure the flow lines start on the x-axis with $\gamma_t = 0$. On the x-axis, there is value $t/(1+t) \sim 0.5$ below which the RG flows to a state with zero t and finite value of γ_t. The critical line originating from this value of t is shown by a thicker line. At large value of γ_t this critical line is well described by the approximate formula given in the text. For initial larger values of t, the RG flow is qualitatively similar to the two-dimensional case.

due to the scaling behavior of $t_c \sim L^{-x_t}$, i.e.,

$$\mu = \nu(\epsilon - x_t). \tag{6.13}$$

On the critical line $x_t = \epsilon$ and $\mu = 0$. On the other hand γ_t compensates the vanishing of t and diverges like

$$\gamma_t \sim L^{\epsilon}. \tag{6.14}$$

The equation for Z, in addition, gives now

$$\frac{\mathrm{d}Z}{\mathrm{d}s} \sim \frac{3}{2}\epsilon Z, \Rightarrow Z \sim L^{3\epsilon}. \tag{6.15}$$

In contrast to the finite value of σ, according to the eqs. (5.45),(5.46) the spin and heat diffusion constants vanish, due to the divergenece of Z_t and Z. Higher order correction terms could modify this result leading to a vanishing conductivity also in agreement with the experiments. Alternatively we can hypothize that the critical line does not characterize the metal-insulator transition. The strong spin fluctuations which are the relevant physical effect associated with $D_s \to 0$ ($\chi \to \infty$) lead instead to an instability line before the localization takes place. In this case the system before reaching the instability, should make a crossover to one of the universality classes with magnetic couplings, which will be discussed later. By assigning scaling exponents in terms of inverse length scale $x_Z = -3\epsilon$ and $x_{Z_2} = -4\epsilon$ to Z and Z_2 and considering that the combination $ZT \sim L^{-(x_T+x_Z)}$ must scale as $Dq^2 \sim L^{-2}$ since D remains finite, one gets

$$x_T = 2 - x_Z = 2 + 3\epsilon, \tag{6.16}$$

which yields for the specific heat and spin susceptibility

$$\frac{C}{T} \sim T^{-3\epsilon/(2+3\epsilon)}, \;\chi \sim T^{-4\epsilon/(2+3\epsilon)}. \tag{6.17}$$

At $\epsilon = 1$, one has the temperature power laws $-3/5$ and $-4/5$. Hence, as for the two-dimensional case, a clear prediction of the theory is a low temperature enhancement of the specific heat and spin susceptibility, the latter being generally stronger. A stronger enhancement of the spin susceptibility has been indeed observed in $Si:P$[26]. Theoretically, as mentioned before, the divergence of the spin susceptibility at low temperature, as predicted by the renormalization group flow, has led to the suggestion that the system, because of the slowing-down of spin diffusion, tends to form regions of localized magnetic moments, which would eventually drive the system into the universality class of magnetic impurities[72, 73]. In a number of experimental papers[30, 27, 77, 32], where the enhancements of specific heat and spin susceptibility have been compared systematically, some sort of an effective two-component system made of localized and itinerant electrons has been proposed to interpret the data.

In the presence of any mechanism that inhibits the spin fluctuation enhancement, the localizing term in the eq.(6.1) for t dominates and one has a metal-insulator transition with $t_c \sim \mathcal{O}(\epsilon)$. For instance, in the presence of a magnetic field only the ladders in the triplet channel with projection $M = \pm 1$ are suppressed. From eq.(5.50) for the correction to the thermodynamic potential, one sees immediately that the spin susceptibility is no longer singular, i.e., Z_t is invariant upon renormalization. By using eq.(5.57) and eliminating the contribution of the triplet component with $M = \pm 1$ in eq.(6.3) for Z one gets

$$\frac{\mathrm{d}Z}{\mathrm{d}s} = -\frac{t}{2} Z \left(1 - \gamma_t\right), \tag{6.18}$$

$$\frac{\mathrm{d}\gamma_t}{\mathrm{d}s} = \frac{t}{2}(1 - \gamma_t^2). \tag{6.19}$$

The above equations have a fixed point $\gamma_t^* = 1$ with a constant Z. It is now direct to obtain the equation for the parameter t. After suppressing the $M = \pm 1$ triplet channel contributions in eq.(6.1) and by using the fixed-point condition $\gamma_t^* = 1$, one obtains

$$\frac{\mathrm{d}t}{\mathrm{d}s} = -\epsilon\frac{t}{2} + (2 - 2\ln 2)t^2, \tag{6.20}$$

which has a fixed point $t^* = \epsilon/(2(2 - 2\ln 2))$ and gives $\mu = 1$ as in the non-magnetic impurity case for the non-interacting system.

In the case of magnetic impurities or spin-orbit scattering, we have seen in subsection **4**˙5 that only the ladder in the singlet channel remains diffusive (cf. eqs.(4.38) and (4.42)).

Since all triplet channels are massive, γ_t drops out in the equations for Z and t, which now read

$$\frac{\mathrm{d}t}{\mathrm{d}s} = -\epsilon\frac{t}{2} + t^2, \tag{6.21}$$

$$\frac{\mathrm{d}Z}{\mathrm{d}s} = -\frac{t}{2}Z. \tag{6.22}$$

The equation for t gives the fixed point $t^* = \epsilon/2$ and conductivity scaling exponent $\mu = 1$. By using the fixed point value for t in the equation for Z, one obtains

$$Z \approx e^{-(\epsilon/4)\ln s} = T^{\epsilon/4}. \tag{6.23}$$

Notice that the identical behavior for the cases of magnetic impurities and spin-orbit scattering only holds when neglecting the contribution of the pure localization effects. When the latter is also taken into account nothing happens for the magnetic impurities case, since all cooperon ladders are massive (cf. eqs.(4.40) and (4.41)). For the spin-orbit case, on the other hand, the ladder in the cooperon singlet channel is still diffusive and contributes by minus one half to the standard localization term, as we have discussed at the end of subsection **4**˙5. Hence the combination of the antilocalizing contribution from pure interference with the localizing term due to interaction in the singlet channel does not change the qualitative behavior of t and gives $\mu = 1$, even though the fixed point value and the approach to it will differ giving $Z \sim T^{\epsilon/2}$. This is relevant in the experiments[47, 48, 49, 50] (already discussed in points 2),3), and 4) of subsect. **4**˙6), where a value of $\mu = 1$ is observed both in the absence and presence of magnetic field. This is exactly what is predicted by the present theory of combined disorder and interaction effects, where a magnetic field simply controls the contribution of the antilocalizing pure interference effect in the Cooper channel and changes the approach to the fixed point. Such a change is indeed observed in [49]. From a theoretical point of view, we finally comment that in order to perform a quantitative analysis in the presence of both diffuson and cooperon diffusive channels requires however the inclusion of the interaction amplitude V_3 in the Cooper channel. For details we refer the reader to [78, 6]. We hence see that all the universality classes share the same conductivity exponent $\mu = 1$, but differ as far as the behavior of Z (and hence of the specific heat) is concerned. To the best of our knowledge there are no experiments available to check this last prediction.

We are at the end of our journey through the fascinating world of disordered electron systems. It is time to draw a few conclusions. We have seen that the non-interacting theory is not sufficient to interpret the existing experiments. In two dimensions the most relevant result is the prediction of the metallic phase, which is observed to be suppressed by the magnetic field. However, a full account of the experimental situation is far from being reached. In three dimensions, the predictions of the theory of disordered interacting electron systems agree with the experiments whenever there is a magnetic coupling in the system and most of the puzzles met while discussing the non-interacting case are resolved. In the general case, with no magnetic coupling present, although the strong enhancement for the specific heat and spin susceptibility predicted by the theory appear to be confirmed by the experiments, a deeper understanding is clearly needed and further theoretical and experimental work is required with particular emphasis on the magnetic instability problem.

* * *

R. Raimondi acknowledges partial financial support from MIUR under grant COFIN 2002022534. C. Di Castro acknowledges partial financial support from MIUR under grant COFIN 2001023848.

APPENDIX A.

Useful integrals

In the evaluation of diagrams, as we have seen, we leave the $\mathbf{q}$-integration at the end, i.e, the integration over the momenta flowing in the ladder. Due to the presence of the diffusive pole, which makes the small-$\mathbf{q}$ region dominant, the remaining integrals over the fast momenta can be expanded in powers of $\mathbf{q}$ and ω. To this end it is useful to expand the Green's function as

$$G(\mathbf{p}+\mathbf{q},\epsilon+\omega) = G\left[1-(\omega-\mathbf{v}\cdot\mathbf{q})G+(\omega-\mathbf{v}\cdot\mathbf{q})^2G^2+...\right], \tag{A.1}$$

where on the right-hand side $G = G(\mathbf{p},\epsilon)$. Then, the integration over the fast momenta involves integrals containing products of retarded and advanced Green's functions with the same argument. Finally, by using the residue theorem and the formula for the residue of poles we get the useful formula

$$(m,n) = \sum_{\mathbf{p}} (G^R)^m (G^A)^n = (-1)^m \mathrm{i}^{n+m} 2\pi N_0 \frac{n(n+1)...(n+m-1)}{(m-1)!}\tau^{n+m-1}. \tag{A.2}$$

The most frequent cases are

$$(1,1) = 2\pi N_0 \tau \tag{A.3}$$

$$(2,2) = 2\ 2\pi N_0 \tau^3 \tag{A.4}$$

$$(1,2) = \mathrm{i}\ 2\pi N_0 \tau^2 \tag{A.5}$$

$$(2,1) = -\mathrm{i}\ 2\pi N_0 \tau^2 \tag{A.6}$$

$$(1,3) = -\ 2\pi N_0 \tau^3 \tag{A.7}$$

$$(3,1) = -\ 2\pi N_0 \tau^3 \tag{A.8}$$

$$(1,4) = -\mathrm{i}\ 2\pi N_0 \tau^4 \tag{A.9}$$

$$(4,1) = \mathrm{i}\ 2\pi N_0 \tau^4 \tag{A.10}$$

$$(2,4) = -4\ 2\pi N_0 \tau^5 \tag{A.11}$$

$$(4,2) = -4\ 2\pi N_0 \tau^5 \tag{A.12}$$

$$(3,3) = 6\ 2\pi N_0 \tau^5 . \tag{A.13}$$

Integrals containing scalar products are evaluated as

$$\sum_{\mathbf{p}} (\mathbf{p}\cdot\mathbf{q})^2 (G^R)^m (G^A)^n = \frac{p_F^2 q^2}{d} \sum_{\mathbf{p}} (G^R)^m (G^A)^n . \tag{A.14}$$

Appendix B.

Magnetic impurities

To see this, let us consider the following term in the Hamiltonian

$$H_{disorder} = \int \mathrm{d}\ \mathbf{r}\ \psi^\dagger_\alpha(\mathbf{r}) \left[u(\mathbf{r}) \delta_{\alpha\beta} + u_s(\mathbf{r}) \mathbf{S}\cdot\sigma_{\alpha\beta} \right] \psi_\beta(\mathbf{r}), \tag{B.1}$$

where $\mathbf{S}$ is the spin of a paramagnetic impurity located at $\mathbf{r}$ having a scattering amplitude $u_s(\mathbf{r})$, whereas $u(\mathbf{r})$ is the scattering amplitude due to non magnetic impurities and already taken into account within the self-consistent Born approximation. The first step amounts to recompute the Green's function in the presence of the full term eq.(B.1). One gets for the Green's function

$$G^R(\mathbf{p},\epsilon) = \left[\epsilon - \xi_{\mathbf{p}} + \frac{\mathrm{i}}{2} \left(\frac{1}{\tau} + \frac{1}{\tau_s} \right) \right]^{-1} , \tag{B.2}$$

where $\tau^{-1} = 2\pi N_0 \overline{u^2}(\mathbf{r})$, $\tau_s^{-1} = 2\pi N_0 \overline{u_s^2}(\mathbf{r}) S(S+1)$ and for the single impurity line

$$U_{\alpha\beta\gamma\delta} = \frac{1}{2\pi N_0 \tau} \left[\delta_{\alpha\beta}\delta_{\gamma\delta} + \frac{\tau}{3\tau_s} \sigma_{\alpha\beta}\cdot\sigma_{\gamma\delta} \right] , \tag{B.3}$$

where the meaning of the spin greek indices is shown in fig.22. To find the expression for the diffuson and cooperon ladders in the presence of magnetic impurities, it is convenient to exploit the conservation of the total spin of the pair (particle-hole for the diffuson $(\alpha - \delta)$ and particle-particle for the cooperon $(\alpha + \gamma)$). To this end we use the singlet and triplet spin projection operator, which for the diffuson are given by

$$S^{p-h}_{\alpha\beta\gamma\delta} = \frac{1}{2} \delta_{\alpha\delta}\delta_{\beta\gamma} = \frac{1}{4} \left[\delta_{\alpha\beta}\delta_{\gamma\delta} + \sigma_{\alpha\beta}\cdot\sigma_{\gamma\delta} \right] , \tag{B.4}$$

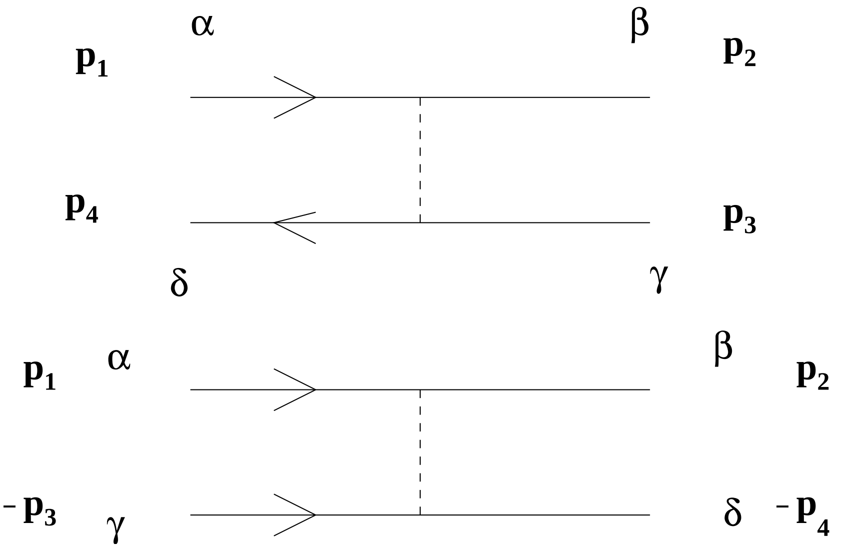

Fig. 22. – A single impurity line with the spin and momentum structure which are related to the diffuson and cooperon ladder. (See fig.12).

$$T^{p-h}_{\alpha\beta\gamma\delta} = \frac{1}{2}\sigma_{\alpha\delta}\cdot\sigma_{\beta\gamma} = \frac{1}{4}\left[3\delta_{\alpha\beta}\delta_{\gamma\delta} - \sigma_{\alpha\beta}\cdot\sigma_{\gamma\delta}\right], \tag{B.5}$$

and for the cooperon by inverting one of the Green's function:

$$S^{p-p}_{\alpha\beta\gamma\delta} = \frac{1}{4}\left[\delta_{\alpha\beta}\delta_{\gamma\delta} - \sigma_{\alpha\beta}\cdot\sigma_{\gamma\delta}\right], \tag{B.6}$$

$$T^{p-p}_{\alpha\beta\gamma\delta} = \frac{1}{4}\left[3\delta_{\alpha\beta}\delta_{\gamma\delta} + \sigma_{\alpha\beta}\cdot\sigma_{\gamma\delta}\right], \tag{B.7}$$

where S and T stand for singlet and triplet, respectively. If we indicate with the $L^{(0)S,T}$ and $L^{(0)}_c$ the the single-impurity line contribution for both singlet (S) and triplet (T) components,

$$L^{(0)S} = Tr(US^{p-h}) = \frac{1}{2\pi N_0\tau}\left(1+\frac{\tau}{\tau_s}\right), \tag{B.8}$$

$$L^{(0)T} = Tr(UT^{p-h}) = \frac{1}{2\pi N_0\tau}\left(1-\frac{\tau}{3\tau_s}\right), \tag{B.9}$$

$$L^{(0)S}_c = Tr(US^{p-p}) = \frac{1}{2\pi N_0\tau}\left(1-\frac{\tau}{\tau_s}\right), \tag{B.10}$$

$$L^{(0)T}_c = Tr(UT^{p-p}) = \frac{1}{2\pi N_0\tau}\left(1+\frac{\tau}{3\tau_s}\right), \tag{B.11}$$

one has for $L^{S,T}$ and $L_c^{S,T}$ the diffuson and cooperon ladders

$$L^{S,T} = \frac{L^{(0)S,T}}{1 - \Pi L^{(0)S,T}},\ L_c^{S,T} = \frac{L_c^{(0)S,T}}{1 - \Pi L_c^{(0)S,T}}. \tag{B.12}$$

The trace sign implies summation over four spin indices. The quantity Π is defined as in eq.(4.11) with the appropriate Green's function for this case. Its evalution leads to eq.(4.13) with $1/\tau$ replaced by $1/\tau + 1/\tau_s \approx 1/\tau(1 - \tau/\tau_s)$.

APPENDIX C.

Spin-orbit scattering

In the presence of spin-orbit interaction, in the scattering Hamiltonian one adds a term

$$H_{SO} = \frac{\hbar}{4m^2c^2} \sum_{\mathbf{R}} \psi_\alpha^\dagger(\mathbf{r}) \left[\sigma_{\alpha\beta} \cdot \nabla V(\mathbf{r} - \mathbf{R}) \wedge \mathbf{p}\right] \psi(\mathbf{r}) \tag{C.1}$$

where $\mathbf{R}$ indicates a ion site and $V(\mathbf{r} - \mathbf{R})$ is the corresponding potential. The matrix element between states of momentum $\mathbf{p}$ and $\mathbf{p}'$ is

$$< \mathbf{p}|H_{SO}|\mathbf{p}' > = \frac{\hbar}{4m^2c^2} \sum_{\mathbf{R}} \sigma_{\alpha\beta} \cdot \int \mathrm{d}\mathbf{r}\, e^{-\mathrm{i}\mathbf{p}\cdot\mathbf{r}} \left[\nabla V(\mathbf{r} - \mathbf{R}) \wedge \mathbf{p}\right] e^{\mathrm{i}\mathbf{p}'\cdot\mathbf{r}} \tag{C.2}$$

$$\equiv \mathrm{i}u_{so} \sum_{\mathbf{R}} e^{\mathrm{i}(\mathbf{p}-\mathbf{p}')\cdot\mathbf{R}} \sigma_{\alpha\beta} \cdot \frac{(\mathbf{p} \wedge \mathbf{p}')}{p_F^2}. \tag{C.3}$$

Since the scattering depends on the momenta of the particles involved, one has to consider separately the contribution to the self-energy and to the single-impurity line in a ladder resummation. For the self-energy one has

$$\Sigma_{so\alpha\beta}(\mathbf{p}, \epsilon) = -\overline{u^2}_{so} \sum_{\mathbf{p}'} \frac{(\mathbf{p} \wedge \mathbf{p}')}{p_F^2} \cdot \sigma_{\alpha\gamma} \frac{(\mathbf{p}' \wedge \mathbf{p})}{p_F^2} \cdot \sigma_{\gamma\beta} G(\mathbf{p}', \epsilon) \tag{C.4}$$

$$\equiv -\mathrm{i}\frac{sign(\epsilon)}{2\tau_{so}} \delta_{\alpha\beta} \tag{C.5}$$

so that the Green's function reads

$$G^R(\mathbf{p}, \epsilon) = \left[\epsilon - \xi_{\mathbf{p}} + \frac{\mathrm{i}}{2}\left(\frac{1}{\tau} + \frac{1}{\tau_{so}}\right)\right]^{-1}. \tag{C.6}$$

For the contribution of a single impurity line one has, by performing the angle average (indicated with a bar) over $\mathbf{p}$ and $\mathbf{p}'$,

$$U_{\alpha\beta\gamma\delta}(\mathbf{p}_1, \mathbf{p}_2, \mathbf{p}_3, \mathbf{p}_4) = -\overline{u^2}_{so} \overline{\frac{(\mathbf{p}_1 \wedge \mathbf{p}_2)}{p_F^2} \cdot \sigma_{\alpha\beta} \frac{(\mathbf{p}_3 \wedge \mathbf{p}_4)}{p_F^2} \cdot \sigma_{\gamma\delta}} \tag{C.7}$$

with the condition that the total momentum is conserved, $\mathbf{p}_1+\mathbf{p}_3=\mathbf{p}_2+\mathbf{p}_4$. In the case of the diffuson ladder one has $\mathbf{p}_1\sim\mathbf{p}_4$, while for the cooperon $\mathbf{p}_1\sim-\mathbf{p}_3$ (See fig.22). As a result

$$U^{p-h}_{\alpha\beta\gamma\delta}=\frac{1}{2\pi N_0\tau_{so}}\sigma_{\alpha\beta}\cdot\sigma_{\gamma\delta} \tag{C.8}$$

$$U^{p-p}_{\alpha\beta\gamma\delta}=-\frac{1}{2\pi N_0\tau_{so}}\sigma_{\alpha\beta}\cdot\sigma_{\gamma\delta}. \tag{C.9}$$

As in the case of magnetic impurities one calculates the single-impurity line contribution

$$L^{(0)S}=\frac{1}{2\pi N_0\tau}\left(1+\frac{\tau}{\tau_{so}}\right) \tag{C.10}$$

$$L^{(0)T}=\frac{1}{2\pi N_0\tau}\left(1-\frac{\tau}{d\tau_{so}}\right) \tag{C.11}$$

$$L^{(0)S}_c=\frac{1}{2\pi N_0\tau}\left(1+\frac{\tau}{\tau_{so}}\right) \tag{C.12}$$

$$L^{(0)T}_c=\frac{1}{2\pi N_0\tau}\left(1-\frac{\tau}{d\tau_{so}}\right) \tag{C.13}$$

In the diagram giving the weak localization correction, in general the spin structure has the form $\delta_{\alpha\delta}\delta_{\gamma\beta}$. By using the projection operators developed in the previous Appendix, one can separate the singlet and triplet contribution to the weak-localization correction in the Cooper channel

$$Tr(S^{p-p}_{\alpha\beta\gamma\delta}\delta_{\alpha\delta}\delta_{\gamma\beta})=-1 \tag{C.14}$$

$$Tr(T^{p-p}_{\alpha\beta\gamma\delta}\delta_{\alpha\delta}\delta_{\gamma\beta})=3. \tag{C.15}$$

We see that, while the triplet is localizing, the singlet has an opposite effect. In the absence of spin-orbit scattering both the singlet and triplet are massless and since the triplet contribution is three times larger, its effect prevails. In the presence of spin-orbit scattering, the triplet becomes massive and does not contribute to the logarithmic singularity term in $d=2$. The latter therefore changes sign and becomes antilocalizing.

APPENDIX D.

The long-range interaction case

The effective screened interaction is given by

$$V^R(q,\omega)=\frac{V_C(q)}{1+V_C(q)K^{00}(q,\omega)}=\frac{2\pi e^2}{q}\frac{Dq^2-\mathrm{i}\omega}{Dq^2+Dq\kappa-\mathrm{i}\omega}, \tag{D.1}$$

where we used the two-dimensional expressions for the $V_C=2\pi e^2/q$ and the Thomas-Fermi inverse screening length $\kappa=4\pi e^2N_0$. In the energy and momentum region given

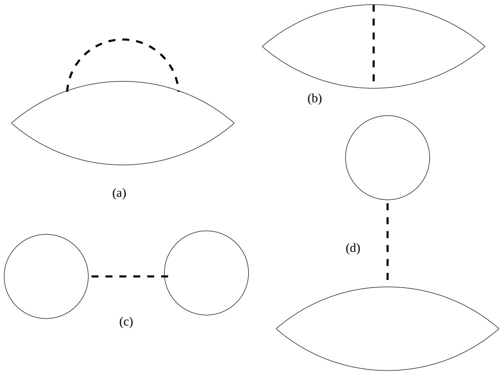

Fig. 23. – Diagrams for the conductivity to the lowest order in the interaction. (a) and (b) Exchange, (c) and (d) Hartree. Interaction is shown as a thick dashed line.

by $\omega < Dq\kappa$ and $Dq^2 < \omega$, the correction to the density of states becomes

$$\delta N(\epsilon) = \frac{1}{2\pi}\mathcal{I}m\int_{-\infty}^{\infty}\mathrm{d}\omega\ f(\omega-\epsilon)\sum_{\omega/D\kappa<|\mathbf{q}|<\sqrt{\omega/D}}\frac{1}{Dq^2(Dq^2-\mathrm{i}\omega)} \tag{D.2}$$

$$= -\frac{t}{4}\ln\left(|\epsilon|\tau\right)\ln\left(\frac{|\epsilon|}{\tau D^2\kappa^4}\right). \tag{D.3}$$

We see that the correction becomes log-square! This is a peculiar feature of the single-particle density of states. In fact, all other physical quantities that we deal with in these lecture notes acquire logarithmic corrections only even in the presence of Coulomb interaction. As we shall see in Appendix H, the density of states can be reabsorbed into the definition of the scattering amplitudes and drops out from the renormalization group equations.

APPENDIX E.

Details on the evaluation of the interaction correction to the conductivity

In this Appendix, we show how to obtain the correction to the electrical conductivity due to the combined effect of disorder and interaction. The diagrams contributing to electrical conductivity to lowest order in the interaction are shown in fig.23. Diagrams (a) and (d) are obtained by inserting a self-energy correction into the Green's function and one has to consider also the symmetric ones with the self-energy insertion in the bottom electron line. Diagrams (b) and (c) are due to vertex corrections. We begin our discussion with diagrams (a) and (b). The extension to diagrams (c) and (d) is straightforward. The expression for diagram (a) reads

$$R^{ij}_{(a)}(\mathbf{r},\mathbf{r}';\Omega) = 2T\sum_{\epsilon_n}\gamma^i(\mathbf{r})\gamma^j(\mathbf{r}')\int \mathrm{d}\mathbf{r}_1\mathrm{d}\mathbf{r}_2 T\sum_{\omega_m}\mathcal{V}(\mathbf{r}_1,\mathbf{r}_2;\omega_m)$$

$$\mathcal{G}(\mathbf{r},\mathbf{r}_1;\epsilon_n+\Omega_\nu)\mathcal{G}(\mathbf{r}_1,\mathbf{r}_2;\epsilon_n+\Omega_\nu-\omega_m)\mathcal{G}(\mathbf{r}_2,\mathbf{r}';\epsilon_n+\Omega_\nu)\mathcal{G}(\mathbf{r}',\mathbf{r};\epsilon_n). \tag{E.1}$$

To this expression one has to add the one corresponding to having the interaction line in the bottom electron line. $\gamma^i(\mathbf{r})$ is the real-space representation of the current vertices. We do not need to write here its explicit expression since at the end, after the impurity average, we recover translational invariance and go back to the momentum representation. Diagram (b) is instead given by

$$\begin{aligned}R^{ij}_{(b)}(\mathbf{r},\mathbf{r}';\Omega) = 2T\sum_{\epsilon_n}\gamma^i(\mathbf{r})\gamma^j(\mathbf{r}')\int \mathrm{d}\mathbf{r}_1\mathrm{d}\mathbf{r}_2\mathcal{G}(\mathbf{r},\mathbf{r}_1;\epsilon_n+\Omega_\nu)\mathcal{G}(\mathbf{r}_2,\mathbf{r};\epsilon_n)\\ T\sum_{\omega_m}\mathcal{G}(\mathbf{r}_1,\mathbf{r}';\epsilon_n+\Omega_\nu-\omega_m)\mathcal{G}(\mathbf{r}',\mathbf{r}_2;\epsilon_n-\omega_m)\mathcal{V}(\mathbf{r}_1,\mathbf{r}_2;\omega_m).\end{aligned} \tag{E.2}$$

In both the eqs.(E.1),(E.2), the Matsubara frequency sums are transformed to contour integrals in the complex plane by means of standard manipulations. Then one gets for diagram (a) (including the other diagram with the two electron lines interchanged)

$$\begin{aligned}R^{ij}_{(a)}(\mathbf{r},\mathbf{r}';\Omega) = {}& -2\gamma^i(\mathbf{r})\gamma^j(\mathbf{r}')\int \mathrm{d}\mathbf{r}_1\mathrm{d}\mathbf{r}_2\int_{-\infty}^{\infty}\frac{\mathrm{d}\epsilon}{2\pi\mathrm{i}}\int_{-\infty}^{\infty}\frac{\mathrm{d}\omega}{2\pi\mathrm{i}}\,[\\
& f(\epsilon-\Omega)b(\omega)(V^R-V^A)_\omega G^R_\epsilon G^R_{\epsilon-\omega}G^R_\epsilon(G^R_{\epsilon-\Omega}-G^A_{\epsilon-\Omega})\\
& +f(\epsilon-\Omega)f(\omega-\epsilon)V^R_\omega G^R_\epsilon(G^R_{\epsilon-\omega}-G^A_{\epsilon-\omega})G^R_\epsilon(G^R_{\epsilon-\Omega}-G^A_{\epsilon-\Omega})\\
& +f(\epsilon)b(\omega)(V^R-V^A)_\omega G^R_\epsilon G^R_{\epsilon-\omega}G^R_\epsilon G^A_{\epsilon-\Omega}\\
& +f(\epsilon)f(\omega-\epsilon)V^R_\omega G^R_\epsilon(G^R_{\epsilon-\omega}-G^A_{\epsilon-\omega})G^R_\epsilon G^A_{\epsilon-\Omega}\\
& -f(\epsilon)b(\omega)(V^R-V^A)_\omega G^A_\epsilon G^A_{\epsilon-\omega}G^A_\epsilon G^A_{\epsilon-\Omega}\\
& -f(\epsilon)f(\omega-\epsilon)V^A_\omega G^A_\epsilon(G^R_{\epsilon-\omega}-G^A_{\epsilon-\omega})G^A_\epsilon G^A_{\epsilon-\Omega}\\
& +f(\epsilon-\Omega)b(\omega)(V^R-V^A)_\omega G^R_\epsilon G^R_{\epsilon-\omega-\Omega}G^R_{\epsilon-\Omega}G^R_{\epsilon-\Omega}\\
& +f(\epsilon-\Omega)f(\omega-\epsilon+\Omega)V^R_\omega G^R_\epsilon G^R_{\epsilon-\Omega}(G^R_{\epsilon-\omega-\Omega}-G^A_{\epsilon-\omega-\Omega})G^R_{\epsilon-\Omega}\\
& -f(\epsilon-\Omega)b(\omega)(V^R-V^A)_\omega G^R_\epsilon G^A_{\epsilon-\Omega}G^A_{\epsilon-\omega-\Omega}G^A_{\epsilon-\Omega}\\
& -f(\epsilon-\Omega)f(\omega-\epsilon+\Omega)V^A_\omega G^R_\epsilon G^A_{\epsilon-\Omega}(G^R_{\epsilon-\omega-\Omega}-G^A_{\epsilon-\omega})G^A_{\epsilon-\Omega}\\
& +f(\epsilon)b(\omega)(V^R-V^A)_\omega(G^R_\epsilon-G^A_\epsilon)G^A_{\epsilon-\Omega}G^A_{\epsilon-\omega-\Omega}G^A_{\epsilon-\Omega}\\
& +\ f(\epsilon)f(\omega-\epsilon+\Omega)V^A_\omega(G^R_\epsilon-G^A_\epsilon)G^A_{\epsilon-\Omega}(G^R_{\epsilon-\omega-\Omega}-G^A_{\epsilon-\omega-\Omega})G^A_{\epsilon-\Omega}]\,.\end{aligned} \tag{E.3}$$

Diagram (b) gives

$$\begin{aligned}R^{ij}_{(b)}(\mathbf{r},\mathbf{r}';\Omega) = {}& -2\gamma^i(\mathbf{r})\gamma^j(\mathbf{r}')\int \mathrm{d}\mathbf{r}_1\mathrm{d}\mathbf{r}_2\int_{-\infty}^{\infty}\frac{\mathrm{d}\epsilon}{2\pi\mathrm{i}}\int_{-\infty}^{\infty}\frac{\mathrm{d}\omega}{2\pi\mathrm{i}}\,[\\
& f(\epsilon)b(\omega)(V^R-V^A)_\omega G^R_{\epsilon+\Omega}G^R_\epsilon G^R_{\epsilon+\Omega-\omega}G^R_{\epsilon-\omega}\\
& f(\epsilon)f(\omega-\epsilon)V^R)_\omega G^R_{\epsilon+\Omega}G^R_\epsilon G^R_{\epsilon+\Omega-\omega}(G^R_{\epsilon-\omega}-G^A_{\epsilon-\omega})\\
& f(\epsilon)f(\omega-\epsilon-\Omega)V^R_\omega G^R_{\epsilon+\Omega}G^R_\epsilon(G^R_{\epsilon+\Omega-\omega}-G^A_{\epsilon+\Omega-\omega})G^A_{\epsilon-\omega}\\
& -f(\epsilon)b(\omega)(V^R-V^A)_\omega G^R_{\epsilon+\Omega}G^A_\epsilon G^R_{\epsilon+\Omega-\omega}G^A_{\epsilon-\omega}\end{aligned}$$

$$\begin{aligned}
&- f(\epsilon)f(\omega-\epsilon)V^A_\omega G^R_{\epsilon+\Omega}G^A_\epsilon G^R_{\epsilon+\Omega-\omega}(G^R_{\epsilon-\omega}-G^A_{\epsilon-\omega})\\
&- f(\epsilon)f(\omega-\epsilon-\Omega)V^R_\omega G^R_{\epsilon+\Omega}G^A_\epsilon(G^R_{\epsilon+\Omega-\omega}-G^A_{\epsilon+\Omega-\omega})G^A_{\epsilon-\omega}\\
&+ f(\epsilon+\Omega)b(\omega)(V^R-V^A)_\omega G^R_{\epsilon+\Omega}G^A_\epsilon G^R_{\epsilon+\Omega-\omega}G^A_{\epsilon-\omega}\\
&+ f(\epsilon+\Omega)f(\omega-\epsilon)V^A_\omega G^R_{\epsilon+\Omega}G^A_\epsilon G^R_{\epsilon+\Omega-\omega}(G^R_{\epsilon-\omega}-G^A_{\epsilon-\omega})\\
&+ f(\epsilon+\Omega)f(\omega-\epsilon-\Omega)V^R_\omega G^R_{\epsilon+\Omega}G^A_\epsilon(G^R_{\epsilon+\Omega-\omega}-G^A_{\epsilon+\Omega-\omega})G^A_{\epsilon-\omega}\\
&- f(\epsilon+\Omega)b(\omega)(V^R-V^A)_\omega G^A_{\epsilon+\Omega}G^A_\epsilon G^A_{\epsilon+\Omega-\omega}G^A_{\epsilon-\omega}\\
&- f(\epsilon+\Omega)f(\omega-\epsilon)V^A_\omega G^A_{\epsilon+\Omega}G^A_\epsilon G^R_{\epsilon+\Omega-\omega}(G^R_{\epsilon-\omega}-G^A_{\epsilon-\omega})\\
&- f(\epsilon+\Omega)f(\omega-\epsilon-\Omega)V^A_\omega G^A_{\epsilon+\Omega}G^A_\epsilon(G^R_{\epsilon+\Omega-\omega}-G^A_{\epsilon+\Omega-\omega})G^A_{\epsilon-\omega}\big]\,.
\end{aligned}\tag{E.4}$$

Since we are discussing the frequency structure, in eqs.(E.3) and (E.4) we have dropped the explicit dependence on space coordinates. The Green's functions are presented in the same order as in eqs.(E.1) and (E.2) where the space dependence is shown. In eqs.(E.3) and (E.4) we may now perform the impurity average. First, averaging impurity pairs belonging to the same Green's function line implies the replacement of the Green's function with its self-consistent Born approximation expression. Secondly, we have to perform the average of impurity pairs belonging to different Green's function lines. This can be performed by arranging the Green's functions on the sides of a square and inserting ladders wherever possible. At the leading order in the expansion parameter, we neglect, as a rule, all the diagrams in which a crossing of impurity lines occurs. Depending on the sequence of retarded and advanced Green's functions around the sides of the square, we may insert two or three ladders. For instance, terms with four retarded Green's functions give zero since all poles lie on the same side of the real axis. In eq.(E.3), the terms that allow two or three ladder insertions are the second, fourth, sixth, eigthth, tenth, and twelfth:

$$\begin{aligned}
R^{ij}_{(a)}(\mathbf{0},\Omega) = -2\sum_{\mathbf{q}}\int_{-\infty}^{\infty}\frac{\mathrm{d}\epsilon}{2\pi\mathrm{i}}\int_{-\infty}^{\infty}\frac{\mathrm{d}\omega}{2\pi\mathrm{i}}\big[&\\
&+ f(\epsilon-\Omega)f(\omega-\epsilon)V^R_\omega(\mathbf{q})\overline{\gamma^i\gamma^j G^R_\epsilon(G^R_{\epsilon-\omega}-G^A_{\epsilon-\omega})G^R_\epsilon(G^R_{\epsilon-\Omega}-G^A_{\epsilon-\Omega})}\\
&+ f(\epsilon)f(\omega-\epsilon)V^R_\omega(\mathbf{q})\overline{\gamma^i\gamma^j G^R_\epsilon(G^R_{\epsilon-\omega}-G^A_{\epsilon-\omega})G^R_\epsilon G^A_{\epsilon-\Omega}}\\
&- f(\epsilon)f(\omega-\epsilon)V^A_\omega(\mathbf{q})\overline{\gamma^i\gamma^j G^A_\epsilon(G^R_{\epsilon-\omega}-G^A_{\epsilon-\omega})G^A_\epsilon G^A_{\epsilon-\Omega}}\\
&+ f(\epsilon-\Omega)f(\omega-\epsilon+\Omega)V^R_\omega(\mathbf{q})\overline{\gamma^i\gamma^j G^R_\epsilon G^R_{\epsilon-\Omega}(G^R_{\epsilon-\omega-\Omega}-G^A_{\epsilon-\omega-\Omega})G^R_{\epsilon-\Omega}}\\
&- f(\epsilon-\Omega)f(\omega-\epsilon+\Omega)V^A_\omega\overline{\gamma^i\gamma^j G^R_\epsilon G^A_{\epsilon-\Omega}(G^R_{\epsilon-\omega-\Omega}-G^A_{\epsilon-\omega})G^A_{\epsilon-\Omega}}\\
&+ f(\epsilon)f(\omega-\epsilon+\Omega)V^A_\omega(\mathbf{q})\overline{\gamma^i\gamma^j(G^R_\epsilon-G^A_\epsilon)G^A_{\epsilon-\Omega}(G^R_{\epsilon-\omega-\Omega}-G^A_{\epsilon-\omega-\Omega})G^A_{\epsilon-\Omega}}\Big]\,.
\end{aligned}\tag{E.5}$$

In the same way, from eq.(E.4) we pick up the third and the eleventh term

$$\begin{aligned}
R^{ij}_{(b)}(\mathbf{0},\Omega) = -2\sum_{\mathbf{q}}\int_{-\infty}^{\infty}\frac{\mathrm{d}\epsilon}{2\pi\mathrm{i}}\int_{-\infty}^{\infty}\frac{\mathrm{d}\omega}{2\pi\mathrm{i}}\big[&\\
&+ f(\epsilon)f(\omega-\epsilon-\Omega)V^R_\omega(\mathbf{q})\overline{\gamma^i\gamma^j G^R_{\epsilon+\Omega}G^R_\epsilon(G^R_{\epsilon+\Omega-\omega}-G^A_{\epsilon+\Omega-\omega})G^A_{\epsilon-\omega}}\\
&- f(\epsilon+\Omega)f(\omega-\epsilon)V^A_\omega(\mathbf{q})\overline{\gamma^i\gamma^j G^A_{\epsilon+\Omega}G^A_\epsilon G^R_{\epsilon+\Omega-\omega}(G^R_{\epsilon-\omega}-G^A_{\epsilon-\omega})}\Big]\,.
\end{aligned}\tag{E.6}$$

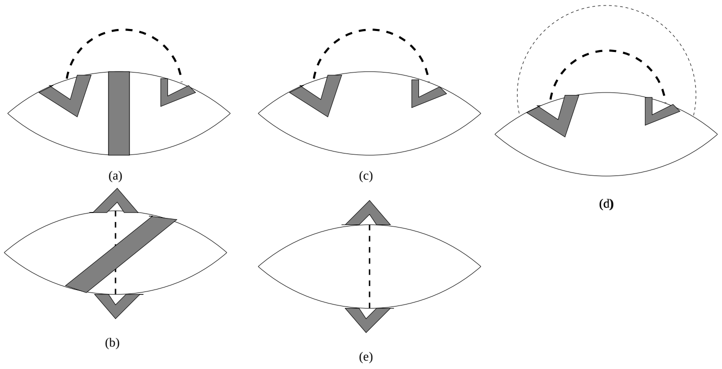

Fig. 24. – Effective conductivity diagrams.

The bar over the products of Green's function indicates the impurity average. Notice that in eqs.(E.5) and (E.6) the current vertices appear under the impurity average bar. After the average and the restoration of traslational invariance, there appear summations over momenta. The sum over the *slow* momenta that enter the interaction and the ladders are performed at the end, while the sum over the *fast* momenta entering the Green's functions are performed with the help of residue theorem within the approximations explained in detail in Appendix A. To this end, all frequencies in the Green's function can be set to zero in the leading order in the diffusive regime expansion $\omega\tau < 1$. As a result, the impurity average of the product of Green's functions does not depend on the energy. Since, the ladders depend only on the *slow* frequencies ω and Ω, we can perform the ϵ-integration at once by using the useful identity

$$\text{(E.7)} \qquad \int_{-\infty}^{\infty} \mathrm{d}\, \epsilon \; f(\epsilon) \; f(\omega - \epsilon) = \frac{\omega}{2} \left(\coth \left(\frac{\omega}{2T} \right) - 1 \right) \equiv F(\omega).$$

We may finally consider explicitly the impurity average. To illustrate the procedure, let us consider the first term in eq.(E.5). It contains four products of four Green's functions each. The first product $G^R_\epsilon G^R_{\epsilon-\omega} G^R_\epsilon G^R_{\epsilon-\Omega}$ gives zero upon averaging. The term $G^R_\epsilon G^R_{\epsilon-\omega} G^R_\epsilon G^A_{\epsilon-\Omega}$ vanishes because of the vector nature of the current vertices. There remain the terms $G^R_\epsilon G^A_{\epsilon-\omega} G^R_\epsilon G^R_{\epsilon-\Omega}$ and $G^R_\epsilon G^A_{\epsilon-\omega} G^R_\epsilon G^A_{\epsilon-\Omega}$. Upon averaging, the first term gives rise to an effective diagram with three ladders, corresponding to (a) of fig.24. The second term, on the other hand, yields effective diagrams with two ladders only, corresponding to (c) and (d) in fig.24. By following this line of reasoning, one obtains all the diagrams of fig.24, including those obtained by interchanging the top and bottom Green's function lines. One key point to notice is that the diagrams with two ladders cancel each other, i.e., the sum of (c),(d), and (e). This cancellation is shown in detail in ref.[59]. To see it, let us consider the terms in eqs.(E.3-E.4) which contain the retarded interaction V^R_ω (a similar analysis can be done for the terms containing V^A_ω). By using eq.(E.7), we get from eqs.(E.5-E.6)

$$-2 \sum_{\mathbf{q}} \int_{-\infty}^{\infty} \frac{\mathrm{d}\omega}{2\pi \mathrm{i}} V^R_\omega \Big(F(\omega - \Omega) \Big[\overline{\gamma^i \gamma^j G^R_\epsilon G^A_{\epsilon-\omega} G^R_\epsilon G^A_{\epsilon-\Omega}} - \overline{\gamma^i \gamma^j G^R_\epsilon G^A_{\epsilon-\omega} G^R_\epsilon G^R_{\epsilon-\Omega}} \Big]$$

$$-F(\omega)\overline{\gamma^i\gamma^j G^R_\epsilon G^A_{\epsilon-\omega}G^R_\epsilon G^A_{\epsilon-\Omega}} - F(\omega)\overline{\gamma^i\gamma^j G^R_\epsilon G^A_{\epsilon-\omega}G^R_\epsilon G^R_{\epsilon-\Omega}}$$
$$-F(\omega-\Omega)\overline{\gamma^i\gamma^j G^R_{\epsilon+\Omega}G^R_\epsilon G^A_{\epsilon+\Omega-\omega}G^A_{\epsilon-\omega}}\Big),$$

which is readily seen to vanish by considering the following averages:

$$\overline{\gamma^i\gamma^j G^R_\epsilon G^A_{\epsilon-\omega}G^R_\epsilon G^R_{\epsilon-\Omega}} = -\delta_{ij}\frac{v_F^2}{d}2\pi N_0\tau^3\left(\frac{1}{2\pi N_0\tau^2}\frac{1}{Dq^2-\mathrm{i}\omega}\right)^2$$
$$\overline{\gamma^i\gamma^j G^R_\epsilon G^A_{\epsilon-\omega}G^R_\epsilon G^A_{\epsilon-\Omega}} = \delta_{ij}\frac{v_F^2}{d}2\pi N_0\tau^3\left(\frac{1}{2\pi N_0\tau^2}\frac{1}{Dq^2-\mathrm{i}\omega}\right)^2$$
$$\overline{\gamma^i\gamma^j G^R_{\epsilon+\Omega}G^R_\epsilon G^A_{\epsilon+\Omega-\omega}G^A_{\epsilon-\omega}} = \delta_{ij}\frac{v_F^2}{d}4\pi N_0\tau^3\left(\frac{1}{2\pi N_0\tau^2}\frac{1}{Dq^2-\mathrm{i}\omega}\right)^2.$$

As a final comment, we note that each individual diagram with two ladders, in the presence of long-range forces, will suffer from the strong singularity as in the case of the density of states, as discussed in Appendix D. However, it has been shown that the singularity due to the long-range forces can be incorporated into a gauge factor, which drops out in the evaluation of gauge-invariant quantities. This is the origin of the cancellation of the diagrams with two ladders[79].

Let us now turn our attention to the diagrams with three ladders. The impurity average needed for the diagram(a) of fig.24 is

$$\begin{aligned}\overline{\gamma^i\gamma^j G^R_\epsilon G^A_{\epsilon-\omega}G^R_\epsilon G^R_{\epsilon-\Omega}} &= \sum_{\mathbf{p}}\gamma^i G^R_\epsilon(\mathbf{p})G^A_{\epsilon-\omega}(\mathbf{p})G^R_{\epsilon-\Omega}(\mathbf{p}-\mathbf{q})\\ &\quad \sum_{\mathbf{p}'}\gamma^j G^R_\epsilon(\mathbf{p}')G^A_{\epsilon-\omega}(\mathbf{p}')G^R_{\epsilon-\Omega}(\mathbf{p}'-\mathbf{q})(\Gamma^0(\mathbf{q},\omega))^2 L(\mathbf{q},\omega-\Omega)\\ &= \frac{(-4\pi e N_0 D\tau^2 q^i)(-4\pi e N_0 D\tau^2 q^j)}{2\pi N_0\tau^4}\frac{1}{(D\mathbf{q}^2-\mathrm{i}\omega)^2(D\mathbf{q}^2-\mathrm{i}(\omega-\Omega))}\\ &= 4\pi\sigma_0\frac{Dq^iq^j}{(D\mathbf{q}^2-\mathrm{i}\omega)^2(D\mathbf{q}^2-\mathrm{i}(\omega-\Omega))}\end{aligned} \tag{E.8}$$

where the factors in round brackets, in the second line, arise from the integration of the three Green's functions with a current vertex. Notice that in diagram (b) of fig.24, the two integrations over products of three Green's functions produce an opposite sign. This gives an overall minus sign for diagram (b) with respect to (a). In the last line $\sigma_0 = 2e^2N_0D$ is the Drude conductivity. By collecting in eqs.(E.5) (first, third, fourth, and sixth line) and (E.6) all the terms giving rise to diagrams with three ladders we get

$$R^{ij}(\mathbf{0},\Omega) = -4\sigma_0\sum_{\mathbf{q}}\int_{-\infty}^{\infty}\frac{\mathrm{d}\omega}{2\pi}\,[$$
$$F(\omega-\Omega)V^R_\omega(\mathbf{q})\frac{Dq^iq^j}{(D\mathbf{q}^2-\mathrm{i}\omega)^2(D\mathbf{q}^2-\mathrm{i}(\omega-\Omega))}$$
$$+\,F(\omega)\;\;V^A_\omega(\mathbf{q})\frac{Dq^iq^j}{(D\mathbf{q}^2+\mathrm{i}\omega)^2(D\mathbf{q}^2+\mathrm{i}(\omega-\Omega))}$$

$$
\begin{aligned}
&+ F(\omega)\ \ V^R_\omega(\mathbf{q})\frac{Dq^iq^j}{(D\mathbf{q}^2-\mathrm{i}\omega)^2(D\mathbf{q}^2-\mathrm{i}(\omega+\Omega))}\\
&+ F(\omega+\Omega)V^A_\omega(\mathbf{q})\frac{Dq^iq^j}{(D\mathbf{q}^2+\mathrm{i}\omega)^2(D\mathbf{q}^2+\mathrm{i}(\omega+\Omega))}\\
&- F(\omega-\Omega)V^R_\omega(\mathbf{q})\frac{Dq^iq^j}{(D\mathbf{q}^2-\mathrm{i}\omega)^2(D\mathbf{q}^2-\mathrm{i}(\omega+\Omega))}\\
&- F(\omega-\Omega)V^R_\omega(\mathbf{q})\frac{Dq^iq^j}{(D\mathbf{q}^2-\mathrm{i}\omega)^2(D\mathbf{q}^2-\mathrm{i}(\omega-\Omega))}\\
&- F(\omega+\Omega)V^A_\omega(\mathbf{q})\frac{Dq^iq^j}{(D\mathbf{q}^2+\mathrm{i}\omega)^2(D\mathbf{q}^2+\mathrm{i}(\omega+\Omega))}\\
&- F(\omega+\Omega)V^A_\omega(\mathbf{q})\frac{Dq^iq^j}{(D\mathbf{q}^2+\mathrm{i}\omega)^2(D\mathbf{q}^2+\mathrm{i}(\omega-\Omega))}\ ]
\end{aligned}
\tag{E.9}
$$

Notice that the first term cancels with the sixth and the fourth with the seventh. By diving by $-\mathrm{i}\Omega$ and sending Ω to zero we get eq.(5.11) quoted in the text.

APPENDIX F.

Details of the evaluation of the thermodynamic potential

To begin with, let us consider, at fixed impurity configuration, the first-order exchange interaction correction to the thermodynamic potential (see the second diagram in fig. 16, without the inserted ladder)

$$
\Delta\Omega=\int_0^1\frac{\mathrm{d}\lambda}{\lambda}\frac{1}{2}T^2\sum_{\omega_m,\epsilon_n}\int \mathrm{d}\mathbf{r}\mathrm{d}\mathbf{r}'\mathcal{V}(\mathbf{r}-\mathbf{r}',\omega_m,\lambda)\mathcal{G}(\mathbf{r},\mathbf{r}';\epsilon_n)\mathcal{G}(\mathbf{r}',\mathbf{r};\epsilon_n+\omega_m),
\tag{F.1}
$$

where we have used the standard trick[44] to multiply the interaction by a parameter $0<\lambda<1$

$$
\mathcal{V}(\mathbf{r}-\mathbf{r}',\omega_m,\lambda)=\lambda\mathcal{V}(\mathbf{r}-\mathbf{r}',\omega_m).
$$

The sum over the Fermionic Matsubara frequency gives

$$
\begin{aligned}
&T\sum_{\epsilon_n}\mathcal{G}(\mathbf{r},\mathbf{r}';\epsilon_n)\mathcal{G}(\mathbf{r}',\mathbf{r};\epsilon_n+\omega_m)|_{\mathrm{i}\omega_m=\omega+\mathrm{i}0^+}=\\
&\int_{-\infty}^{\infty}\frac{\mathrm{d}\epsilon}{2\pi\mathrm{i}}f(\epsilon)\left[(G^R(\mathbf{r},\mathbf{r}';\epsilon)-G^A(\mathbf{r},\mathbf{r}';\epsilon))G^R(\mathbf{r}',\mathbf{r};\epsilon+\omega)\right.\\
&\left.+\,G^A(\mathbf{r},\mathbf{r}';\epsilon-\omega)(G^R(\mathbf{r}',\mathbf{r};\epsilon)-G^A(\mathbf{r}',\mathbf{r};\epsilon))\right].
\end{aligned}
\tag{F.2}
$$

By performing the impurity average we need to keep only terms with both retarded and advanced Green's functions. This selects in eq.(F.2) the term

$$
\int_{-\infty}^{\infty}\frac{\mathrm{d}\epsilon}{2\pi\mathrm{i}}f(\epsilon)\left[-\overline{G^A(\mathbf{r},\mathbf{r}';\epsilon)G^R(\mathbf{r}',\mathbf{r};\epsilon+\omega)}+\overline{G^A(\mathbf{r},\mathbf{r}';\epsilon-\omega)G^R(\mathbf{r}',\mathbf{r};\epsilon)}\right]
$$

$$= \int_{-\infty}^{\infty} \frac{\mathrm{d}\epsilon}{2\pi \mathrm{i}} \left[f(\epsilon+\omega) - f(\epsilon) \right] \overline{G^A(\mathbf{r}, \mathbf{r}'; \epsilon) G^R(\mathbf{r}', \mathbf{r}; \epsilon+\omega)}$$

$$= \frac{\mathrm{i}\omega}{2\pi} (2\pi N_0 \tau)^2 L(\mathbf{q}, \omega), \tag{F.3}$$

where, making use of the fact that the impurity average of the product of Green's functions does not depend on the energy, we have performed the integration over the frequency. As a result, eq.(F.1) becomes

$$\Delta\Omega = -\int_0^1 \frac{\mathrm{d}\lambda}{\lambda} T \sum_{\omega_m} \sum_{\mathbf{q}} \frac{N_0 \mathcal{V}(\mathbf{q}, \omega_m, \lambda) |\omega_m|}{D\mathbf{q}^2 + |\omega_m|}, \tag{F.4}$$

from which, by taking $N_0 \mathcal{V}(\mathbf{q}, \omega_m, \lambda) = \lambda(V_1 - 2V_2)$, one obtains the eq.(5.14) of the main text. Whence the dynamical amplitude resummation is inserted into the diagrams of fig.16 one obtains the final expressions (5.50),(5.51) for the thermodynamic potential.

Appendix G.

Ladder in the presence of Zeeman coupling

In the presence of a magnetic field, electron energies are changed by the Zeeman energy, so that the Green's function reads

$$G^R_\alpha(\mathbf{p}, \epsilon) = \left[\epsilon - \xi_{\mathbf{p}} + \alpha\omega_s + \frac{\mathrm{i}}{2\tau} \right]^{-1}, \tag{G.1}$$

where $\omega_s = g\mu_B B$ with g the Landè factor and μ_B the Bohr magneton. The spin projection takes values $\alpha = \pm 1/2$. One sees that the Zeeman energy $\alpha\omega_s$ enters the Green's function as an energy in shift. This allows to get immediately the ladder in the presence of magnetic Zeeman coupling, since the energy difference ω is shifted by the difference of the Zeeman energies of the particle-hole pair. For instance, by making reference to the spin structure of fig.22 and taking into account the spin conservation along a Green's function line, one has

$$L_{\alpha\delta}(q, \omega) = \frac{1}{2\pi N_0 \tau^2} \frac{1}{Dq^2 - \mathrm{i}\omega - \mathrm{i}(\alpha - \delta)\omega_s}. \tag{G.2}$$

This show that only the triplet components with total spin projection $\alpha - \delta \equiv M = \pm 1$ are affected by the magnetic field.

Appendix H.

The ladder renormalization

In this Appendix we show that the logarithmic corrections found for the physical quantities can be absorbed into a renormalization of the parameters characterizing the

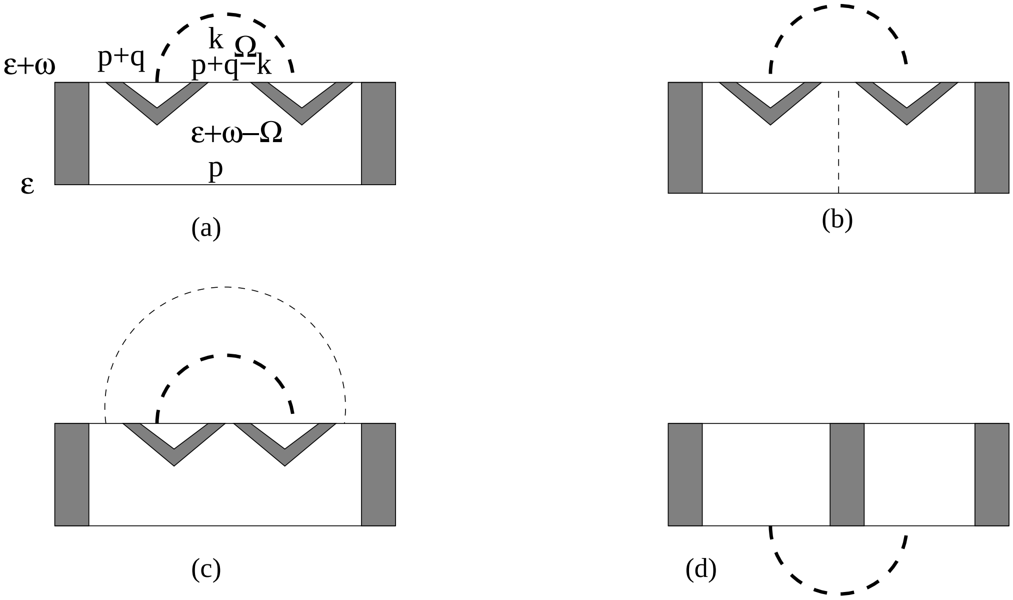

Fig. 25. – Diagrams for the ladder self-energy. A similar set of diagrams is generated by the interchange of the interaction line (tick-dashed line) between top and bottom Green's function lines.

ladder propagator. This identification is the formal basis of the renormalizability of the effective field theory, whose physical meaning is discussed in the text via the Ward identities. Let us assume that the ladder, in the presence of interaction, gets renormalized as

$$L(q,\omega)=\frac{1}{2\pi N_0\tau^2}\frac{1}{Dq^2-\mathrm{i}\omega}\rightarrow\frac{1}{2\pi N_0\tau^2}\frac{\zeta^2}{D_Rq^2-\mathrm{i}Z\omega} \tag{H.1}$$

where ζ, D_R, and Z represent the effective wave function renormalization, the renormalized diffusion coefficient, and the renormalization of the frequency. By expanding

$$\frac{\zeta^2}{D_Rq^2-\mathrm{i}Z\omega}-\frac{1}{Dq^2-\mathrm{i}\omega}=\frac{(2\delta\zeta-\delta D/D)Dq^2-\mathrm{i}(2\delta\zeta-\delta Z)\omega}{(Dq^2-\mathrm{i}\omega)^2}\equiv\frac{\Sigma_L(q,\omega)}{(Dq^2-\mathrm{i}\omega)^2} \tag{H.2}$$

and the last equation defines the ladder self-energy. The diagrams for the self-energy are shown in fig.25. The first step is the integration over the *fast* momenta running within the Green's functions. This integration amounts to the evaluation of several integrals of products of the type $(G^R)^m(G^A)^n$, whose result is given in Appendix A. For diagrams (a-c), in the small k, Ω, q and ω limit, we obtain

$$I_{abc}=(2\pi N_0\tau)^2 2\pi N_0\tau^4\left[D(q^2+k^2)-\mathrm{i}(\omega+\Omega)-2\mathbf{q}\cdot\mathbf{k}\right], \tag{H.3}$$

where the first factor $(2\pi N_0\tau)^2$ represents the two integrations over the two Green's functions at the interaction vertices. The rest gives the integration over the remaining

Green's functions. In a similar way, integration over Green's functions gives for diagram (d)

$$I_d = -(2\pi N_0 \tau^2)^3. \tag{H.4}$$

The diagrams (a),(b),(c) shown in fig.25 finally yield

$$\Sigma_{L,abc} = -2T \sum_{\epsilon_n+\omega_\nu<\Omega_m} \sum_{\mathbf{k}} \frac{I_{abc}(\mathbf{k},\mathbf{q},\Omega_m,\omega_\nu)\mathcal{V}(\mathbf{k},\Omega_m)}{(2\pi N_0\tau^2)^3(Dk^2+|\Omega_m|)^2} \tag{H.5}$$

and diagram (d)

$$\Sigma_{L,d} = 2T \sum_{\epsilon_n<\Omega_m} \sum_{\mathbf{k}} \frac{I_d \mathcal{V}(\mathbf{k},\Omega_m)}{(2\pi N_0\tau^2)^3(D(\mathbf{k}+\mathbf{q})^2+|\Omega_m+\omega_\nu|)}. \tag{H.6}$$

In eqs.(H.5-H.6) we have used Matsubara frequencies. The relative minus sign comes from the integration over the *fast* momenta. The factor of 2 is due to the fact that there is another set of diagrams generated by interchanging the interaction line between the two electron lines. One may check that the sum of eqs.(H.5-H.6) vanishes in the limit $q=0$ and $\omega=0$. For small, but finite external momentum and frequency, we rewrite eq.(H.5) in the form

$$\begin{aligned}\Sigma_{L,abc} = & -2T \sum_{\epsilon_n+\omega_\nu<\Omega_m} \sum_{\mathbf{k}} \frac{\mathcal{V}(\mathbf{k},\Omega_m)}{Dk^2+|\Omega|} \\ & -2T \sum_{\epsilon_n+\omega_\nu<\Omega_m} \sum_{\mathbf{k}} \frac{(Dq^2+|\omega_\nu|)\mathcal{V}(\mathbf{k},\Omega_m)}{(Dk^2+|\Omega_m|)^2}\end{aligned} \tag{H.7}$$

and eq.(H.6) as

$$\begin{aligned}\Sigma_{L,d} = & \, 2T \sum_{\epsilon_n<\Omega_m<\epsilon_n+\omega_\nu} \sum_{\mathbf{k}} \frac{\mathcal{V}(\mathbf{k},\Omega_m)}{D(\mathbf{k}+\mathbf{q})^2+|\Omega_m+\omega_\nu|} \\ & + 2T \sum_{\epsilon_n+\omega_\nu<\Omega_m} \sum_{\mathbf{k}} \left[\frac{\mathcal{V}(\mathbf{k},\Omega_m)}{D\mathbf{k}^2+|\Omega_m|} + \frac{\mathcal{V}(\mathbf{k},\Omega_m)}{D(\mathbf{k}+\mathbf{q})^2+|\Omega_m+\omega_\nu|} - \frac{\mathcal{V}(\mathbf{k},\Omega_m)}{D\mathbf{k}^2+|\Omega_m|}\right],\end{aligned} \tag{H.8}$$

where less divergent terms have been neglected. The first term in the square brakets of eq.(H.8) cancels with the first term in eq.(H.7). Let us analyze the first term of eq.(H.8). By transforming the Matsubara sum into an integral in the complex plane and analytically continuing $\epsilon \to -\mathrm{i}\epsilon$ and $\epsilon+\omega \to -\mathrm{i}(\epsilon+\omega)$, it reads

$$\begin{aligned}\Sigma^1_{L,d} = & \, 2T \sum_{\epsilon_n<\Omega_m<\epsilon_n+\omega_\nu} \sum_{\mathbf{k}} \frac{\mathcal{V}(\mathbf{k},\Omega_m)}{D(\mathbf{k}+\mathbf{q})^2+|\Omega_m+\omega_\nu|} \\ \approx & -\frac{2}{2\pi\mathrm{i}} \int_{-\infty}^{\infty} \mathrm{d}\Omega \, [f(\Omega-\epsilon-\omega)-f(\Omega-\epsilon)] \sum_{\mathbf{k}} \frac{V^R(0,0)}{D\mathbf{k}^2-\mathrm{i}(\Omega+\omega)}\end{aligned}$$

$$
\begin{aligned}
&= -\frac{2\omega}{2\pi \mathrm{i}} \sum_{\mathbf{k}} \frac{V^R(0,0)}{D\mathbf{k}^2 - \mathrm{i}(\epsilon+\omega)} \\
&= \mathrm{i}\omega \frac{V_1 - 2V_2}{4\pi^2 D} \ln\left(\frac{1}{\epsilon\tau}\right) \\
&= -\mathrm{i}\omega \ \mathrm{I}_3, \qquad \text{(H.9)}
\end{aligned}
$$

having used $f(\Omega-\epsilon-\omega) - f(\Omega-\epsilon) \approx \omega \ \partial_\Omega f(\Omega-\epsilon)$. In the last line we have also included the contribution of the Hartree diagrams. The difference between the second and third term in the square brakets of eq.(H.8) may be expanded in powers of q and ω_ν. The lowest order term reads

$$
\begin{aligned}
\Sigma^2_{L,d} &= 2T \sum_{\epsilon_n+\omega_\nu<\Omega_m} \sum_{\mathbf{k}} \mathcal{V}(\mathbf{k},\Omega_m) \left[\frac{2D^2q^2\mathbf{k}^2}{(D\mathbf{k}^2+|\Omega_m|)^3} - \frac{(Dq^2+|\omega_\nu|)}{(D\mathbf{k}^2+|\Omega_m|)^2}\right] \\
&= -\frac{2}{2\pi\mathrm{i}} \int_{-\infty}^{\infty} \mathrm{d}\Omega f(\Omega-\epsilon-\omega) \sum_{\mathbf{k}} \left[\frac{Dq^2D\mathbf{k}^2V^R(0,0)}{(D\mathbf{k}^2-\mathrm{i}\Omega)^3} - \frac{(Dq^2-\mathrm{i}\omega)V^R(0,0)}{(D\mathbf{k}^2-\mathrm{i}\Omega)^2}\right] \\
&= Dq^2\frac{V_1-2V_2}{4\pi^2D}\ln\left(\frac{1}{\epsilon\tau}\right) - (Dq^2-\mathrm{i}\omega)\frac{V_1-2V_2}{4\pi^2D}\ln\left(\frac{1}{\epsilon\tau}\right) \\
&= Dq^2 \ \mathrm{I}_2 - (Dq^2-\mathrm{i}\omega)\mathrm{I}_1. \qquad \text{(H.10)}
\end{aligned}
$$

Finally, the second term in eq.(H.7) reads

$$
\begin{aligned}
\Sigma_{L,abc} &= -(Dq^2+|\omega_\nu|)2T \sum_{\epsilon_n+\omega_\nu<\Omega_m} \sum_{\mathbf{k}} \frac{\mathcal{V}(\mathbf{k},\Omega_m)}{(Dk^2+|\Omega_m|)^2} \\
&= -(Dq^2-\mathrm{i}\omega)\frac{2}{2\pi\mathrm{i}} \int_{-\infty}^{\infty} \mathrm{d}\Omega f(\Omega-\epsilon-\omega) \sum_{\mathbf{k}} \frac{V^R(0,0)}{(Dk^2-\mathrm{i}\Omega)^2} \\
&= -(Dq^2-\mathrm{i}\omega)\frac{V_1-2V_2}{4\pi^2D}\ln\left(\frac{1}{\epsilon\tau}\right) \\
&= -(Dq^2-\mathrm{i}\omega) \ \mathrm{I}_1. \qquad \text{(H.11)}
\end{aligned}
$$

One sees that the by inserting the self-energy results (H.9-H.11) into eq.(H.2) one gets

$$\zeta = 1 - \mathrm{I}_1, \qquad \text{(H.12)}$$

$$\frac{D_R}{D} = 1 - \mathrm{I}_2, \qquad \text{(H.13)}$$

$$Z = 1 - \mathrm{I}_3. \qquad \text{(H.14)}$$

In the main text the renormalized diffusion coefficient D_R will be renamed D. We conclude this Appendix by remarking that the above renormalizations coincide with the perturbative corrections of the single-particle density of states, eq.(5.10), conductivity, eq.(5.12) and specific heat, eq.(5.17), satisfying at this order the Ward identities identifications.

REFERENCES

[1] BERGMANN G., *Phys. Rep.*, **107** (1984) 1.

[2] LEE P. A. and RAMAKRISHNAN T. V., *Rev. Mod. Phys.*, **57** (1985) 287.

[3] ALTSHULER B. L. and ARONOV A. G., in *Electron-Electron Interactions in Disordered Systems*, edited by POLLAK M. and EFROS A. L. (North-Holland, Amsterdam) 1985, p. 1.

[4] CASTELLANI C. and DI CASTRO C., in *Lecture Notes in Physics 216* edited by GARRIDO L. (Springer-Verlag) 1985.

[5] CASTELLANI C., DI CASTRO C. and STRINATI G., in *Lecture Notes in Physics 268* edited by GARRIDO L. (Springer-Verlag) 1985.

[6] FINKELSTEIN A. M. , *Soviet Scientific Reviews*, **14** (1990) .

[7] KRAMER B. AND MACKINNON A., *Rep. Prog. Phys.*, **56** (1993) 1469 .

[8] BELITZ D. and KIRKPATRICK T. R., *Rev. Mod. Phys.*, **66** (1994) 261.

[9] IOFFE A. F. and REGEL A. R., *Prog. Semicond.*, **4** (1960) 237.

[10] MOTT N. F.,*Philos. Magazine*, **26** (1972) 1015.

[11] DOLAN G. J. and OSHEROFF D. D., *Phys. Rev. Lett.*, **43** (1979) 721.

[12] ROSENBAUM T. F., MILLIGAN R. F., PAALANEN M. A., THOMAS G. A., BHATT R. N., and LIN W., *Phys. Rev. B* , **27** (1983) 7509.

[13] ROSENBAUM T. F. ANDRES K., THOMAS G. A., and BHATT R. N., *Phys. Rev. Lett.*, **45** (1980) 1723.

[14] STUPP H., HORNUNG M., LAKNER M., MADEL O., and V.LÖHNEYSEN H., *Phys. Rev. Lett.*, **71** (1993) 2634.

[15] ROSENBAUM T. F., THOMAS G. A., and PAALANEN M. A., , *Phys. Rev. Lett.*, **72** (1994) 2121.

[16] STUPP H., HORNUNG M., LAKNER M., MADEL O., and V.LÖHNEYSEN H., *Phys. Rev. Lett.*, **72** (1994) 2122.

[17] CASTNER T. G., *Phys. Rev. Lett.*, **73** (1994) 3600.

[18] STUPP H., HORNUNG M., LAKNER M., MADEL O., and V.LÖHNEYSEN H., *Phys. Rev. Lett.*, **73** (1994) 3601.

[19] THOMAS G. A., OOTUKA Y., KATSUMOTO S., KOBAYASHI S., and SASAKI S., *Phys. Rev. B*, **25** (1982) 4288.

[20] HERTEL G., BISHOP D. J., SPENCER E. G., ROWELL J. M., and DYNES R. C., *Phys. Rev. Lett.* , **50** (1983) 743.

[21] YAMAGUCHI M., NISHIDA N., FURUBAYASHI T., MORIGAKI K., ISHIMOTO H., and ONO K., *Physica B (Amsterdam)*, **118** (1983) 694.

[22] RHODE M. and MICKLITZ H., *Phys. Rev. B*, **36** (1987) 7572.

[23] MCMILLAN W. L. and MOCKEL J., *Phys. Rev. Lett.* , **46** (1981) 556.

[24] KOBAYASHI S., IKEATA S., KOBAYASHI S., and SASAKI W., *Solid State Communications*, **32** (1979) 1174.

[25] THOMAS G. A., OOTUKA Y., KOBAYASHI S., and SASAKI W., *Phys. Rev. B*, **24** (1981) 4886.

[26] PAALANEN M. A., GRAEBNER J. E., BHATT R. N., and SACHDEV S.,(1988) *Phys. Rev. Lett.*, **61** (1988) 597.

[27] LAKNER M. and V.LÖHNEYSEN H., *Phys. Rev. Lett.*, **63** (1989) 648.

[28] IKEATA S. and KOBAYASHI S., *Solid State Communications*, **56** (1985) 607.

[29] Paalanen M. A., Sachdev S., Bhatt R. N., and Ruckenstein A. E., *Phys. Rev. Lett.*, **57** (1986) 2061.

[30] Alloul H. and Dellouve P., *Phys. Rev. Lett.*, **59** (1987) 578.

[31] Hirsch M. J. Holcomb D. F., Bhatt R. N., and Paalanen M.A. , *Phys. Rev. Lett.*, **68** (1992) 1418.

[32] Schlager H. G. and v. Löhneysen H., *Europhys. Lett.*, **40** (1997) 661.

[33] Kravchenko S. V., Mason W. E., Bower G. E., Furneaux J. E., Pudalov V. M. , and D'Iorio M., *Phys. Rev. B*, **51** (1995) 7038.

[34] Abrahams E., Kravchenko S. V., and Sarachik M. P., *Rev. Mod. Phys.*, **73** (2001) 251.

[35] Kravchenko S. V., and Sarachik M. P., *Rep. Prog. Phys.*, **67** (2004) 1.

[36] Anderson P. W., *Physical Review* , **109** (1958) 1492.

[37] Mott N. F., *Advances in Physics (Philosophical Magazine Supplement*, **16** (1967) 49.

[38] Edwards J. T. and Thouless D. .J, *J. Phys. C*, **5** (1972) 807.

[39] Licciardello D. C. and Thouless D. .J, *Phys. Rev. Lett.*, **35** (1975) 1475.

[40] Abrahams E., Anderson P. W., LicciardelloD. C., and Ramakrishnan T. V. , *Phys. Rev. Lett.*, **42** (1979) 673.

[41] Wegner F.,*Z. Phys. B*, **25** (1976) 327.

[42] Langer J. S. and Neal T., *Phys. Rev. Lett.*, **16** (1966) 984 .

[43] Castellani C., Di Castro C., Forgacs G., and Tabet E., *J. Phys. C: Solid State Phys.*, **16** (1983) 159.

[44] A. A. Abrikosov, L. P. Gorkov, and I. E. Dzyaloshinski, *Methods of Quantum Field Theory in Statistical Physics*, Dover Publications Inc, New York (1975), Sec 1.3.

[45] Zala G., Narozhny B. N., and Aleiner I. L. , *Physical Review B*, **64** (2001) 214204.

[46] Gorkov L. P., Larkin A. I., and Khmelnitskii D. E., *Pis'ma Zh. Eksp. Teor. Fiz.*, **30** (1979) 248 [*JETP Lett.*, **30** (1979) 228].

[47] Okuma S., Komori F., and Kobayashi S., in *Anderson Localization. Proceedings of the International Symposium* edited by Ando, T.; Fukuyama, H. (Springer-Verlag) 1988, p.78.

[48] Nishida N., Furubayashi T. and Yamaguchi M., *Solid State Physics*, **19** (1984) 410.

[49] Katsumoto S., Komori F. Sano N., and Kobayashi S., *Journal of the Physical Society of Japan*, **56** (1987) 2259.

[50] Katsumoto S., in *Anderson Localization. Proceedings of the International Symposium* edited by Ando, T.; Fukuyama, H. (Springer-Verlag) 1988, p.45.

[51] Paalanen M. A., Rosenbaum T. F., Thomas G. A., Bhatt R. N., and Lin W., *Phys. Rev. Lett.* , **48** (1982) 1284.

[52] Shafarman W. N., Koon D. W., and Castner T. G., *Phys. Rev. B*, **40** (1989) 1216.

[53] Dai P., Zhang Y., and Sarachik M.P., *Phys. Rev. Lett.*, **67** (1991) 1914.

[54] Dai P., Zhang Y., Bogdanovich S., and Sarachik M.P., *Phys. Rev. B*, **48** (1993) 4941.

[55] Attaccalite C., Moroni S., Gori-Giorgi P., and Bachelet G.B. , *Phys. Rev. Lett.*, **88** (2002) 256601.

[56] Simonian D. Kravchenko S. V., and Sarachik M. , *Phys. Rev. Lett.*, **79** (1997) 2304.

[57] Altshuler B. L. and Aronov A. G., *Pis'ma Zh. Eksp. Teor. Fiz.*, **30** (1979) 514 [*JETP Lett.*, **30** (1979) 482].

[58] Altshuler B. L., Aronov A. G., and Lee P. A. , *Phys. Rev. Lett.*, **44** (1980) 1288.

[59] Altshuler B. L., Khmelnitskii D. E., Larkin A. I., and Lee P. A. , *Phys. Rev. B*, **22** (1980) 5142.

[60] Altshuler B. L. and Aronov A. G., *Solid State Communications*, **46** (1983) 429.
[61] Finkelstein A. M. , *Zh. Eksp. Teor. Fiz.*, **84** (1983) 168 [*Sov. Phys. JETP* , **57** (1983) 97].
[62] Castellani C., Di Castro C., Lee P. A., and Ma M., *Phys. Rev. B*, **30** (1984) 527.
[63] Castellani C. and Di Castro C., *Phys. Rev. B*, **34** (1986) 5935.
[64] Castellani C., Kotliar G., and Lee P. A., *Phys. Rev. Lett.*, **59** (1987) 323.
[65] Castellani C., Di Castro C., Forgacs G., and Tabet E., *Nucler Phys. B*, **225** (1983) 441.
[66] Altshuler B. L., Aronov A. G., and Zyuzin A. Yu. , *Zh. Eksp. Teor. Fiz.*, **84** (1983) 1537 [*Sov. Phys. JETP* , **57** (1983) 889].
[67] Castellani C., Di Castro C., Lee P. A., Ma M., Sorella S., and Tabet E., *Phys. Rev. B*, **33** (1986) 6169.
[68] Raimondi R., Castellani C., and Di Castro C., *Physical Review B*, **42** (1990) 4724.
[69] Castellani C., Di Castro C., Kotliar G., Lee P.A., and Strinati G., *Physical Review Letters*, **59** (1987) 477.
[70] Castellani C., Di Castro C., Kotliar G., Lee P.A., and Strinati G., *Physical Review B*, **37** (1988) 9046.
[71] Di Castro C., in *Anderson Localization. Proceedings of the International Symposium* edited by Ando, T.; Fukuyama, H. (Springer-Verlag) 1988, p.96.
[72] Finkelstein A. M. , *Z. Phys. B*, **56** (1984) 189.
[73] Castellani C., Di Castro C., Lee P. A., Ma M., Sorella S., and Tabet E., *Phys. Rev. B*, **30** (1984) 1596.
[74] Castellani C., Di Castro C., and Lee P. A., *Phys. Rev. B*, **57** (1998) 9381.
[75] Punnoose A. and Finkel'stein A. M., *Phys. Rev. Lett.*, **88** (2002) 016802.
[76] Prus O., Yaish Y., Reznikov M., Sivan U., and Pudalov V., *Phys. Rev. B*, **67** (2003) 205407.
[77] Lakner M., v.Löhneysen H., Langenfeld A., and Wölfle P., *Phys. Rev. B*, **50** (1994) 17064.
[78] Castellani C., Di Castro C., Forgacs G., and Sorella S., *Solid State Communications*, **52** (1984) 261.
[79] Kopietz P., *Phys. Rev. Lett.*, **81** (1998) 2120.